Studies on Synthesis and Physical Properties of Highly Isotactic Poly(vinyl alcohol) Derived from Poly(*tert*-butyl vinyl ether)

HIROYUKI OHGI

2007

Contents

Chapter 1

General Introduction

Chapter 2

Preparation of Highly Isotactic Poly(vinyl alcohol)s Derived from Poly(*tert*-butyl vinyl ether)s

Chapter 3

Heterogeneous Cationic Polymerization of *tert*-Butyl Vinyl Ether

Chapter 4

Some Physical Properties, Structure and Hydrogen Bonding of Highly Isotactic Poly(vinyl alcohol) Films

Chapter 5

Solid-State ^{13}C NMR Investigation of the Structure and Hydrogen Bonding for Stereoregular Poly(vinyl alcohol) Films in the Hydrated State

Chapter 6

Viscoelastic Behavior of Highly Isotactic Poly(vinyl alcohol) Films

Chapter 7

Investigation of the Complex formation between Highly Isotactic Poly(vinyl alcohol) and Iodine

Chapter 1

General Introduction

1.1. Backgrounds

1.1.1. Preparation and characterization of stereoregular PVAs

The stereoregular polymerization of vinyl monomers was first accomplished by Schildknecht et al. in their studies on the polymerization of vinyl alkyl ethers. In their work, *iso*-butyl vinyl ether gave the most stereospecific polymerization, rapidly yielding crystalline polymer with boron trifluoride etherate ($BF_3^.OEt_2$) catalyst in hydrocarbon solvent at -80 ^{o}C.[1] Natta et al. showed that poly(*iso*-butyl vinyl ether) prepared in this fashion has an isotactic structure.[2] A number of other catalyst systems capable of giving crystalline poly(alkyl vinyl ethers) have been reported.[3]

Poly(vinyl alcohol) (PVA) holds a unique and significant position in the field of polymer stereochemistry. Its high crystalline nature has been noted since the early days of polymer science.[4,5] Three different steric configurations, which coincide with isotactic,[6] atactic,[7] and syndiotactic structures,[8] had been postulated to account for the X-ray fiber diagram of PVA before these structures were designated by Natta et. al.[9] The discovery of stereoregular polymerization methods described above, evoked great interest in the preparation and characterization of stereoregular PVAs. The problem has been studied intensely, particularly in Japan, because of its industrial potential.

A number of investigations have been reported on the synthesis of stereoregular PVAs - both syndiotactic and isotactic PVAs. Although they are rich in syndiotactic or isotactic sequences, a marked dependence of stereoregularity on their properties has been recognized, which may primarily be a result of the changing of intra- and inter-molecular hydrogen bonding.[4,5]

A series of vinyl esters has been polymerized by free radical polymerization to convert to stereoregular PVAs with a rich syndiotactic or isotactic sequence. The physical and solution properties of the PVAs were also studied in relation to their stereoregularity. The stereoregularity of the PVA derived from poly(vinyl acetate) (PVAc), which is available commercially, is approximately atactic.[4,5] Vinyl pivalate[10] and vinyl trifluoroacetate[11] yield somewhat syndiotacticity-rich PVAs compared to commercially available PVA, whereas vinyl benzoate and its derivatives yield slightly isotacticity-rich PVAs.[12]

Vinyl ethers such as benzyl vinyl ether (BzVE), *tert*-butyl vinyl ether (*t*BVE), and trimethylsilyl vinyl ether (VOSi) have been also studied as starting monomers in order to obtain stereoregular PVAs. Murahashi et al. successfully prepared isotacticity-rich PVA by the cationic polymerization of BzVE followed by hydrolysis with hydrogen bromide.[13] Yuki et al. closely studied the relationship between the polymerization conditions of BzVE and the polymer tacticity by analyzing the ^{1}H NMR spectrum of methylene protons at the side chain of polyBzVE.[14] The mole fraction (f_{mm}) of *mm* increased with decreasing polymerization temperature and

reducing monomer concentration, and it was also influenced by the polarity of the polymerization medium. In an attempt to attain higher stereoregularity and easier conversion to PVA, tBVE was investigated by Okamura et al.[15] They studied in detail the relationship between the polymerization conditions of tBVE and the polymer tacticity, and isotacticity-rich PVA was produced by polymerization with $BF_3^{.}OEt_2$ in non-polar media. Murahashi et al. prepared PVAs with a wider range of tacticity by using VOSi whose polymer could be converted to PVA immediately by being dissolved only in methanol.[16] On one hand, isotacticity-rich PVA was obtained by the cationic polymerization of VOSi with ethyl aluminum dichloride ($EtAlCl_2$) in toluene; on the other hand, syndiotacticity-rich PVA was obtained with stannic chloride in nitroethane.

Considerable effort has been invested for preparing stereoregular PVAs as described above; however, the stereoregularity has remained at low levels: f_{mm}=0.7 at best for the so-called isotactic PVA derived from polyVOSi.[16,17]

1.1.2. Solid-state ^{13}C NMR spectroscopy

The characterization of structure and dynamics of crystalline polymers is very important to establish structure-property relationships and to develop high-performance polymer materials. For example, physical properties of PVA films may significantly depend on the structure and hydrogen bonding in the crystalline region as well as in the dried or water-swollen noncrystalline region. There are many techniques that are used for the

polymer characterization, and solid-state ^{13}C NMR spectroscopy is one of the useful methods for characterization of structure and dynamics of solid polymers. A main advantage of solid-state ^{13}C NMR spectroscopy is the selective measurements of the respective components building polymer materials; the separation of the contributions from the crystalline, crystalline-amorphous interfacial, and amorphous regions is possible by using the difference in magnetic relaxation times such as ^{13}C spin-lattice relaxation times (T_{1C}) and spin-spin relaxation times (T_{2C}).[18-24]

Since the stereoregularity dependence of the physical properties of PVA may be closely related to inter- and intra-molecular hydrogen bonding, it is very important to characterize such hydrogen bonding for the stereoregular PVAs in detail. As mentioned above, the solid-state ^{13}C NMR analyses are powerful for the characterization of hydrogen bonding of PVA in the solid state. In the case of the crystalline component of solid atactic PVA samples, the CH resonance line splits into a triplet due to the formation of 2, 1, and 0 intramolecular hydrogen bond(s) in the triad sequences having the all-*trans* conformation.[25-30] As for the noncrystalline component, the characterization becomes more complicated because of the effects of the *gauche* conformation and it may be successful when the statistical treatment will be allowable for the formation of intramolecular hydrogen bonding and for the generation of the *gauche* conformation.[28-30]

On the other hand, the hydration process and resulting hydrogen bonding for A-PVA films have been investigated by the solid-state ^{13}C NMR analysis.[31] It was found that there were three components with different

T_{1C} values assigned to the crystalline, less mobile, and mobile components in the hydrated A-PVA films. In the crystalline component, the probability f_a of the formation of intramolecular hydrogen bonding for the OH groups in the *meso* unit is significantly increased by the addition of water. In the less mobile component, two types of hydrogen bonds are found to still remain even in the presence of water, and the mobile component is subjected to rapid exchanges among different conformations and hydrogen bonds.

1.2. Outline of This Thesis

As described in the previous section, many investigations have been reported on the synthesis and the characterization of stereoregular PVAs which are rich in isotactic sequences, however, the stereoregularity has remained at low levels. Recently, we have succeeded in preparing a PVA having the highest isotactic sequence among all the isotactic PVAs reported so far.[32] This highly isotactic PVA (HI-PVA) showed some interesting physical properties that are different from those of the previously reported isotactic PVAs as well as the commercial atactic PVA. In this thesis, details of the preparation of the HI-PVA derived from poly*t*BVE are dealt with. In addition, we study the physical properties of PVA samples with different tacticities including HI-PVA.

In Chapter 2, the preparation of highly isotactic poly(vinyl alcohol)s (HI-PVAs) are investigated. First, the polymerization of *t*BVE is carried out with various $BF_3 \cdot OEt_2$ concentrations in toluene at $-78\ ^oC$, and then the

resultant poly*t*BVEs are converted into the PVAs.　PVA which has the highest isotacticity ever reported is derived from poly*t*BVE polymerized with $BF_3{\cdot}OEt_2$ catalyst.　In order to clarify the reason why these HI-PVAs are obtained by using an identical catalyst as in previously reported experiments, we study the polymerization conditions such as monomer concentration, polymerization temperature, solvents, and water content. We also study the polymerization of *t*BVE with various BF_3 complexes, and propose the model and mechanism of isospecific propagation in controlling the stereoregularity of the poly*t*BVE.

In Chapter 3, we investigate the heterogeneous cationic polymerization of *t*BVE with Vandenberg type catalysts or metal sulfate-sulfuric acid complexes, because the heterogeneous polymerization of *t*BVE is of considerable interest in both methods in order to obtain the stereoregular PVAs as well as for theoretical consideration.　We determine the stereoregularity of the resultant PVAs derived from these poly(vinyl ether)s and discuss a mechanism for the isospecific heterogeneous polymerization on the basis of a statistical analysis of the tacticity data.

In Chapter 4, some basic physical properties of PVA samples with different tacticities including HI-PVA are systematically examined by different analytical methods as functions of the f_{mm} at the wide range. Intramolecular and intermolecular hydrogen bondings are also characterized for HI-PVA in detail by using high-resolution solid-state ^{13}C NMR spectroscopy.

In Chapter 5, we apply similar ^{13}C NMR analyses to the characterization

6

of the structure and hydrogen bonding for the hydrated HI-PVA and syndiotactic PVA (S-PVA) films. We also investigate the possibility of the partitioning of the different triad sequences into the crystalline and noncrystalline regions in these samples by selectively measuring the triad tacticities for the mobile components that are produced by swelling with water. The clarification of such partitioning is very important to understand the molecular motion in the noncrystalline region for stereoregular PVA samples in relation to the triad tacticity, as described in Chapter 6.

In Chapter 6, we examine dynamic viscoelasticity of HI-PVA in comparison with S-PVA and A-PVA to elucidate the effect of the stereoregularity on the motion of the PVA chains. We study the β_a (local twisting motion) and α_a (micro-Brownian motion) in the noncrystalline region, and the β_c (local motion in crystals due to defects) and the α_c (axial motion of the chain in the crystal lattices) in the crystalline region for each stereoregular PVA samples.

In Chapter 7, we investigate the complex formation of the HI-PVA with iodine in order to compare it with that for A-PVA and S-PVA in aqueous solutions and in film states. We study the absorption maximum λ_{max} and absorbance at λ_{max} of each stereoregular PVA–iodine complexes in aqueous solution under several experimental conditions, i.e. concentration of the boric acid or temperature. To clarify the effect of the stereoregularity of PVA on the complexes with iodine, we study the structure of polyiodine in the complex with HI-PVA by using Resonance Raman spectroscopy and X-ray diffractometry, and propose a model of the HI-PVA and iodine

complexes.

References

(1)   (a) Schildknecht, C. E.; Gross, S. T.;Davidson, H. R.; Lambert, J. M.; Zoss, A. O. *Ind. Eng. Chem.* **1948**, 40, 2104.

(b) Schildknecht, C. E.; Gross, S. T.; Zoss, A. O. *Ind. Eng. Chem.* **1949**, 41, 1998.

(c) Schildknecht, C. E. *Ind. Eng. Chem.* **1958**, 50, 107.

(2)   Natta, G.; Corradini, P.; Bassi, I. W. *Makromol. Chem.* **1956**, 18/19, 455.

(3)   (a) Lal, J. *J. Polym. Sci.* **1958**, 31, 179.

(b) Natta, G.; Dall'Asta, G.; Mazzanti, G.; Gianniti, U.; Cesca, S.*Angew. Chem.* **1959**, 71, 205.

(c) Vandenberg, E. J. *J of Polymer Sci. Part C1* **1963**, 207.

(d) Roch, R. M.; Saunders, J. *J. Polymer Sci.* **1959**, 38, 554.

(4)   Fujii, K. *J. Polym. Sci., Part D* **1971**, 5, 431.

(5)   (a) Finch, C. A. In *Polyvinyl Alcohol*; John Wiley & Sons: New York, **1973**; Chapter 6 and 10.

(b) Finch, C. A. In *Polyvinyl Alcohol-Developments*; John Wiley & Sons: New York, **1992**; Chapter 9 and 10.

(6)   Mooney, R. C. L. *J. Am. Chem. Soc.* **1941**, 63, 2828.

(7)   Bunn, C. W. *Nature* **1948**, 161, 929.

(8)   Sakurada, I.; Fuchino, K.; Okada, N. *Bull. Inst. Chem. Res., Kyoto Univ.* **1950**, 23, 78.

(9)   Natta, G.; Pino, P.; Corradini, P.; Danusso, F.; Mantica, E.; Mazzanti, E.; Moraglio, G. *J. Am. Chem. Soc.* **1955**, 77, 1708.

(10) (a) Yamamoto, T.; Yoda, S.; Sangen, O.; Fukae, R.; Kamachi, M. *Polym. J.* **1989**, 21, 1053.

(b) Yamamoto, T.; Yoda, S.; Sangen, O.; Fukae, R.; Kamachi, M. *Polym. J.* **1990**, 22, 636.

(11) Ofstead, R. F.; Poser, C. I. *Polym. Mater. Sci. Eng.* **1987**, 57, 361.

(12) (a) Imai, K.; Shiomi, T.; Tezuka, Y.; Kawanishi, T.; Jin, T. *J. Polym. Sci., Part A* **1988**, 26, 1961.

(b) Imai, K.; Shiomi, T.; Tezuka, Y.; Fujioka N.; Hosokawa, T.; Ueda, N.; Fujita, K. *Kobunshi Kagaku* **1989**, 46, 261.

(13) Murahasi, S.; Yuki, H.; Sano, T., Yonemura, U.; Tadokoro, T.; Chatani, Y. *J. Polym. Sci.* **1962**, 62, S77.

(14) Yuki, H.; Hatada, K.; Oda, K.; Kinoshita, Murahashi, S.; Ono, K.; Ito, Y. *J. Polym. Sci.* **1969**, Part A-1, 7, 1517.

(15) (a) Okamura, S.; Kodama, T.; Higashimura, T. *Makromol. Chem.* **1962**, 53, 180.

(b) Higashimura, T.; Suzuki, K.; Okamura, S. *Makromol. Chem.* **1965**, 86, 259.

(16) (a) Murahashi, S.; Nozakura, S.; Sumi, M. *J. Polym. Sci.* **1965**, B, 3, 245.

(b) Murahashi, S.; Nozakura, S.; Sumi, M.; Yuki, H.; Hatada, K. *J. Polym. Sci., Polym. Lett. Ed.* **1966**, 4, 65.

(c) Murahashi, S.; Nozakura, S.; Sumi, M.; Yuki, H.; Hatada, K.

Kobunshi Kagaku **1966**, 23, 550.

(17) Wu, T. K.; Ovenall, D. W. *Macromolecules* **1973**, 6, 582.

(18) Tsuji, H.; Horii, F.; Nakagawa, M.; Ikada, Y.; Odani, H.; Kitamaru, R.; *Macromolecules* **1992**, *25*, 4114.

(19) Ishida, H.; Kaji, H.; Horii, F., *Macromolecules* **1997**, *30*, 5799.

(20) Kuwabara, K.; Kaji, H.; Horii, F.; Bassett, D. C.; Olley, R. H., *Macromolecules* **1997**, *30*, 7516.

(21) Kuwabara, K.; Kaji, H.; Horii, F. *Macromolecules* **2000**, *33*, 4453.

(22) Ohira, Y.; Horii, F.; Nakaoki, T. *Macromolecules* **2000**, *33*, 5566.

(23) Ohira, Y.; Horii, F.; Nakaoki, T. *Macromolecules* **2001**, *34*, 1655.

(24) Murakami, M.; Ishida, H.; Miyazaki, M.; Kaji, H.; Horii, F. *Macromolecules*, **2003**, 36, 4160.

(25) Horii, F.; Hu, S.; Ito, T.; Odani, H.; Kitamaru, R.; Matsuzawa, S.; Yamaura, K. *Polymer* **1992,** 33, 2299.

(26) Hu, S.; Horii, F.; Odani, H.; Narukawa, H.; Akiyama, A.; Kajitani, K. *Kobunshi Ronbunshu* **1992**, 49, 361.

(27) Hu, S.; Tsuji, M.; Horii, F. *Polymer* **1994**, 35, 2516.

(28) Masuda, K.; Horii, F. *Macromolecules* **1998**, 31, 5810.

(29) Masuda, K.; Kaji, H.; Horii, F. *Polym. J.* **1999**, 31, 105.

(30) Masuda, K.; Kaji, H.; Horii, F. *J. Polym. Sci., Part B: Polym. Phys.* **2000**, 38, 1060.

(31) Masuda, K.; Kaji, H.; Horii, F. *Polym. J* **2001**, 33, 356.

(32) Ohgi, H.; Sato, T. *Macromolecules* **1993**, *26*, 559.

Chapter 2

Preparation of Highly Isotactic Poly(vinyl alcohol)s Derived from Poly(*tert*-butyl vinyl ether)s

2.1. Introduction

A number of investigations have been reported on the synthesis of stereoregular PVAs both syndiotactic and isotactic PVAs.[1-5] Vinyl ethers are well known as attractive starting monomers for the preparation of stereoregular PVAs. Ionic polymerization of vinyl ethers has long been known to produce isotactic poly(alkyl vinyl ether)s, e.g., poly(benzyl vinyl ether) (polyBzVE) has been shown to be isotactic.[1] Murahashi et al. successfully prepared isotacticity-rich PVA by the cationic polymerization of BzVE followed by hydrolysis with hydrogen bromide. They also studied the effect of the conditions of polymerization of BzVE on polymer structures in detail.[6] In the high-resolution NMR spectrum of polyBzVE, the side chain methylene signal was a triplet that seemed to correspond to *mm*, *mr*, and *rr* sequences in the order of increasing field strength. The fraction of *mm* sequence (f_{mm}) increased as the polymerization temperature and monomer concentration were lowered. The f_{mm} was also influenced by the polarity of the polymerization medium,[7] as in the cationic polymerization of alkyl vinyl ethers.[1]

In an attempt to attain easier polymer transformation and greater stereoregularity, *tert*-butyl vinyl ether (*t*BVE) was employed by

Higashimura's group. Predominantly isotactic polymers were produced by polymerization with boron trifluoride etherate ($BF_3 \cdot OEt_2$) in non-polor solvent, and atactic polymers were obtained with stannic chloride in polor solvent such as methylene chloride.[8] They studied the effect of polymerization conditions on polymer tacticity and observed a further increase in syndiotacticity with polymerization in nitroethane.[8] Stereoregular PVA samples derived from poly*t*BVE have been used as the references samples in many studies of the stereoregularity of PVA.[1]

The synthesis of PVA samples with a wider range of tacticity was made possible by the use of vinyl trimethylsilyl ether (VOSi). Murahashi et al. applied this monomer to PVA synthesis.[9] VOSi was polymerized with cationic initiators, and was converted to PVA by methanolysis immediately after polymerization. Although polymerization with ethyl aluminum dichloride ($EtAlCl_2$) in toluene gave an isotacticity-rich PVA, stannic chloride in nitroethane led to syndiotacticity-rich PVA.[9]

Conciderable effort has been invested for preparing stereoregular PVAs as described above; however, the stereoregularity has remained at low levels: f_{mm}=0.7 at best for the so-called isotactic PVA derived from polyVOSi.[9,10] We have succeeded in preparing PVA having the highest isotactic sequence among all the isotactic PVAs reported so far.[11] In this chapter, details of the preparation and the characterization of the HI-PVA have been dealt with.

2.2. Experimental Section

2.2.1. Reagents

tert-butyl vinyl ether (*t*BVE) monomer was prepared by alkyl exchange reaction between *tert*-butyl alcohol and lauryl vinyl ether in the presence of $Hg(OAc)_2$. In order to eliminate traces of alcohols, the monomer was washed with water, dehydrated over potassium hydroxide, and distilled over calcium hydride before use: b.p.78 ^{o}C (Lit. 76.5-78 ^{o}C). The purity was further confirmed by gas chromatography. Solvents were purified and dehydrated carefully by the usual methods. Boron trifluoride diethyl etherate ($BF_3 {}^. OEt_2$) was purified by distillation under reduced nitrogen pressure and used as a toluene or methylene chloride solution. Other boron trifluoride complexes were used as toluene solutions without further purification.

2.2.2. Polymerization

The polymerization of *t*BVE was carried out with boron trifluoride complexes in several solvents such as toluene or methylene chloride at various temperatures. An ampoule equipped with a three-way stopcock was flushed with dry nitrogen, and then the solvent and the catalyst were introduced with a syringe. To this catalyst solution cooled at a given temperature the monomer solution was added slowly with a syringe and the ampoule was sealed off immediately. Adding a small amount of methanol that was cooled to the same temperature as the reaction mixture terminated the polymerization. The mixture was then poured into a large amount of methanol, and the precipitated polymer was washed with methanol and

dried under vacuum.

2.2.3. Preparation of PVA from poly*t*BVE

Poly*t*BVE was converted into PVA with hydrogen bromide (HBr) gas at
0 $^{\circ}$C.   Before dry HBr gas was passed slowly through a 1-5 wt% solution
of poly*t*BVE in methylene chloride or toluene with stirring, dry nitrogen
being passed to remove oxygen dissolved in the solution.   After 5-10 min.
blowing of HBr gas a white precipitate appeared.   The reaction mixture
was then poured into a large amount of ammoniacal methanol and the
precipitate was collected by filtration, washed with methanol and dried
under vacuum.

2.2.4. Acetylation of PVA

1 g of PVA powder was suspended in 10 ml of dry pyridine at room
temperature.   After the PVA was swollen, 5 ml of acetic anhydride was
added.   Then the reaction mixture was heated at 100 $^{\circ}$C with shaking at
intervals, and heated for another 1 hr after the PVA was dissolved
absolutely.   After the reaction, the mixture was poured into 500 ml of
water and the precipitated polymer was collected by filtration.   The PVAc
thus obtained was purified by precipitation from acetone with water and
then dried under vacuum.

2.2.5. Molecular weight measurements

Molecular weights and their distributions of poly*t*BVE were measured

by GPC at 38 $^{\circ}$C in THF as an eluent with Shimazu Model 802A hichromatograph equipped with a differential refractometer detector. The molecular weight calibration was obtained by using standard polystyrenes. The degrees of polymerization of PVAc (P_{rac}) were measured by the same method described in the previous paper.[11]

2.2.6. NMR measurements

^{1}H NMR measurements were performed on a JEOL JNM-GSX270 spectrometer operating at 270.17MHz. The spectra of PVA were measured in dimethyl sulfoxide (DMSO)-d_6 at 25.0 $^{\circ}$C.

2.2.7. Stereoregularity determination

The triad sequence fractions of PVA can be determined by ^{1}H NMR spectrum measured in DMSO-d_6.[12] Figure 2-1 illustrates the ^{1}H NMR spectra of several stereoregular PVAs derived from poly*t*BVEs.

2.3. Results and Discussion

2.3.1. Preparation of highly isotactic PVAs

The polymerization of *t*BVE was carried out with various BF$_3$·OEt$_2$ concentrations in toluene at −78 $^{\circ}$C, and then the resultant poly*t*BVEs were converted into the PVAs. The results are summarized in Table 2-1 and the mol fraction of *mm* (f_{mm}) of the PVAs is shown in Figure 2-2 as a function of BF$_3$·OEt$_2$ concentration. The f_{mm} increased with decreasing BF$_3$·OEt$_2$ concentration and reached as high as 78-79% when the BF$_3$·OEt$_2$

concentration was reduced below 0.5 x 10^{-3} mol/l.

Because the stereoregularity of PVA can be determined by several spectroscopic methods,[1,12,13] the method used to measure the stereoregularity of the polymers must be noted. The observation of the methyl proton signal of PVAc by ^{1}H NMR spectrum was the most popular method to determine the stereoregularity of PVA because PVA is easily converted to PVAc along with the retention of its stereoregularity. However, it is difficult to determine the tacticity by using this method because of their close chemical shifts and broad *rr* absorption peaks.[1,14] The relative peak height analysis may overestimate the f_{mm}. On the other hand, Moritani et al.[12] and DeMember et al.[13] found that the hydroxyl proton absorption splits three separate peaks due to the triad tacticity in the ^{1}H NMR spectrum of PVA in DMSO-d_6. These three peaks are sharp and sufficiently separate to make the stereoregularity distinguishable, as shown in Figure 2-1.

It is believed that the ^{1}H NMR measurement of PVA in DMSO-d_6 can give a more accurate tacticity than that of the corresponding PVAc. For the purpose of comparison, Table 2-1 includes f_{mm} values determined by ^{1}H NMR spectra on PVAc and PVA of some typical isotactic PVAs reported so far. The f_{mm} value of PVA derived from poly*t*BVE, which is obtained by a process proposed by Okamura et al.,[8] is 0.79 for PVAc and 0.55 for PVA,[13] and the f_{mm} value of PVA derived from polyVOSi, which is prepared by Murahashi et al.,[9] is 0.86 for PVAc and 0.70 for PVA.[10] This fact indicates that the f_{mm} value determined for PVAc is considerably larger than that
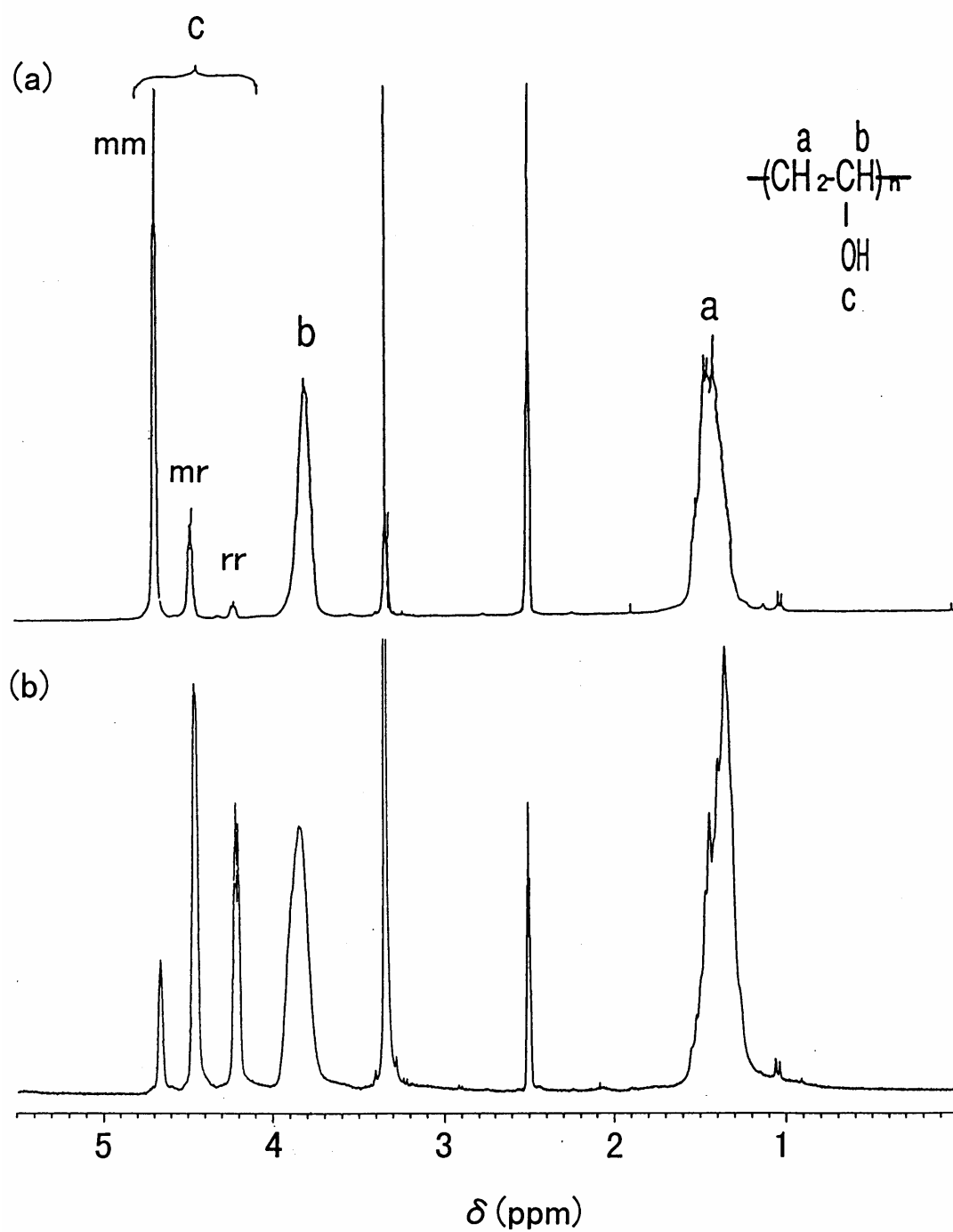
Figure 2-1. ^{1}H NMR spectra of stereoregular PVAs in DMSO-d_6, at 25 ^{o}C and 270 MHz: (a) highly isotactic (run 2 in Table 2-1); (b) moderately syndiotactic (run 2 in Table 2-3). *mm, mr,* and *rr* are assigned to *meso-meso, meso-racemo, and racemo-racemo* sequence fraction, respectively.

17

determined for PVA, and suggests that the f_{mm} of the isotactic PVA derived from polyBzVE, whose f_{mm} is 0.89 determined for PVAc, reported by Yuki et al.[7] may likewise be similar to that of the PVA prepared by Murahashi et al.   It has also been reported that a PVA derived from poly$t$BVE prepared with BF$_3$·OEt$_2$ in toluene at -78 ^{o}C has a f_{mm} of 0.50, as determined for PVA.[12]   In any case, the PVA prepared in this work seems to be the most highly isotactic PVA (HI-PVA) ever reported.   Figure 2-1(a) shows the ^{1}H NMR spectrum of the HI-PVA (run2 in Table 2-1) derived from poly$t$BVE, which is prepared with BF$_3$·OEt$_2$ at a very low catalyst concentration.

In order to clarify the reason why these highly isotactic PVAs (poly$t$BVEs) were obtained by using an identical catalyst as in previously reported experiments, we studied the polymerization conditions closely.

2.3.2. Effect of monomer concentration

The effect of tBVE monomer concentration on the polymerization carried out with 0.25 x 10^{-3} mol/l of BF$_3$·OEt$_2$ in toluene at -78 ^{o}C is summarized in Table 2-2.   The f_{mm} of the PVA (poly$t$BVE) increased from 0.65 to 0.77 with decreasing initial tBVE concentration from 50 vol% to 2.5 vol%.   Our results seem to agree with Okamuras' result that the dielectric constant of the polymerization system affects the stereoregularity of the produced polymer.[8]   By comparing Tables 2-1 and 2-2, it is apparent that reducing the tBVE monomer concentration is not as effective

Table 2-1. Characterization of isotactic PVAs derived from poly tBVE prepared with $BF_3 \cdot OEt_2$ in toluene at $-78\ ^\circ C$.

No.	[tBVE] (vol%)	[$BF_3 \cdot OEt_2$] (mM)	Time (h)	Conv. (%)	Poly$t$BVE M_n	M_w	M_w/M_n	PVA triad mm	mr	rr	P_{rac}
1	5	1.25	3	73.1	59000	121200	2.05	0.67	0.30	0.03	1400
2	5	0.50	2	80.9	58290	120720	2.07	0.80	0.18	0.02	1370
3	5	0.25	4	85.2	212900	507820	2.39	0.79	0.19	0.02	6800
4	10	0.25	10	78.7	32030	60680	1.89	0.78	0.19	0.03	490
5[a]								0.55	0.32	0.13[b]	
								(0.79	0.17	0.04)[c]	
6[d]								0.70	0.23	0.07[e]	
								(0.86	0.10	0.04)[c]	

[a] Isotactic PVA derived from poly$t$BVE reported by Okamura et al.(ref 8). [b] Triad sequence fractions determined by ^{1}H NMR spectrum on PVA (ref 13). [c] Triad sequence fractions determined by ^{1}H NMR spectrum on PVAc (ref 9). [d] Isotactic PVA derived from polyVOSi prepared by Murahashi et al.(ref 9). [e] Triad sequence fractions determined by ^{1}H NMR spectrum on PVA (ref 10).
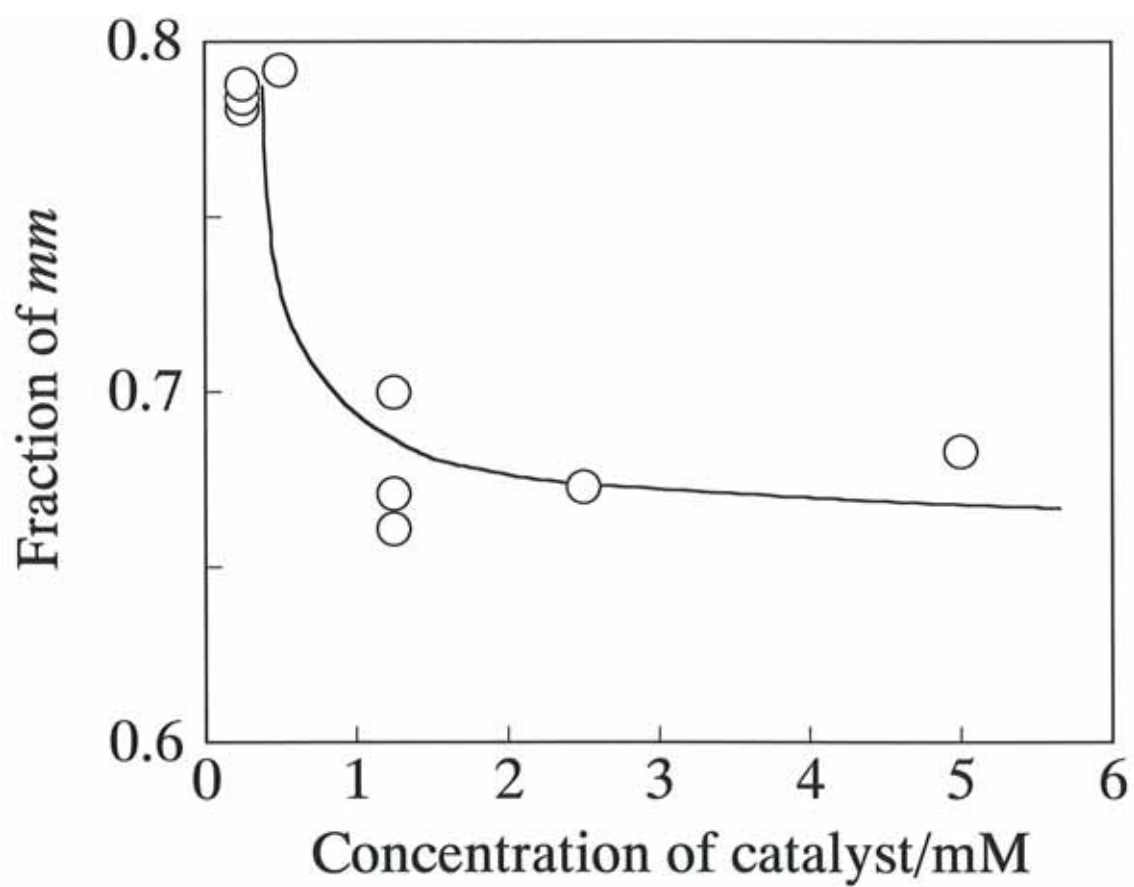
Figure 2-2. Effect of catalyst concentration on the *mm* sequence fraction of PVAs derived from poly*t*BVE prepared with $BF_3{\cdot}OEt_2$ in toluene at -78 $^{\circ}$C.

as achieving greater catalyst concentration in increasing the f_{mm} of the produced polymer.

2.3.3. Polymerization in various solvents

The results of the polymerization carried out in various solvents and the characterizations of the resultant PVAs are summarized in Table 2-3. By using polar solvents such as methylene chloride (CH_2Cl_2) or nitroethane ($EtNO_2$), the *rr* sequence fraction (f_{rr}) increased, while the f_{mm} increased in non-polar solvents such as n-hexane, n-heptane, or methylcyclohexane (MCH).

In CH_2Cl_2, the polymerization proceeded homogeneously as is the case with toluene, but the polymerization rate was slower and the molecular weight of the obtained poly*t*BVE was lower compared to that obtained in toluene. However, the polymerization in $EtNO_2$ proceeded heterogeneously due to the low solubility of poly*t*BVE in $EtNO_2$, and therefore, the *rr* sequence fraction of the resultant PVA was lower than that obtained in CH_2Cl_2.

The stereoregularity of PVAs (poly*t*BVEs) polymerized in toluene/CH_2Cl_2 mixtures are shown in Figure 2-3 as a function of the volume ratio of toluene, indicating that the f_{mm} increased monotonically with increasing toluene fraction. These results may be interpreted according to the theory proposed by Okamura et al.[8] that the isotactic propagation preferred homogeneous and non-polar conditions at low temperature. The f_{mm} of PVAs (poly*t*BVEs) obtained in toluene,

Table 2-2. Characterization of isotactic PVAs derived from poly*t*BVE prepared at various monomer concentrations with $BF_3 \cdot OEt_2$ in toluene at - 78 ^{o}C .

No.	[*t*BVE] (vol%)	Time (hr)	Conv. (%)	Poly*t*BVE			PVA	triad	
				M_n	M_w	M_w/M_n	*mm*	*mr*	*rr*
1	50	3	21.5	101500	221800	2.19	0.65	0.29	0.06
2	25	3	34.8	91700	167500	1.83	0.72	0.24	0.04
3	10	7.5	61.6	30400	52100	1.71	0.76	0.21	0.03
4	5	3	80.6	81300	140600	1.73	0.77	0.20	0.03
5	2.5	19	51.3	47500	85500	1.80	0.77	0.20	0.03

however, was much higher than that obtained in n-hexane, n-heptane, or methylcyclohexane, whose f_{mm} were almost the same despite their different dielectric constants and solubility parameters.   This fact may suggest that in the case of toluene, some kind of interaction between the propagation site and π electron of toluene should be allowed as a factor that influences the stereospecific propagation.   It is well known that the aromatic groups of solvents, additives, monomers, and polymers interact with a growing chain in carbocationic polymerization.[15] Therefore, the local polarity around the propagation site in toluene may be lower than the average polarity of the polymerization mixture due to the selective solvation of toluene to the carbeniumion caused by π electron interaction, which would promote isospecific propagation. In contrast, the local polarity in aliphatic solvents such as methylcyclohexane may be higher than the average polarity because of the selective solvation of tBVE to the carbeniumion. We conclude that toluene is one of the best solvents for obtaining highly isotactic polymers by the polymerization of tBVE with $BF_3^.OEt_2$.

2.3.4. Effect of polymerization temperature

We then examined the effect of temperature on the polymerization of tBVE.   Table 2-4 indicates the results of the polymerization conducted in toluene with 0.25 x 10^{-3} mol/l of $BF_3^.OEt_2$ at various temperatures between -78 and 0 ^{o}C.   Barring the polymerization at 0 ^{o}C, a high molecular weight and high f_{mm} of the poly$t$BVEs (PVAs) were obtained, and both increased with decreasing polymerization temperature.   This result means that

Table 2-3. Characterization of stereoregular PVAs derived from poly*t*BVE prepared with $BF_3 \cdot OEt_2$ at - 78 $^\circ$C in various solvents.

No.	solv.	[*t*BVE] (vol%)	[$BF_3 \cdot OEt_2$] (mM)	Time (hr)	Conv. (%)	Poly*t*BVE M_n	M_w	M_w/M_n	PVA triad mm	mr	rr
1	CH_2Cl_2	10	2.50	60	70.0	26000	56900	2.19	0.19	0.49	0.32
2	CH_2Cl_2	10	0.25	60	70.0	52100	99300	1.91	0.11	0.54	0.35
3	$EtNO_2$	10	2.50	3	67.2	1640	5000	3.05	0.19	0.55	0.26
4	$EtNO_2$	10	0.25	3	2.8	26800	38100	1.42	0.16	0.53	0.31
5	Hexane	10	2.50	3	89.1	74300	360300	4.85	0.51	0.38	0.11
6	Hexane	10	0.25	3	8.9	103500	284500	2.75	0.50	0.37	0.13
7	Heptane	5	2.50	3	92.5	136000	966000	7.10	0.54	0.36	0.10
8	Heptane	5	0.25	3	75.5	187000	642000	3.43	0.54	0.35	0.11
9	MCH	5	2.50	6	99.0	110000	281000	2.55	0.50	0.39	0.11
10	MCH	5	0.50	6	89.0	33700	111000	3.29	0.52	0.37	0.11

decreasing the polymerization temperature to the lowest possible extent is really effective to obtain high molecular weight and highly isotactic PVAs (poly$t$BVEs).

Nozakura et al.[16] have reported that the mechanism of stereoregulation could be inferred from Fordham's equation (eq 1).[17] Here, P_i and P_s denote the mole fractions of *meso* and *racemo*, respectively; R is the gas constant, and T is the absolute temperature.

$$\ln(P_i/P_s) = (\Delta S_i^{\neq} - \Delta S_s^{\neq})/R - (\Delta H_i^{\neq} - \Delta H_s^{\neq})/RT \tag{1}$$

By analyzing the stereoregularity of the resultant polymers according to eq 1, we can obtain the following information regarding the regulation of the polymerization: Is monomer addition governed enthalpically or entropically? In Figure 2-4, the relationships between the reciprocal temperature (1/T) and logarithm of *meso*/*racemo* ratio ($\ln(P_i/P_s)$) for two BF$_3$·OEt$_2$ concentration levels of 0.25 x 10^{-3} mol/l and 2.5 x 10^{-3} mol/l are plotted, and the activation parameters calculated are listed in Table 2-5. Both activation enthalpy and activation entropy of the isotactic propagation are smaller than those of the syndiotactic propagation, and their differences are 1140 cal/mol and 1.7 cal/deg·mol for 0.25 x 10^{-3} mol/l, and 770 cal/mol and 0.85 cal/deg·mol for 2.5 x 10^{-3} mol/l, respectively. This indicates that the isotactic propagation was preferred to the syndiotactic propagation enthalpically, although the syndiotactic propagation is predominant entropically.   In other words, the
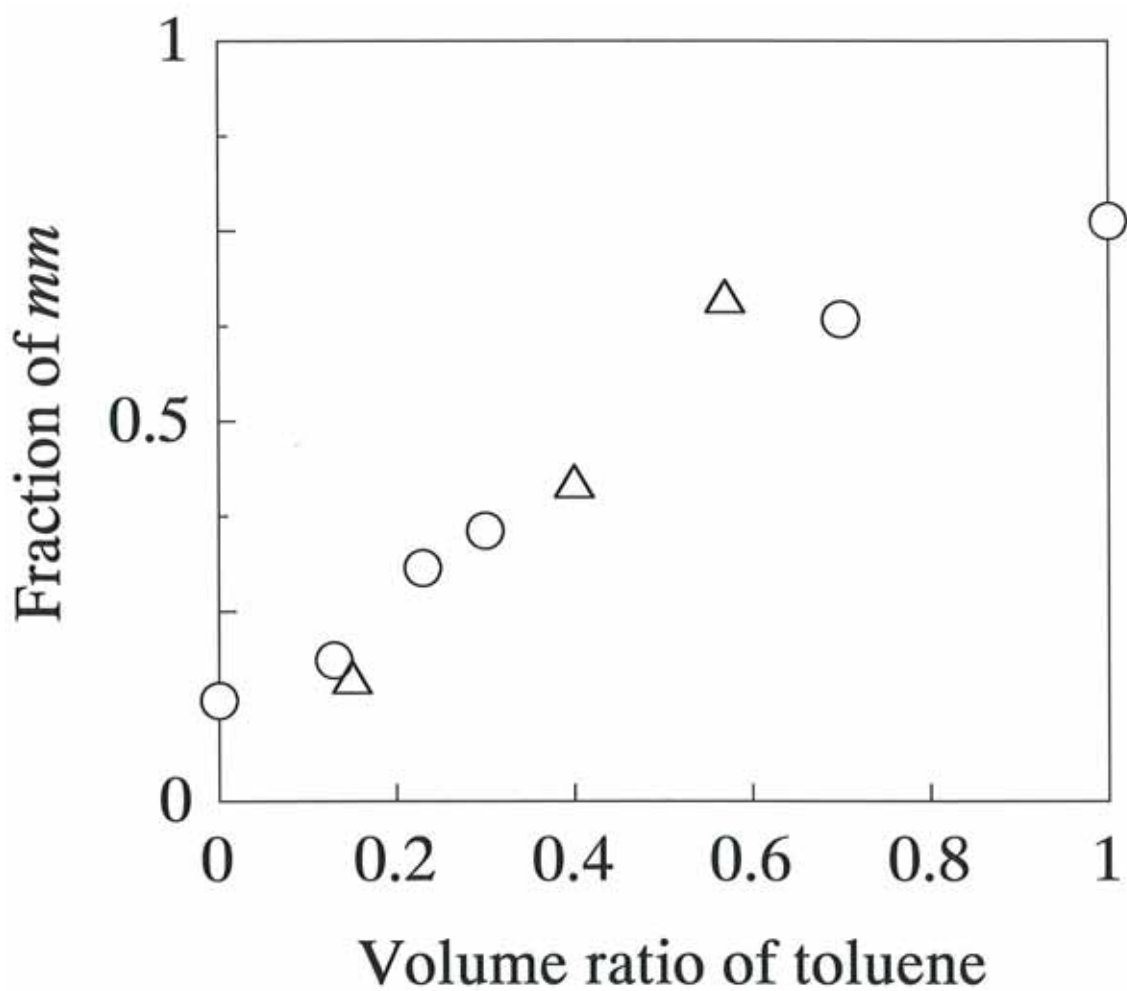
Figure 2-3. Effect of the solvent polarity on the *mm* sequence fraction of PVAs derived from poly*t*BVE prepared with $BF_3 \cdot OEt_2$ in toluene-methylene chloride mixture at -78 ^{o}C. Initial concentrations of *t*BVE were 10 (circle) and 5 (triangle) vol%.

Table 2-4. Characterization of isotactic PVAs derived from poly*t*BVE prepared with $BF_3 \cdot OEt_2$ of 0.25 x 10^{-3} mol/l in toluene at various temperatures.

No.	Temp. (°C)	Time (hr)	Conv. (%)	Poly*t*BVE			PVA			
				M_n	M_w	M_w/M_n	triad			P_{rac}
							mm	*mr*	*rr*	
1	0	3	0	2380	3620	1.52				
2	-20	3	57.5	26500	40200	1.52	0.65	0.30	0.05	
3	-40	3	37.5	41000	87600	2.14	0.72	0.24	0.04	1070
4	-60	3	62.5	70100	142500	2.03	0.76	0.21	0.03	2020
5	-78	3	25.1	74200	150000	2.02	0.79	0.19	0.02	3540

stereoregulation of *t*BVE polymerization with $BF_3 \cdot OEt_2$ in toluene is governed by an enthalpical factor, which is similar to the results obtained by Sumi et al.[18] for VOSi polymerization with $EtAlCl_2$ in toluene. A more noteworthy fact is that a smaller value of $\Delta H_i^{\neq} - \Delta H_s^{\neq}$ for the lower concentration of $BF_3 \cdot OEt_2$ was obtained. This suggests that a new kind of propagation species generated under low $BF_3 \cdot OEt_2$ concentration has high isospecific selectivity to lead to the most highly isotactic PVA (poly*t*BVE) as mentioned above.

From the kinetic study of the polymerization of alkyl vinyl ether in diethyl ether with $BF_3 \cdot OEt_2$,[19] it has been stated that the initiation of the polymerization occurs with an ion pair formed by the direct reaction between $BF_3 \cdot OEt_2$ and monomer as follows:

$$BF_3 \cdot OEt_2 + CH_2 = CHOR \qquad EtCH_2CH^+[BF_3 \cdot OEt]^- \qquad (2)$$
$$| \atop OR$$
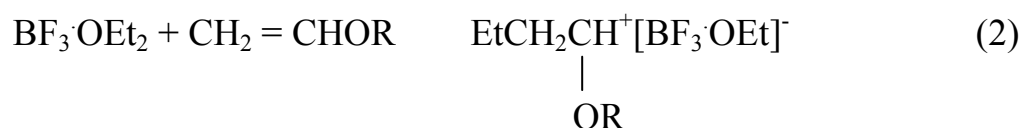
In the polymerization system, there actually exist a small amount of water; however, the exchange reaction described in eq 3 occurs and the reactions in eqs 2 and 4 seem to compete in the initiation followed by the propagation.[7]

$$BF_3 \cdot OEt_2 + H_2O \qquad BF_3 \cdot OH_2 \ + \ Et_2O \qquad (3)$$

$$BF_3 \cdot OH_2 + CH_2 = CHOR \qquad HCH_2CH^+[BF_3 \cdot OH]^- \qquad (4)$$
$$| \atop OR$$
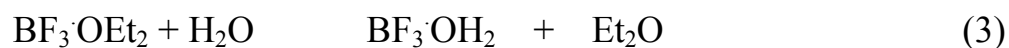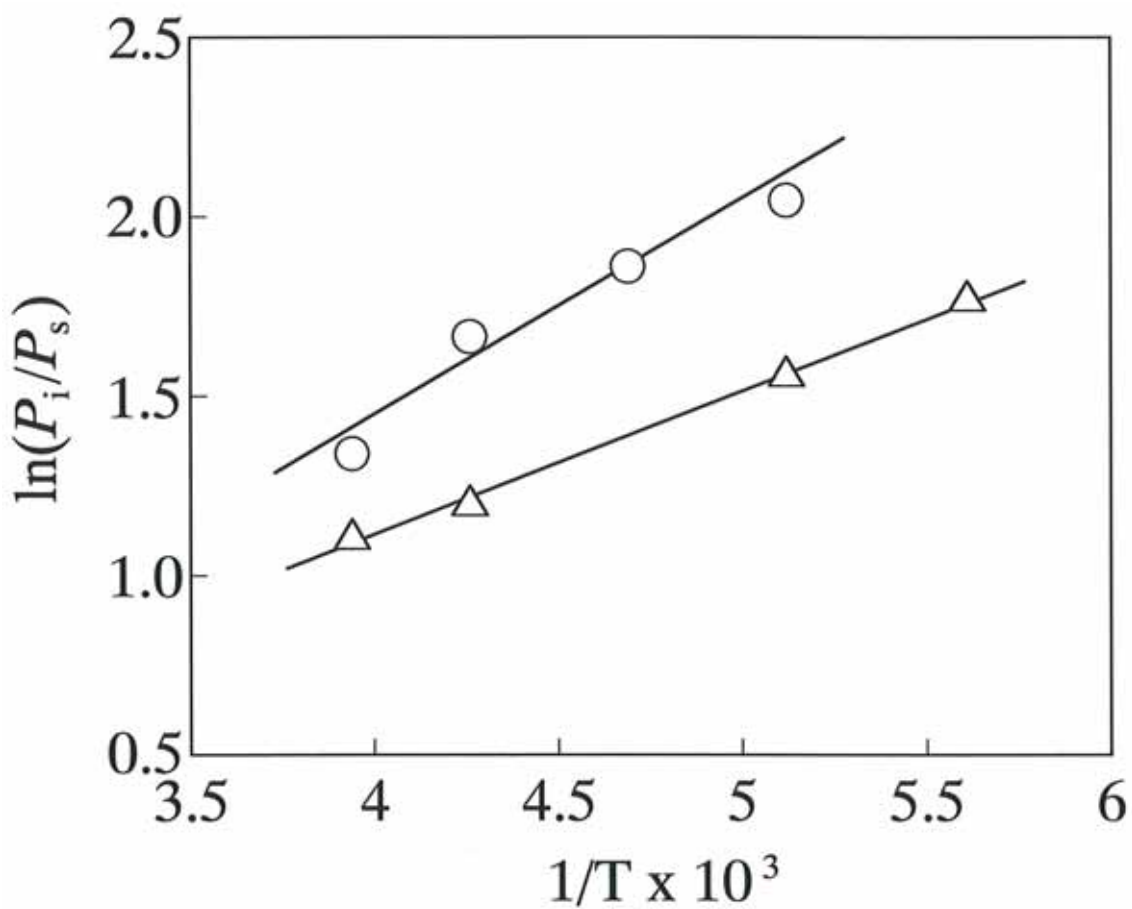
Figure 2-4. Temperature dependencies on the stereoregularity of isotactic PVAs derived from poly*t*BVE prepared with $BF_3 \cdot OEt_2$ in toluene. Catalyst concentrations were 0.25 mmol/l (circle), and 2.5 mmol/l (tringle).

Table 2-5. Activation parameters in isotactic and syndiotactic propagation of isotactic PVAs.

Concentration of catalyst	$\Delta H_i^{\neq} - \Delta H_s^{\neq}$ (cal/mol)	$\Delta S_i^{\neq} - \Delta S_s^{\neq}$ (cal/deg·mol)
Low (0.25mM)	-1140	-1.70
High (2.50mM)	-770	-0.85

The reaction described in eq 4 will be dominant in the polymerization reaction when the ratio of the catalyst to residual water in the reaction mixture is low. We consider that the increase in isotacticity may be caused by highly isospecific polymerization with a new species generated from the ligand exchange of catalyst from ether to water as shown in eq 3.

2.3.5. Effect of water on the polymerization

Then, we examined the polymerization in the presence of various amounts of water in order to investigate the effect of water on the polymerization. The results are shown in Table 2-6 and Figure 2-5. The f_{mm} sequence fraction increased sharply only when the water/catalyst ratio reduced considerably to become as low as around 10^{-1} in the concentration range of $BF_3 \cdot OEt_2$ between 0.25 to 5.00 mol/l. However, for water contents equal to the value given by as run 8 in Table 2-6, polymerization barely occurred because water acts as a strong inhibitor or chain transfer agent. This result supports our assumption that the reaction described in eq 4 is dominant in the presence of an equimolar or more amount of water as compared to a catalyst even in the case of high catalyst concentration, which would cause a higher isospecific propagation by a new active species generated from ligand exchange reaction according to eq 3.

2.3.6. Effect of the ligand of BF_3 complexes on the polymerization

As mentioned above, the f_{mm} increased when the catalyst concentration

Table 2-6. Characterization of isotactic PVAs derived from poly$t$BVE prepared with BF$_3$·OEt$_2$ in the presence of various amount of water in toluene at $-78\ ^{\circ}$C.

| No.	[BF$_3$·OEt$_2$] (mM)	[H$_2$O] (mM)	Time (hr)	Conv. (%)	Poly$t$BVE M_n	M_w	M_w/M_n	PVA triad mm	mr	rr
1	5.00	1.00	3	94.6	94500	307000	3.25	0.68	0.27	0.05
2	2.50	1.12	4	76.6	33930	72240	2.13	0.67	0.27	0.06
3	1.25	0.96	2	71.5	116900	258300	2.21	0.66	0.28	0.06
4	1.25	9.38	5	60.6	27300	47300	1.73	0.74	0.22	0.04
5	1.25	22.1	12	70.6	24400	40700	1.67	0.75	0.21	0.04
6	0.25	0.96	3	71.2	115600	291500	2.52	0.78	0.19	0.03
7	0.25	9.38	16	60.0	23300	39600	1.70	0.79	0.19	0.02
8	0.25	22.1	36	0						
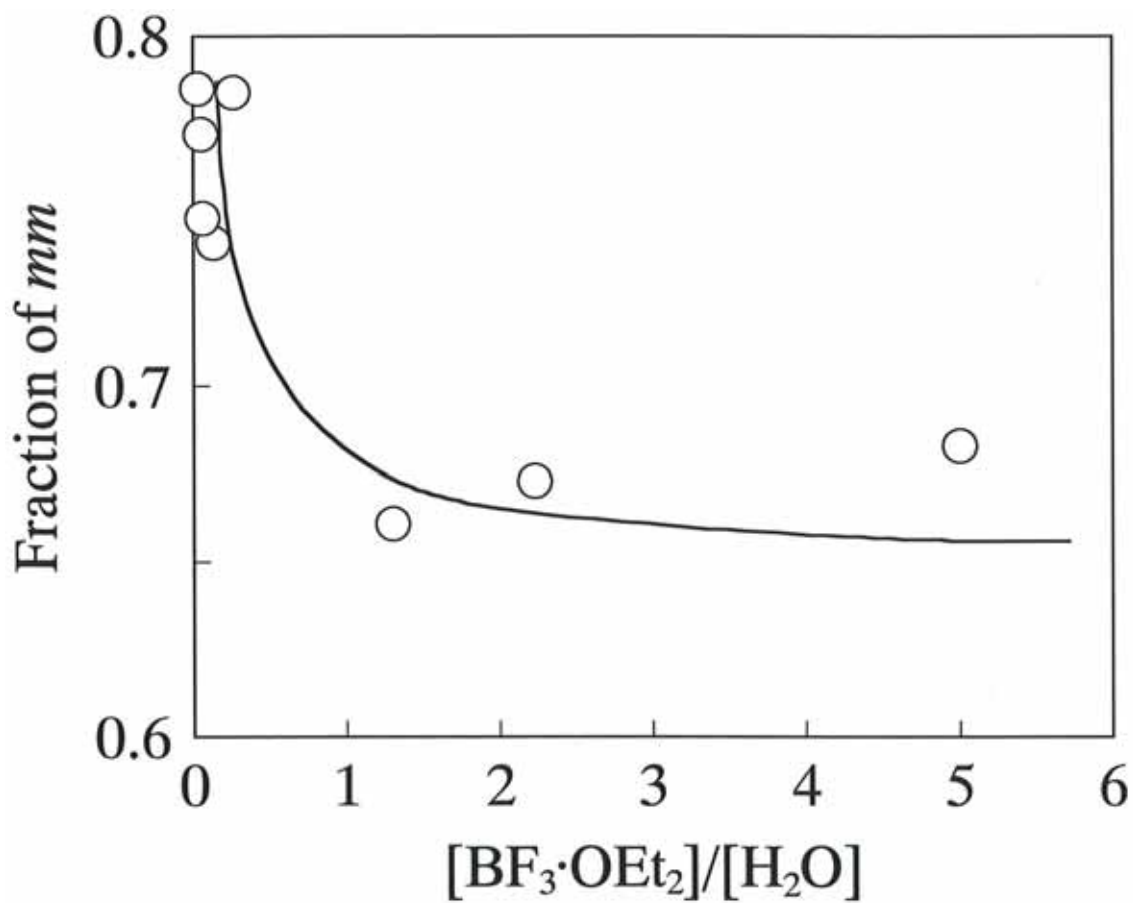
Figure 2-5. Effect of water on the *mm* sequence fraction of PVAs derived from poly*t*BVE prepared with $BF_3 \cdot OEt_2$ in toluene at -78 ^{o}C.
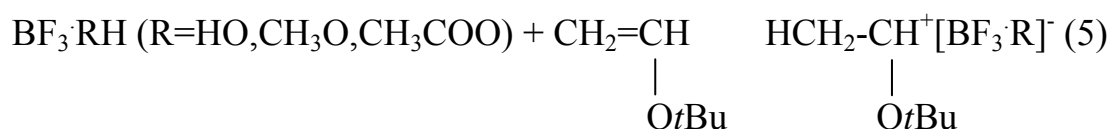
was reduced (Figure 2-2), which is thought to be caused by highly isospecific polymerization with a new kind of species generated by ligand exchange from ether to water. These results suggest that the ligand of BF_3 complexes play an important role in this stereospecific polymerization. Then we studied the polymerization of tBVE with various BF_3 complexes at -78 ^{o}C in toluene. The results are shown in Table 2-7 and Figure 2-6.

In the case of $BF_3 \cdot 2H_2O$, especially at high catalyst concentrations, the polymerization system became heterogeneous by the precipitation of the resulted polymer because of the low solubility of $BF_3 \cdot 2H_2O$ in toluene, and the molecular weight of poly$t$BVE increased with increasing catalyst concentration. The polymerization with $BF_3 \cdot 2CH_3OH$ proceeded homogeneously despite the low solubility of $BF_3 \cdot 2CH_3OH$ in toluene and no precipitation was observed. The molecular weight of poly$t$BVE increased with increasing catalyst concentration, although it decreased at a high concentration because a small amount of free CH_3OH appears to act as a chain transfer agent during polymerization. The polymerization with $BF_3 \cdot 2CH_3COOH$ proceeded very fast and yielded poly$t$BVE with a relatively wide distribution of molecular weight. The *mm* sequence fraction increased in the following order: $BF_3 \cdot 2CH_3COOH < BF_3 \cdot OEt_2 < BF_3 \cdot 2CH_3OH < BF_3 \cdot 2H_2O$, and increased with reducing concentration for each type of catalyst.

Some models and mechanisms of isospecific propagation in homogeneous systems have been proposed for mainly vinyl ethers. Kunitake et al. proposed that the important factors in controlling the

34

stereochemistry of chain growth in alkyl vinyl ether polymerization are the degree of association of a growing cation and its counter anion, and the physical size of the counter anion.[20,21] Steric repulsion of the bulky substituents of terminal and penultimate monomer units could be minimized, and assuming a planar carbocation, a monomer attack on the same side of the counter anion (front side attack) or on the opposite side (backside attack) leads to mainly syndiotactic placement or isotactic placement, respectively. Non-polar solvents such as toluene would be expected to favor a tight association between the propagating cation and its counter anion so that they favor back-side attack with the formation of an isotactic configuration that minimized the steric repulsion between the bulky substituent in monomers and growing polymer chains. Polar solvents such as CH_2Cl_2 favor an inversely front side attack with the formation of syndiotactic configuration because they can stabilize separated ion pairs. These suggest that the tighter association of the growing ion pair will yield higher isotacticity at the isospecific polymerization. Kunitake et al. carried out isospecific polymerization of *t*BVE at $-78\ ^{\circ}C$ with various triphenylmethyl salts as the initiator, and they observed that the *mm* sequence fraction increased with decreasing counter anion size.[20] Since there may be steric hindrances between the bulky *tret*-butyl group and the counter anion, the binding strength between the growing ion pairs will increase with decreasing counter anion size, which will only lead to more back-side attack, that is, a more isotactic-rich polymer.

The initiation reaction of the cationic polymerization of vinyl ether with BF_3 complex is thought to be as follows: a direct reaction between the monomer and the catalyst for $BF_3 \cdot OEt_2$, and a proton addition for the BF_3 complex whose ligand has acidic proton; the interaction between the excess ligand and growing carbeniumion can be neglected in this case because aromatic group of toluene would interact with the chain end preferably,[15] as shown in eqs 2 (R = tBu) and 5.

$$BF_3 \cdot RH \ (R=HO,CH_3O,CH_3COO) + CH_2=CH \qquad HCH_2-CH^+[BF_3 \cdot R]^- \ (5)$$
$$\qquad\qquad\qquad\qquad\qquad\qquad\qquad\quad | \qquad\qquad\qquad\quad |$$
$$\qquad\qquad\qquad\qquad\qquad\qquad\qquad\quad OtBu \qquad\qquad\quad OtBu$$

The counter anions of BF_3 complexes during the polymerization are thus believed to be $[BF_3 \cdot CH_3COO]^-$, $[BF_3 \cdot OEt]^-$, $[BF_3 \cdot OCH_3]^-$, and $[BF_3 \cdot OH]^-$ for $BF_3 \cdot 2CH_3COOH$, $BF_3 \cdot OEt_2$, $BF_3 \cdot 2CH_3OH$, and $BF_3 \cdot 2H_2O$, respectively. The fact that the size of the BF_3 complexes as the counter anion during polymerization reduces in the following order: $BF_3 \cdot 2CH_3COOH$ < $BF_3 \cdot OEt_2$ < $BF_3 \cdot 2CH_3OH$ < $BF_3 \cdot 2H_2O$ coincides with the content of the *mm* sequence fraction of the resultant poly$t$BVEs.

The f_{mm} increased sharply with decreasing catalyst concentration for each type of catalyst except for $BF_3 \cdot 2H_2O$, as shown in Figure 2-6. This is because the ligand exchange reaction from the original ligand to water according to eqs 6 and 4 (R = tBu) become dominant with increasing concentration ratio of residual water - a small amount but not zero - to the

Table 2-7. Characterization of isotactic PVAs derived from poly$t$BVE prepared with various BF_3 complexes in toluene at - 78 $^{\circ}$C.

| No.	Catalyst	[cat.] (mM)	Time (hr)	Conv. (%)	Poly$t$BVE			PVA		
					M_n	M_w	M_w/M_n	triad		
								mm	*mr*	*rr*
1	BF$_3$·2H$_2$O	10.0	3.5	82.2	81300	170500	2.10	0.73	0.24	0.03
2	BF$_3$·2H$_2$O	5.00	3.5	62.2	55100	105400	1.91	0.75	0.22	0.03
3	BF$_3$·2H$_2$O	2.50	16	67.5	53600	95600	1.78	0.76	0.21	0.03
4	BF$_3$·2CH$_3$OH	10.0	2.5	57.2	23500	53950	2.30	0.67	0.28	0.05
5	BF$_3$·2CH$_3$OH	5.00	2.5	80.6	68670	157600	2.30	0.70	0.27	0.03
6	BF$_3$·2CH$_3$OH	1.25	2.5	76.6	41000	77900	1.90	0.75	0.23	0.02
7	BF$_3$·2CH$_3$COOH	5.00	3	77.8	24300	74100	3.05	0.59	0.34	0.07
8	BF$_3$·2CH$_3$COOH	1.25	3	76.3	61130	275100	4.50	0.62	0.32	0.05
9	BF$_3$·2CH$_3$COOH	0.25	3	72.8	53000	368000	6.94	0.70	0.26	0.04
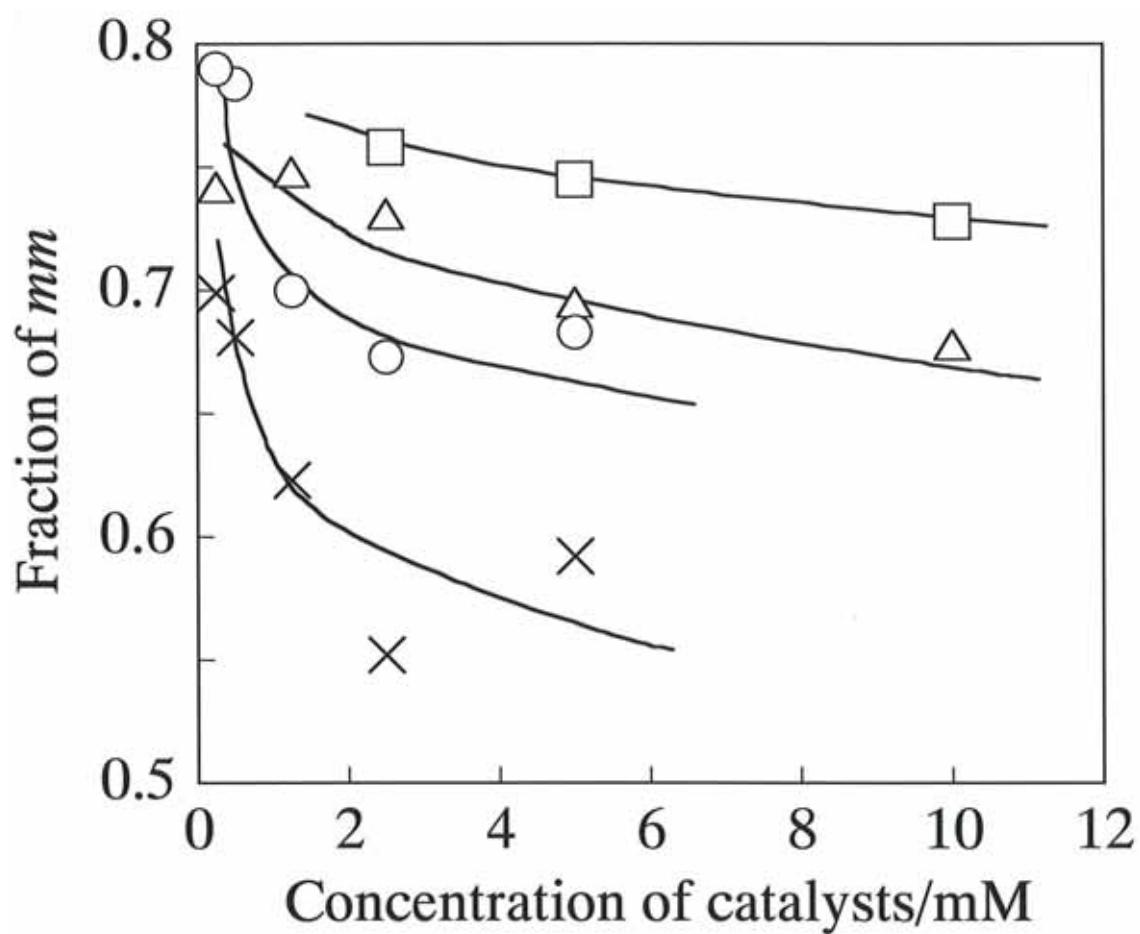
Figure 2-6. Effect of catalyst concentration on the *mm* sequence fraction of PVAs derived from poly*t*BVE prepared with $BF_3 \cdot OEt_2$ (circle), $BF_3 \cdot 2H_2O$ (square), $BF_3 \cdot 2CH_3OH$ (triangle), and $BF_3 \cdot 2CH_3COOH$ (cross) in toluene at -78 ^{o}C.

catalyst. In other words, the counter anion of the growing cation would be almost $[BF_3 \cdot OH]^-$ at a low catalyst concentration irrespective of the BF_3 complexes.

$$BF_3 \cdot X \ (X=CH_3OH, Et_2O, CH_3COOH) + H_2O \quad BF_3 \cdot OH_2 \ + \ X \quad (6)$$
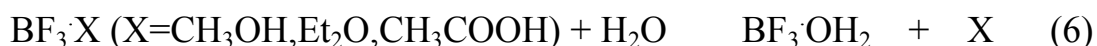
2.4. Conclusions

The preparation and characterization of the HI-PVAs derived from poly*t*BVE polymerized with $BF_3 \cdot OEt_2$ were reported. The f_{mm} increased with decreasing $BF_3 \cdot OEt_2$ concentration, and it reached 0.78–0.79, which seems to be the highest value of all isotactic PVAs reported so far. Such high isotacticity was obtained when the catalyst concentration was reduced to below 0.5×10^{-3} mole/l. An increase in f_{mm} may be caused by highly isospecific propagation of a new kind of species, which is thought to be generated from the ligand exchange of BF_3 complex from ether to water.

We also reported the polymerization of *t*BVE with various BF_3 complexes such as $BF_3 \cdot 2CH_3COOH$, $BF_3 \cdot 2CH_3OH$ or $BF_3 \cdot 2H_2O$. The f_{mm} increased in the following order: $BF_3 \cdot 2CH_3COOH$ < $BF_3 \cdot OEt_2$ < $BF_3 \cdot 2CH_3OH$ < $BF_3 \cdot 2H_2O$ and it increased when the catalyst concentration for each type of catalyst was reduced.

References

(1) Fujii, K. *J. Polym. Sci., Part D* **1971**, 5, 431.

(2) (a) Finch, C. A. In *Polyvinyl Alcohol*; John Wiley & Sons: New York, **1973**; Chapter 6 and 10. (b) Finch, C. A. In *Polyvinyl Alcohol-Developments*; John Wiley & Sons: New York, **1992**; Chapter 9 and 10.

(3) (a) Yamamoto, T.; Yoda, S.; Sangen, O.; Fukae, R.; Kamachi, M. *Polym. J.   (Japan)* **1989**, 21, 1053. (b) Yamamoto, T.; Yoda, S.; Sangen, O.; Fukae, R.; Kamachi, M. *Polym. J. (Japan)* **1990**, 22, 636.

(4) Ofstead, R. F.; Poser, C. I. *Polym. Mater. Sci. Eng*. **1987**, 57, 361.

(5) (a) Imai, K.;Shiomi, T.;Tezuka, Y.;Kawanishi, T.;Jin, T. *J.Polym.Sci.,Part A* **1988**, 26, 1961. (b) Imai, K.;Shiomi, T.;Tezuka, Y.;Fujioka N.;Hosokawa, T.;Ueda, N.;Fujita, K. *Kobunshi Kagaku* **1989**, 46, 261.

(6) Murahasi, S.; Yuki, H.; Sano, T., Yonemura, U.; Tadokoro, T.; Chatani, Y. *J. Polym. Sci.* **1962**, 62, S77.

(7) Yuki, H.; Hatada, K.; Oda, K.; Kinoshita, Murahashi, S.; Ono, K.; Ito, Y. *J. Polym. Sci.* **1969**, Part A-1, 7, 1517.

(8) (a) Okamura, S.; Kodama, T.; Higashimura, T. *Makromol. Chem.* **1962**, 53, 180. (b) Higashimura, T.; Suzuki, K.; Okamura, S. *Makromol. Chem.* **1965**, 86, 259.

(9) (a) Murahashi, S.; Nozakura, S.; Sumi, M. *J. Polym. Sci.* **1965**, B, 3, 245.

(b) Murahashi, S.; Nozakura, S.; Sumi, M.; Yuki, H.; Hatada, K. *J. Polym. Sci., Polym. Lett. Ed*. **1966**, 4, 65. (c) Murahashi, S.; Nozakura, S.; Sumi, M.; Yuki, H.; Hatada, K. *Kobunshi Kagaku* **1966**,

23, 550.

(10) Wu, T. K.; Ovenall, D. W. *Macromolecules* **1973**, 6, 582.

(11) Ohgi, H.; Sato, T. *Macromolecules* **1993**, 26, 559.

(12) Moritani, T.; Kuruma, I.; Shibatani, K. *Macromolecules* **1972**, 5, 577.

(13) DeMember, J. R.; Haas, H. C.; MacDonald, R. L. *J. Polym. Sci., Polym. Lett. Ed.* **1972**, 10, 385.

(14) Fujii, K.; Fujiwara Y.; Brownstein, S. *Preprints 17th Polymer Symp.(Matsuyama, Japan)* **1968**, 1111.

(15) Kennedy, J.P.; Marechal, E. In *Carbocationic Polymerization*; John Wiley & Sons: New York, **1982**; Chapter 4.3, p209.

(16) Nozakura, S.; Sumi, M.; Uoi, M.; Okamoto, T.; Murahashi, S. *J. Polym. Sci.: Polym. Chem. Ed*. **1973**, 11, 279.

(17) Fordham, J. W. L. *J. Polym. Sci.* **1959**, 39, 321.

(18) Sumi, M.; Nozakura, S.; Murahashi, S. *Kobunshi Kagaku* **1967**, 24, 424.

(19) Plesch, P. H. In *The Chemistry of Cationic Polymerization*; Pergamon: Press: New York, **1963**; p392.

(20) Kunitake, T.; Aso, C. *J. Polym. Sci., Part A*, **1970**, 8, 665.

(21) Kunitake, T.; Takarabe, K. *Makromol Chem*. **1981**, 182, 817.

Chapter 3

Heterogeneous Cationic Polymerization of *tert*-Butyl Vinyl Ether

3.1. Introduction

There are many reports on the stereoregular polymerization of BzVE[1,2] or *t*BVE,[3] that is, the precursors of the stereoregular PVA, with a homogeneous cationic catalyst, whereas the heterogeneous polymerization of these vinyl ethers has not been studied well. Vandenberg reported that certain modified Ziegler-type catalysts (the so-called Vandenberg type catalysts) such as VCl_4-Et_3Al mixture or $TiCl_4$-Et_3Al mixture treated with an iBu_3Al-THF complex polymerize some alkyl vinyl ethers such as methyl, ethyl, isobutyl, and *tert*-butyl vinyl ether to yield crystalline polymers.[4] It is noteworthy that the vanadium based initiator led to a highly crystalline poly *t*BVE at room temperature. He proposed that the stereoregular polymerization of vinyl ethers with these catalysts occurs by a cationic insertion mechanism, and the factor that controls the steric structure of the poly(vinyl ether)s is different from that of an ordinal catalyst system such as $BF_3 \cdot OEt_2$. However, the polymerization results and stereoregularity of the obtained poly*t*BVE were not quantitatively discussed.

On the other hand, Higashimura et al. and McGrath et al. found that a series of metal sulfate-sulfuric acid complexes such as $Al_2(SO_4)_3$-H_2SO_4 or $MgSO_4$-H_2SO_4 efficiently polymerizes vinyl ethers at room temperature to

yield crystalline isotactic polymers.[5-7]   They reported that the Al$_2$(SO$_4$)$_3$-H$_2$SO$_4$ catalyst yielded stereoregular poly(methyl vinyl ether) or poly(isobutyl vinyl ether) with higher crystallinity at room temperature than those obtained in the homogeneous polymerization with BF$_3$·OEt$_2$ at low temperatures.   Higashimura et al. determined the stereoregularity of the obtained poly(methyl vinyl ether) with metal sulfate-sulfuric acid complexes by NMR spectroscopy and found that the fraction of the triad tacticity calculated from the enantiomorphic catalyst site model coincided with the experimental results.[8]   This means that only the heterogeneous catalyst, or the structure of the catalyst surface, should dominate the stereoregularity of an added monomer in this catalyst and this case is entirely different from that of homogeneous BF$_3$ complex catalysts. However, there have been no reports on the polymerization of *t*BVE or BzVE with these metal sulfate-sulfuric acid complex catalysts.

In Chapter 2, we showed that most of the highly isotactic PVAs reported so far were derived from poly*t*BVE prepared by homogeneous cationic polymerization with BF$_3$·OEt$_2$ catalyst.[9,10]   We also studied the polymerization of *t*BVE with various BF$_3$ complexes and proposed that the counter anion of the growing chain plays important roles in controlling the stereoregularity of the poly*t*BVE with homogeneous BF$_3$ complexes catalyst.[10]   The heterogeneous polymerization of *t*BVE is of considerable interest in both methods in order to obtain the stereoregular PVAs as well as for theoretical consideration.   In this chapter, we describe the heterogeneous cationic polymerization of *t*BVE and BzVE with

43

Vandenberg type catalysts or metal sulfate-sulfuric acid complexes. We also determine the stereoregularity of the resultant PVAs derived from these poly(vinyl ether)s and discuss a mechanism for the isospecific heterogeneous polymerization on the basis of a statistical analysis of the tacticity data.

3.2. Experimental Section

3.2.1 Reagents

Synthesis of tBVE monomer was carried out according to the ways described in Chapter 2. BzVE monomer was prepared by alkyl exchange reaction between benzyl alcohol and ethyl vinyl ether in the presence of Hg(OAc)$_2$. BzVE, tBVE, and iso-butyl vinyl ether (iBVE) (Tokyo Kasei Kogyo; 99%) were washed with 10% aqueous sodium hydroxide and then with water, dried overnight over potassium hydroxide (pellets), and distilled from calcium hydride before use. All solvents and BF$_3$·OEt$_2$ were purified by the same ways described in Chapter 2.

Modified Ziegler type (Vandenberg type) catalysts were prepared by the procedure described by Vandenberg.[4] The stoichiometric titanium (ST) catalyst (mole ratio of 0.34:1 Et$_3$Al:TiCl$_4$) was prepared under nitrogen in n-heptane diluent at 0.12 M concentration of TiCl$_4$ by addition of the Et$_3$Al. This catalyst was aged 2 hr at room temperature, and then heat treated for 16 hr in a 90 $^{\circ}$C bath. This catalyst was the starting material for the pretreated stoichiometric titanium (PST) catalyst. The vanadium counterpart of ST catalyst that is the SV catalyst (0.36:1 Et$_3$Al:VCl$_4$) was

prepared in the same way except of using VCl_3 as vanadium compound instead of $TiCl_4$. The PST catalyst was prepared by reacting ST catalyst with *iso*-Bu_3Al (1M in *n*-heptane) at a mole ratio of 2:1 *iso*-Bu_3Al:Ti (0.1M titanium concentration) for 5 min. at room temperature. The PSV catalyst was prepared in a similar manner in *n*-heptane. All catalysts were handled under a moisture- and oxygen-free argon atmosphere, and dissolved in dry and distilled *n*-heptane under dry argon before use.

Metal sulfate-sulfuric acid complexes were prepared by the procedure described by Higashimura et al.[5] $Al_2(SO_4)_3 \cdot H_2SO_4$ was prepared by following method. A 12 g portion of finely powdered $Al_2(SO_4)_3$-$18H_2O$ and 60 ml of concentrated sulfuric acid were placed in a 100 ml flask. The mixture was stirred with a magnetic stirrer and maintained at 5 ^{o}C for 24 hr and then maintained at 100 ^{o}C for 1.5 hr. After cooling, it was added to 500 ml of stirred anhydrous diethyl ether. The white precipitate was filtered, washed with additional anhydrous ether and dried under vacuum. $Cr_2(SO_4) \cdot H_2SO_4$, $MgSO_4 \cdot H_2SO_4$, $FeSO_4 \cdot H_2SO_4$ and $Fe_2(SO_4)_3 \cdot H_2SO_4$ were prepared by same method. The composition of the catalysts determined by the atomic absorption (metal composition) and ion chromatographic (SO_4^{2-}) methods corresponding to $Al_2(SO_4)_3 \cdot 1.4H_2SO_4 \cdot 10.4H_2O$, $MgSO_4 \cdot 0.67H_2SO_4 \cdot 4.0H_2O$ and $FeSO_4 \cdot 0.38H_2SO_4 \cdot 3.3H_2O$, respectively. All catalysts were handled under a moisture- and oxygen-free argon atmosphere, and dissolved in dry and distilled toluene under dry argon before use.

3.2.2. Polymerization

The polymerization of *t*BVE, BzVE or *i*BVE were carried out with Vandenberg type catalysts in *n*-heptane or metal sulfate-sulfuric acid complexes in toluene.   An ampoule equipped with a three-way stopcock was flushed with dry nitrogen, and then the solvent and the catalyst solution were introduced with a syringe.   To this catalyst solution kept at a given temperature the monomer solution was added slowly with a syringe and the ampoule was sealed immediately.   Adding a small amount of methanol that was kept to the same temperature as the reaction mixture terminated the polymerization.   The mixture was then poured into a large amount of methanol, and the precipitated polymer was washed with methanol and dried under vacuum.

3.2.3. Preparation and characterizations of stereoregular PVAs

The stereoregular PVAs were obtained from poly*t*BVE by using same procedure described in Chapter 2.   The number-average molecular weight (M_n), the weight-average molecular weight (M_w), and the triad tacticity of obtained PVAs were also determined by the same ways described in Chapter 2. Figure 3-1 illustrates the ^{1}H NMR spectra of several stereoregular PVAs derived from poly*t*BVEs catalyzed by Vandenberg type catalysts.
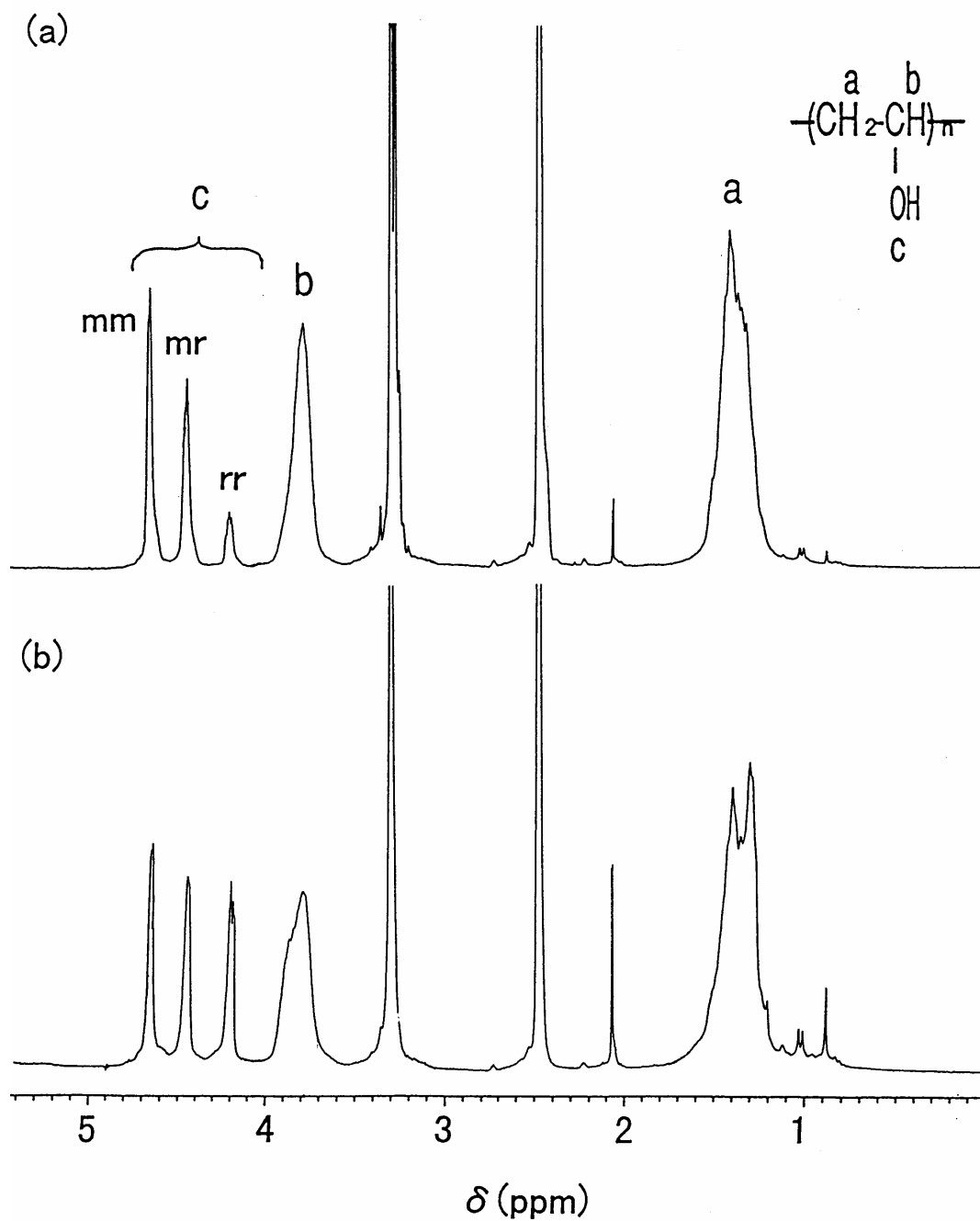
Figure 3-1. ^{1}H NMR spectra of stereoregular PVAs in DMSO-d_6, at 25 °C and 270 MHz: (a) PVA obtained from the poly$t$BVE polymerized with PST catalyst (run 2 in Table 3-1); (b) PVA obtained from the poly$t$BVE polymerized with PSV catalyst (run 4 in Table 3-1). *mm*, *mr*, and *rr* are assigned to *meso-meso*, *meso-racemo*, and *racemo-racemo* sequence fraction, respectively.

47

3.3. Results and Discussion

3.3.1. Polymerization of tBVE with Vandenberg type catalyst

In his report, Vandenberg concluded that the PSV (pretreated stoichiometric vanadium) catalyst that gave the most stereoregular polymerization was the Ziegler type transition metal catalyst.[4]   However, he had not studied the polymerization of vinyl ethers with titanium based catalysts.

Now, the polymerization of tBVE was carried out with several Vandenberg type catalysts, i.e., vanadium based catalysts and titanium based ones, at 30 ^{o}C in n-heptane.   The polymerization results are summarized in Table 3-1.   For comparison, we also studied the polymerization of tBVE with $BF_3 \cdot OEt_2$ in n-heptane.   The ST (stoichiometric titanium) catalyst had a red purple dispersion and the PST (pretreated stoichiometric titanium) catalyst had a dark brown dispersion in n-heptane.   The polymerization of tBVE with titanium based catalysts was found to be slow, and the polymer yield was in the range of 30 - 55% polymerized for 39 hr.   While the rate of the homogeneous polymerization of tBVE with $BF_3 \cdot OEt_2$ was very fast at –78 ^{o}C, only few amounts of the polymer were obtained at 0 ^{o}C.   During the polymerization, the reaction mixture become highly colored, and $BF_3 \cdot OEt_2$ yielded poly$t$BVE with a very low molecular weight at 0 ^{o}C; our results seem to agree with those of Aoshima and Higashimura.[12]   It was very difficult to recover the obtained oligomers by using the precipitation method because of their high solubility in methanol.   Since the titanium based catalysts are insoluble in the

Table 3-1. Characterization of PVAs derived from poly*t*BVEs prepared with several modified Ziegler-type catalysts in *n*-heptane. [*t*BVE]=20vol%.

No.	catalyst	[cat.] (mM)	Temp. (°C)	Time (hr)	Polymer yield (%)	Poly*t*BVE M_n	M_w	M_w/M_n	PVA triad mm	mr	rr
1	PST	0.47	30	39	1.4	13300	25100	1.89	-	-	-
2	PST	1.28	30	39	25.6	12200	23400	1.92	0.52	0.38	0.10
3	ST	0.47	30	39	54.7	14700	41400	2.82	0.51	0.39	0.10
4	PSV	0.47	30	50	25.2	4000	7100	1.78	0.34	0.34	0.32
5	SV	0.47	30	50	22.6	3800	6400	1.68	0.36	0.33	0.32
6[a]	SV	0.47	30	50	32.2	8400	4800	1.75	0.37	0.33	0.30
7	VCl$_3$	0.47	30	50	30.0	3700	6900	1.86	0.32	0.37	0.31
8	BF$_3$·OEt$_2$	0.5	0	50	0	-	-	-	-	-	-
9	BF$_3$·OEt$_2$	0.5	-78	3	91.3	18700	64200	3.42	0.54	0.34	0.12

a [*t*BVE]=50vol%

polymerization medium, such extremely slow polymerization may be caused by some steric factor of the solid catalyst surface.

The polymerization system became heterogeneous because of the low solubility of catalyst; however, the molecular weight distribution (*MWD*) of the polymers obtained from *t*BVE by titanium based catalysts were relatively narrow, and the GPC elution curve of the polymer obtained with the titanium based catalysts showed a monomodal *MWD*.   Higashimura et al. found that a bimodal *MWD* of polystyrenes is formed under suitable conditions, e.g., by the use of acetyl perchlorate or perchloric acid in several solvents at 0 $^{\circ}$C.[13]   They studied the nature of propagating species in the cationic polymerization of styrene under various conditions and suggested that the shape of *MWD* was influenced by the character of the propagating species, such as the fractional contribution of the dissociated and non-dissociated propagating species to polymer formation.   Further, all the poly*t*BVEs polymerized with titanium based catalysts were isolated as nontacky, semicrystalline powdery solids.   On the basis of these results, it may be suggested that the polymerization of *t*BVE proceed with a uniform active center.   However, in cationic polymerization, it is known that the monomodal *MWD* of the polymer is not always proof of a uniform active center because a propagating species can exchange with each other very quickly even if more than two propagating species exist.   More studies on the propagating species during the polymerization of *t*BVE with titanium based catalysts are required to obtain more detailed information.

It is also noticeable that polymers with high molecular weights can be

obtained from tBVE at high temperatures.　As reported in Chapter 2, we examined the effect of temperature on the polymerization of tBVE with $BF_3 \cdot OEt_2$, and a marked decrease in the molecular weight of the polymer was observed at higher reaction temperatures (Figure 3-2).[10]　In contrast, especially with PST catalysts, poly$t$BVEs with high molecular weights were obtained, and the molecular weight of the polymer remained almost constant despite the catalyst concentration.　It is well known that the stability of the propagating species in cationic polymerization suppresses chain transfer, termination, and other side reactions.　The high molecular weight of the poly$t$BVE obtained by the titanium based catalyst may be a result of bulky and sterically hindered counteranions, which may interact with and stabilize the growing carbocation.　Our results and considerations seem to be similar to those in the study reported by Higashimura et al. on iBVE polymerization with metal sulfate-sulfuric acid complexes at room temperature.[14]

The poly$t$BVEs catalyzed by the titanium based catalysts were converted into stereoregular PVAs by hydrolysis with hydrogen bromide.　As shown in Figure 3-1, the hydroxyl proton absorption splits into three separate peaks resulting from the triad tacticity in ^{1}H NMR spectrum of the PVAs obtained from the poly$t$BVEs catalyzed by the titanium based catalysts. The stereoregularities of the PVAs are also summarized in Table 3-1.　It is well known that the fraction of mm sequence (f_{mm}) of the poly vinyl ethers with BF_3 complexes increased with decreasing polymerization temperature.[2,10]　However, the resultant PVAs derived from the poly$t$BVEs

catalyzed by titanium based catalyst yielded a relatively high f_{mm} at high temperatures. The f_{mm} of the PVA obtained from the poly$t$BVE with PST catalyst is 0.52, which is similar to that of the poly$t$BVE prepared with $BF_3 \cdot OEt_2$ in heptane at -78 ^{o}C. We assumed that these unusually high stereospecific polymerization can be attributed to the isospecific species that differs from that an ordinary BF_3 complexes catalyst. To elucidate the reaction mechanism in more detail, the factor that controls the steric structure of an adding monomer was studied by a statistical analysis, as described later.

The vanadium based Vandenberg type catalyst did not work as well as titanium based one with tBVE. The polymerization of tBVE yielded poly$t$BVE of lower molecular weight when catalyzed by vanadium based catalysts than when catalyzed by titanium based ones.

The f_{mm} of the PVAs obtained from the poly$t$BVEs with vanadium based catalysts ranges from 0.32 - 0.37, and the addition of a monomer had little effect on the stereoregularity of the polymer (run 6 in Table 3-1). It is worth noting that the heterotactic PVAs were obtained from the polymerization of tBVE with vanadium based catalysts. These results suggest that the structure of the counter ion, which influences not only the chain transfer reaction but also the stereospecificity of the polymerization, of the system in the case of titanium and vanadium were different.

3.3.2. Polymerization of BzVE with Vandenberg type catalyst

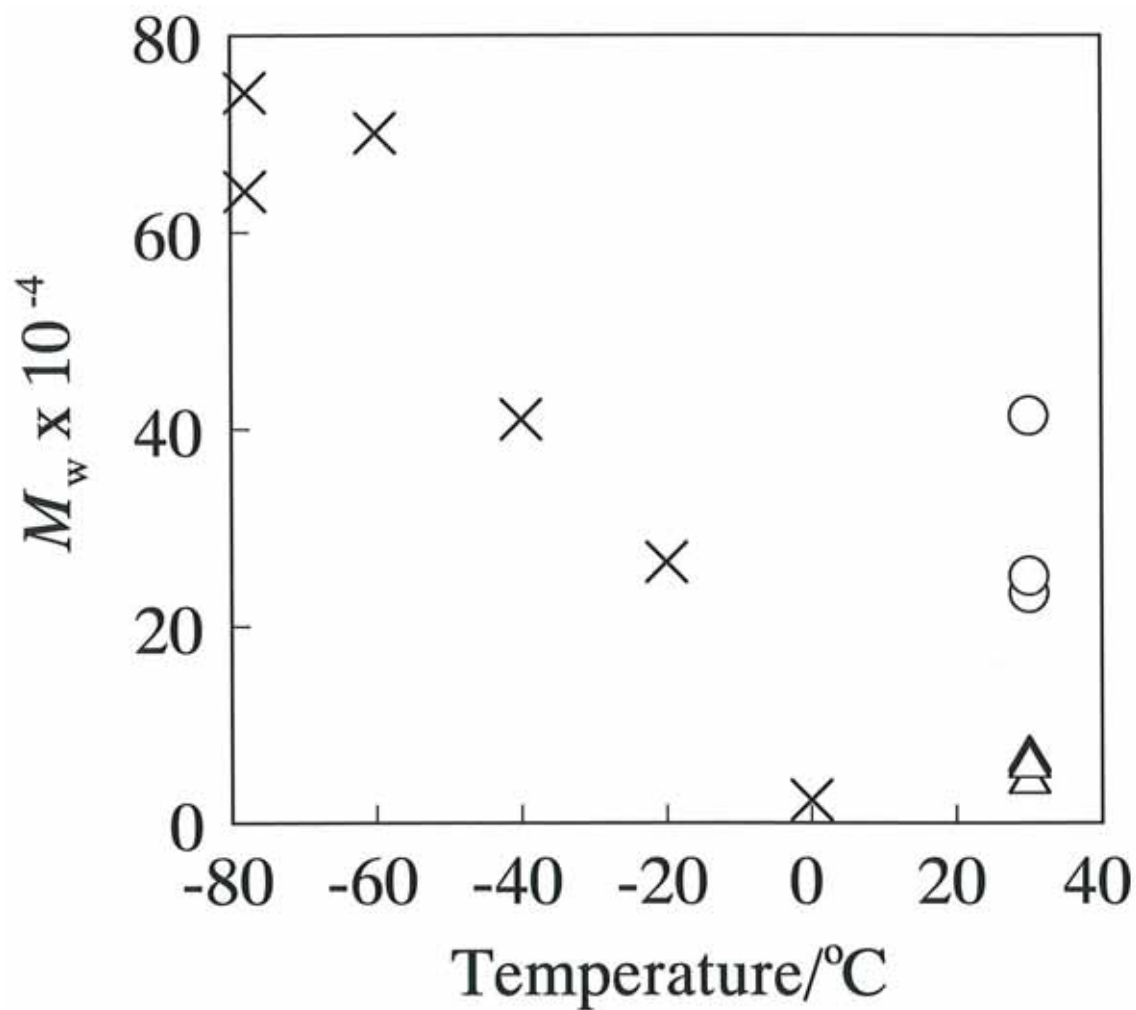Next, we studied the polymerization of BzVE, which is also known as a

Figure 3-2. Effect of polymerization temperature on the weight average of molecular weight (M_w) of poly$t$BVE polymerized with titanium based catalysts (circle), vanadium based catalysts (triangle) or $BF_3 \cdot OEt_2$ (cross) in n-heptane.

starting monomer of isotactic PVA,[2,15] with the titanium or the vanadium based Vandenberg type catalysts; however, only few amounts of the polymer were obtained (Table 3-2). The titanium based catalysts are slightly active in comparison with the corresponding vanadium based catalysts. Interestingly the molecular weight distribution of polyBzVE obtained with the titanium based catalysts was somewhat broader than that of poly*t*BVE with the same catalysts. This result suggests that both chain transfer reactions and different initiating and/or propagating species are present in the system. We assume that the system of BzVE polymerization with the Vandenberg type catalyst is more complex than that of *t*BVE and the interaction between the phenyl substituent of BzVE and that the active site bound to a solid surface may influence the polymerization activity of the complete process.

We also tried to convert the polyBzVE that polymerized with the Vandenberg type catalysts into PVA by using several methods such as by using HBr, HCl, or trifluoroacetic acid. However, the obtained PVAs show gelation and brown color, which may be caused by small amounts of the residual catalyst, and we were inable to estimate the accurate tacticity of the polymer.

3.3.3. Polymerization of *t*BVE with metal sulfate-sulfuric acid complexes

The polymerization of *t*BVE has been investigated in the presence of other heterogeneous catalysts based on metal sulfate-sulfuric acid

Table 3-2. Characterization of polyBzVE prepared with several modified Ziegler-type catalysts in *n*-heptane. [BzVE]=20 vol%.

No.	Catalyst	[cat.] (mM)	Temp. (°C)	Time (hr)	Polymer yield (%)	PolyBzVE M_n	M_w	M_w/M_n	PVA triad *mm*	*mr*	*rr*
1	PST	0.47	30	39	1.7	12800	47000	3.67	-	-	-
2	PST	1.28	30	39	5.5	9800	31300	3.19	-	-	-
3	ST	0.47	30	39	7.0	10000	32400	3.24	-	-	-
4	PSV	0.47	30	50	-	-	-	-	-	-	-
5	SV	0.47	30	50	-	-	-	-	-	-	-
6	VCl$_3$	0.47	30	50	-	-	-	-	-	-	-
7	BF$_3$·OEt$_2$	0.5	0	50	0	-	-	-	-	-	-
8	BF$_3$·OEt$_2$	0.5	-78	3	65.0	224030	425530	1.90	0.50	0.39	0.11

derivatives. For comparison, the polymerization of *i*BVE has also been investigated with the same type of catalysts. As shown in Tables 3-3 and 3-4, all the metal sulfate-sulfuric acid complexes show significantly low activity against *t*BVE polymerization as compared to *i*BVE.

These results agree well with those reported by McGrath et al.[16] They studied the heterogeneous cationic polymerization of several vinyl ethers and found that vinyl ethers having a linear alkyl group polymerized significantly faster than those having a branched alkyl group with the metal sulfate-sulfuric acid complexes, e.g., the apparent rate constant for the polymerization of *n*-butyl vinyl ether at 36 $^\circ$C was approximately 25 times the corresponding value for *i*BVE. From these results, it should be indicated that the bulkiness of the substituent has a greater influence on the rate of polymerization in this heterogeneous system. The bulkiness of the *tert*-butyl substituent might hinder the approach to the active centers of the heterogeneous catalyst and hence significantly decrease the rate of its polymerization.

3.3.4. Mechanism of stereocontrol polymerization of *t*BVE with Vandenberg type catalyst

As mentioned above, highly isotactic PVAs were produced from poly*t*BVEs that polymerized with the use of a heterogeneous modified Ziegler-type catalyst at high temperatures. According to the NMR spectra of PVAs obtained as a result from the poly*t*BVEs, these polymers contain a f_{mm} greater than 0.50. To elucidate the reaction mechanism in more detail,

Table 3-3. Characterization of poly*t*BVE prepared with several metal sulfate-sulfuric acid complexes in toluene. [*t*BVE]=20 vol%.

No.	Metal	Temp. (°C)	Time (hr)	Polymer yield (%)	M_n	M_w	M_w/M_n
1	Al	0	5	0.5	15800	32500	2.06
2	Al	45	5	0.2	13900	22200	1.60
3	Al	60	5	0.1	17400	23200	1.33
4	Cr	0	6	0.1	34700	81500	2.35
5	Cr	30	5	0.3	16800	38700	2.30
6	Cr	60	5	0.1	18400	25900	1.41
7	Mg	0	6	0	-	-	-
8	Mg	30	6	0.3	870	3200	3.68
9	Mg	60	6	0.1	1700	13000	7.65
10	Fe(II)	0	5	0	-	-	-
11	Fe(II)	30	5	0	-	-	-
12	Fe(II)	60	5	0.3	1170	2400	2.05
13	Fe(III)	-40	50	1.8	2500	9920	3.97
14	Fe(III)	-18	26	0.3	23500	63620	2.71
15	Fe(III)	0	5	4.7	2650	45300	17.1
16	Fe(III)	30	5	0.3	16420	27570	1.68
17	Fe(III)	60	5	0.1	520	730	1.40

Table 3-4. Characterization of poly*i*BVE prepared with several metal sulfate-sulfuric acid complexes in toluene. [*i*BVE]=20 vol%.

No.	Metal	Temp. ($^{\circ}$C)	Time (hr)	Polymer yield (%)	M_n	M_w	M_w/M_n
1	Al	0	7	1.8	52600	565000	10.7
2	Al	45	3	48.3	71800	828200	11.5
3	Cr	0	7	0.2	22200	277000	12.5
4	Cr	60	7	20.8	466000	1770000	3.80
5	Mg	0	5	11.2	17400	109300	6.28
6	Mg	60	5	6.2	15200	138000	9.08
7	Fe(II)	0	5	0.4	22200	78900	3.55
8	Fe(II)	60	5	6.6	690	790	1.14
9	Fe(III)	0	5	51.4	23200	196700	8.48
10	Fe(III)	60	5	47.5	9300	92600	9.96

the factor that controls the steric structure of an adding monomer was studied in the same way as reported in the previous paper.[8,17] When δ_1 is defined as the persistence probability that an attacking monomer gives the same configuration (diad *meso*) as that of the last unit at its proceeding unit, according to Bovey et al.,[18] the following relationships hold.

$$f_{mm} = \delta_1^2$$
$$f_{mr} = 2\delta_1(1 - \delta_1) \qquad (1)$$
$$f_{rr} = (1 - \delta_1)^2$$

where f_{mm}, f_{mr}, and f_{rr} are a fraction of the triad for the isotactic, heterotactic, and syndiotactic structures, respectively.   On the other hand, for a system where the configuration of the monomer is determined by the catalyst, a treatment based on the enantiomorphic catalyst model was proposed by Fueno et al.[19]   In this model, each fraction of *mm*, *mr*, and *rr* are expressed by δ_2, as shown in eq. (2).

$$f_{mm} = 1 - 3(\delta_2 - \delta_2^2)$$
$$f_{mr} = 2(\delta_2 - \delta_2^2) \qquad (2)$$
$$f_{rr} = \delta_2 - \delta_2^2$$

where δ_2 represents the persistence probability that a monomer adds to a polymer chain end in either configuration controlled by the catalyst site.

The triad tacticity measured by the NMR spectra of PVAs, which was

obtained from the poly*t*BVE catalyzed by Vandenberg type catalysts, is summarized in Table 3-1.   From the observed values of the f_{mm}, the value of δ_1 can be obtained by calculations using eq.1, and the value of δ_2 can be defined by eq.2.   Figure 3-3 and Figure 3-4 show the relationship between δ_1 or δ_2 and probability (*P*) of each triad tacticity of PVAs (circle for ST and PST).   In Figure 3-3 and 3-4, the *P* values of PVAs derived from poly*t*BVEs polymerized with $BF_3 \cdot OEt_2$ are also plotted against δ_1 and δ_2, respectively, for comparison (cross).   The solid lines in Figure 3-3 and 3-4 are the theoretical values calculated from Bovey's model (eq.1) and the enantiomorphic catalyst site model (eq.2), respectively.   Apparently, the observed values of each fraction of the three kinds of triads (circle in Figure 3-3) show significantly good agreement with the theoretical values calculated from Bovey's model, whereas the plots of *P* (circle in Figure 3-4) seem inconsistent with the calculated ones from the enantiomorphic catalyst site model.   This case gave good agreement with that catalyzed by homogeneous BF_3 complexes, where the growing chain end and penultimate unit control the steric structure of an approaching monomer. Further, this fact suggests that the steric structure of the poly*t*BVEs catalyzed by BF_3 homogeneous catalysts or titanium based heterogeneous catalysts was controlled by the same mechanism.   These results are totally different from the results reported by Higashimura et al.[8]   They studied the mechanism by which the steric structure of a methyl vinyl ether
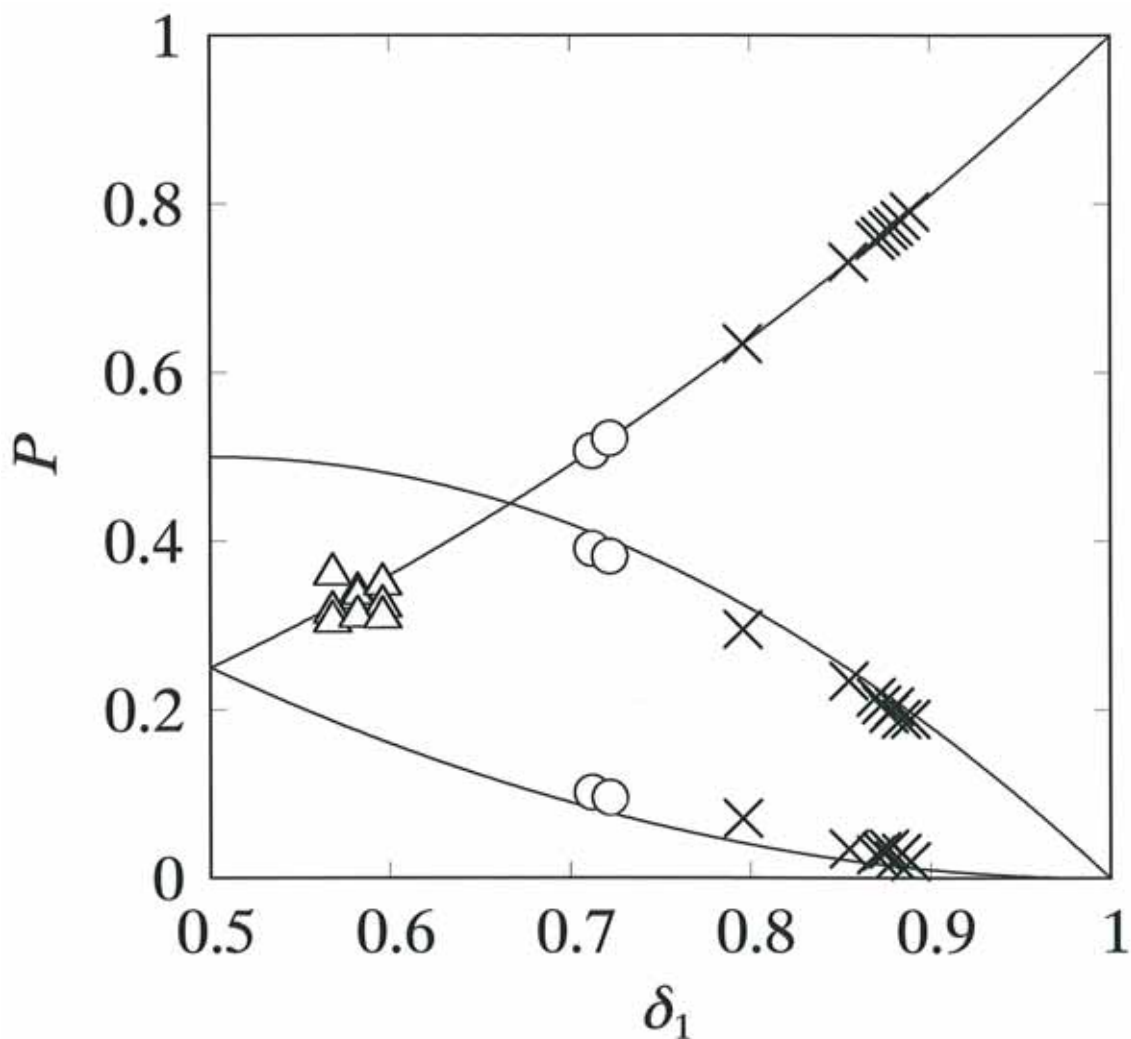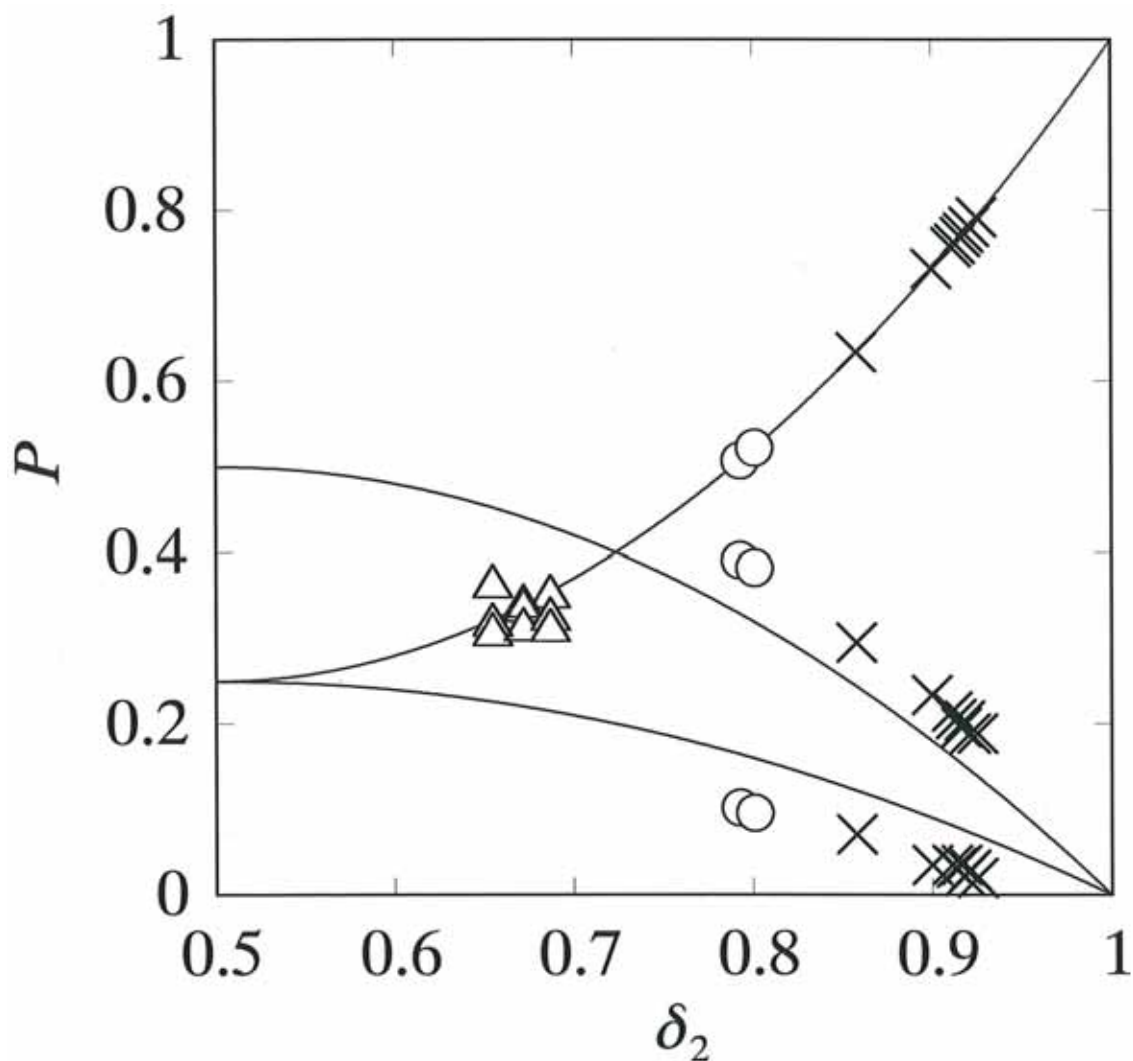
Figure 3-3. Relationships between δ_1 and the probability (P) of the triad tacticity of PVAs obtained from the poly$t$BVEs catalyzed by the titanium based catalysts at 30 $^{\circ}$C (circle), the vanadium based catalyst at 30 $^{\circ}$C (triangle) and BF$_3$·OEt$_2$ at -78 $^{\circ}$C (cross) in n-heptane.   The curves indicate the theoretical values calculated from Bovey's model.

Figure 3-4. Relationships between δ_2 and the probability (P) of the triad tacticity of PVAs obtained from the poly$t$BVEs catalyzed by the titanium based catalysts at 30 $^{\circ}$C (circle), the vanadium based catalyst at 30 $^{\circ}$C (triangle) and BF$_3$·OEt$_2$ at −78 $^{\circ}$C (cross) in n-heptane. The curves indicate the theoretical values calculated from the enantiomorphic site model.

monomer is controlled in the polymerization catalyzed by the sulfuric acid-aluminum sulfate complex, and found that the content of the triad tacticity of poly(methyl vinyl ether) obtained by these catalysts agreed with the value calculated from the enantiomorphic catalyst site model. They confirmed that the steric structure of an adding monomer in the presence of this heterogeneous catalyst is controlled only by a catalyst site. It should be remembered that different factors control the polymer configuration even in the heterogeneous polymerization if different catalyst systems are used.

In Chapter 2, we showed that the most highly isotactic PVA reported so far was derived from poly$t$BVE prepared by cationic polymerization with $BF_3 \cdot OEt_2$ catalyst.[9,10] We also studied the polymerization of tBVE with various BF_3 complexes and reported that the f_{mm} increases in the following order: $BF_3 \cdot 2CH_3COOH < BF_3 \cdot OEt_2 < BF_3 \cdot 2CH_3OH < BF_3 \cdot 2H_2O$.[10] These results suggest that the counter anion of the growing chain should play important roles in controlling the stereoregularity of poly$t$BVE with homogeneous BF_3 complexes catalyst. Some models and mechanisms of isospecific propagation in homogeneous systems have been proposed primarily for vinyl ethers. Kunitake et al. proposed that the important factors for controlling the stereochemistry of chain growth in alkyl vinyl ether polymerization are the degree of association of growing cations and their counter anions, and the bulkiness of the counter anion.[20,21] The steric repulsion of the bulky substituents of terminal and penultimate monomer units could be minimized, and assuming a planar carbocation, a monomer

attack on the same side of the counter anion (front side attack) or on the opposite side (backside attack) leads to mainly syndiotactic placement or isotactic placement, respectively. Non-polar solvents such as n-heptane would be expected to favor a tight association between the propagating cation and its counter anion so that they favor the back-side attack with the formation of isotactic configuration that minimized the steric repulsion between the bulky substituent in monomer and the growing polymer chain. Polar solvents such as CH_2Cl_2 favor inversely front side attack with the formation of a syndiotactic configuration because they could stabilize separated ion pairs. More recently, the stereoregulation in the cationic polymerization of vinyl ethers was studied by Sawamoto et al.[17,22,23] It is proposed that the bulkiness and spatial shape of the counteranions are directly responsible for the stereoregulation, and an effective isospecificity enhancement was demonstrated by a bulky protonic acid and/or a bulky Lewis acid from which the counteranions form. It is noteworthy that the bulky phosphoric acid derivatives coupled with $SnCl_4$ yielded highly isotactic poly*i*BVE. They reported that the high isoselectivity by the phosphoric acids was probably a result of an exchange reaction with $SnCl_4$ to generate a bulkier Lewis acid, and a bulkier counteranion can be formed during polymerization to induce isospecificity.[23] For the polymerization of *t*BVE with titanium based catalysts, considering steric repulsions associated with the heterogeneous nature of the catalyst is very important in determining the mode of insertion of the monomer between the heterogeneous and sterically hindered counteranion and the growing

polymer cation. Hence, we concluded that the high isoselectivity by the titanium based catalyst is a result of bulkier and sterically hindered counteranions as compared to that of the polymerization with $BF_3 \cdot OEt_2$.

In contrast, the steric configuration of PVAs obtained from the poly*t*BVEs with vanadium based catalysts cannot be applied to either Bovey's model or the enantiomorphic catalyst site model. As shown in Figures 3-3 and 3-4, the observed triad faction for polymers obtained with vanadium based catalysts (triangle) does not agree with the theoretical curve calculated from these models. Since an increase in the monomer concentration causes an increase in the polarity of the reaction system, the isotacticity of the polymer decreases. However, the addition of a monomer had little effect on the stereoregularity of the polymer (run 6 in Table 3-1).

This suggests that the stereochemistry of these systems follow some statistics other than chain-end control (Bovey's model) or catalyst site model. It may be difficult to elucidate the exact mechanism of the polymerization of *t*BVE with vanadium based catalysts to form isotactic polymers. It has been reported that the polymerization of *t*BVE with the PSV catalyst yielded a highly crystallinity polymer, but the conversion was very low.[4] Vandenberg also proposed that an amorphous polymer with a high molecular weight obtained with the PSV catalyst may be caused by the aluminum components of the system and it is difficult to avoid the contamination of the alkylaluminum component, which are by-products of the PSV catalyst formation. However, all poly*t*BVEs polymerized with

vanadium based catalysts were isolated as nontacky, semicrystalline powdery solids. Further, a single symmetric GPC elution curve and a relatively narrow molecular weight distribution (Table 3-1) of poly*t*BVEs catalyzed by the vanadium based catalysts may suggest that the polymerization of *t*BVE proceeds with a single active center, and not a mixture of different polymerization species. However, as discussed above, the monomodal *MWD* of the polymer is not always proof of a uniform active center in the cationic polymerization. We need more information on the polymerization of *t*BVE with vanadium based catalysts in order to elucidate the reaction mechanism in greater detail.

3.4. Conclusions

We studied the polymerization of *t*BVE and BzVE with heterogeneous catalysts, i.e., modified Ziegler type (Vandenberg type) catalysts and metal sulfate-sulfuric acid complexes. A Vandenberg type catalyst shows a high activity against *t*BVE at high temperatures, and this result shows that there are few chain transfer reactions during polymerization. The polymerization system became heterogeneous because of the low solubility of the catalyst; however, the molecular weight distribution of the polymers obtained from *t*BVE by titanium based catalysts was relatively narrow. The *mm* sequence fraction of the PVA obtained from poly*t*BVE with PST catalyst is 0.52, which is similar to poly*t*BVE prepared with $BF_3 \cdot OEt_2$ in *n*-heptane at $-78\ ^\circ C$. The observed values of the respective fractions of the triad tacticities show significantly good agreement with the theoretical

values calculated from Bovey's model. These results suggest that the stereoregular polymerization with titanium based catalysts should occur according to the chain-end control model, and the high isoselectivity by the titanium based catalyst is probably due to bulkier and sterically more hindered counter-anions as compared to those for the polymerization with $BF_3 \cdot OEt_2$.

The vanadium based Vandenberg type catalyst did not work as well as the titanium based one with tBVE. The polymerization of tBVE yielded poly$t$BVE of lower molecular weight when catalyzed by vanadium based catalysts than when catalyzed by titanium based ones. The relationships between the observed triad faction for polymers obtained with vanadium based catalysts and the theoretical curves suggested that the stereochemistry of these systems follows some statistics other than the chain-end control (Bovey's model) or enantiomorphic catalyst site model.

References

(1) Murahasi, S.; Yuki, H.; Sano, T.; Yonemura, U.; Tadokoro, T.; Chatani,Y. *J Polym Sci* **1962**, S77, 62.

(2) Yuki, H.; Hatada, K.; Oda, K.; Kinoshita, H.; Murahashi, S.; Ono, K.;Ito,Y. *JPolym Sci Part A1* **1969**, 7, 1517.

(3) Higashimura,T.; Suzuki, K.; Okamura,S. *Makromol Chem* **1965**,86,259.

(4) Vandenberg, E.J. *J of Polym Sci Part C1* **1963**, 207.

(5) Yamaoka,H.;Higashimira,T.;Okamura,S.;*KobunshiKagaku***1961,** 18,561.

(6) Okamura,S.;Higashimura,T.;Watanabe,T.*Makromol Chem* **1961**,50,137.

(7) Lal, J.; McGrath, J.E.; Trick, G.S. *J Polym Sci Part A* **1967**, 5, 795.

(8) Higashimura, T.; Ohsumi, Y.; Kuroda, K.; Okamura, S. *J of Polym Sci PartA* **1967**, 15, 863.

(9) Ohgi, H.; Sato, T. *Macromolecules* **1993**, 26, 559.

(10) Ohgi, H.; Sato, T. *Macromolecules* **1999**, 32, 2403.

(11) Moritani, T.; Kuruma, I.; Shibatani, K. *Macromolecules* **1972**, 5, 577.

(12) Aoshima, S.; Higashimura, T. *Polymer J* **1984**, 16(3), 249.

(13) Higashimura. T.; Takeda, T.; Sawamoto, M.; Matsuzaki, K.; Uryu, T. *J Polym Sci Part A* **197,** 16, 503. and references therein.

(14) Higashimura, T.; Watanabe, T.; Okamura, S. *Kobunshi Kagaku* **1963**, 20, 680.

(15) Murahasi, S.; Yuki, H.; Sano, T.; Yonemura, U.; Tadokoro, T.; Chatani, Y. *J Polym Sci* **1962**, S77, 62.

(16) Lal, J.; McGrath, J.E. *J of Polym Sci Part A* **1964**, 2, 3369.

(17) Ouchi, M.; Kamigaito, M.; Sawamoto, M. *J of Polym Sci Part A* **2001**, 39, 1060.

(18) Bovey, F.A., Tiers, G.V.D. *J of Polym Sci* **1960**, 44, 173.

(19) Shelden, R.A.; Fueno, T.; Tsunetsugu, T.; Furukawa, J. *J of Polym Lett* **1965**, 3, 23.

(20) Kunitake, T.; Aso, C. *J Polym Sci Part A* **1970**, 8, 665.

(21) Kunitake, T.; Takarabe, K. *Makromol Chem* **1981**, 182, 817.

(22) Ouchi,M.;Kamigaito,M.;Sawamoto,M. *Macromolecules* **1999**,32,6407.

(23) Ouchi, M.; Sueoka, M.; Kamigaito, M.; Sawamoto, M. *J of Polym Sci Part A* **2001**, 39, 1067.

Chapter 4

Some Physical Properties, Structure and Hydrogen Bonding of Highly Isotactic Poly(vinyl alcohol) Films

4.1. Introduction

Marked stereoregularity dependencies on the physical properties of stereoregular PVAs were recognized, which may be mainly caused by differences in inter- and intramolecular hydrogen bonding. A series of vinyl esters have been polymerized using free radicals to prepare syndiotacticity-rich polymers and many studies have been reported on the relationships between stereoregularity and physical or solution properties of PVA.[1-3] On the other hand, the synthesis of isotacticity-rich PVA was carried out successfully using vinyl ethers as starting monomers, and their physical or solution properties were also investigated.[1,3-9]

Irrespective of many efforts paid to prepare stereoregular PVAs, the stereoregularity still remained at a low level of f_{mm}=0.70 even for so-called isotactic PVA (LI-PVA) derived from poly(trimethyl silyl vinyl ether) (polyVOSi).[9,10] As described in Chapter 2, we studied in detail the cationic polymerization of tBVE with boron trifluoride diethyl etherate (BF$_3$·OEt$_2$) and successfully prepared the PVAs whose isotacticity is the highest of all isotacticity-rich PVAs reported so far.[10-12] Preliminary experiments partly revealed interesting features of the highly isotactic PVA (HI-PVA) different from those of LI-PVA and ordinary atactic PVA

(A-PVA).[10,13] In this chapter, some basic physical properties of PVA samples with different tacticities including HI-PVA are systematically examined by different analytical methods as functions of the *mm* fraction at the wide range.   Intramolecular and intermolecular hydrogen bondings are also characterized for HI-PVA in detail by using high-resolution solid-state ^{13}C NMR spectroscopy.

4.2. Experimental Section

4.2.1. Preparation of stereoregular PVAs

HI-PVAs with *mm* triad fractions higher than 0.70 were synthesized by the procedure which is described in Chapter 2.   The previously reported LI-PVAs,[11] which have *mm* triads lower than 0.70, were also synthesized by the procedure described in Chapter 2 and used as references to clarify unique solid properties of HI-PVAs.   The commercially available A-PVA derived from poly(vinyl acetate) and syndiotacticitiy-rich PVA (S-PVA) derived from poly(vinyl pivalate) by using the method previously reported[14] were also used as reference samples.

4.2.2. Characterization of the stereoregular PVA samples

The degrees of polymerization and the stereoregularity of each PVA samples were measured by using the method previously reported in Chapter 2.

4.2.3. Preparation of PVA films

All physical properties were measured on the PVA films with a thickness of about 100 μm unless otherwise specified. The PVA films were prepared by casting the 5 wt% DMSO solution on a glass plate, evaporating DMSO at 50 °C for 20 hr, immersing them in hot methanol overnight, and then drying at 50 °C under vacuum.

4.2.4. Thermal analyses

Differential scanning calorimetry (DSC) thermograms were recorded on 10 mg of each PVA sample under nitrogen with a Mettler differential scanning calorimeter. Melting temperatures of the samples were determined as endothermic peak temperatures observed in the thermograms. A thermogravimetric analysis (TGA) was carried out on 10 mg of each sample under a nitrogen atmosphere. The heating rate was 10 °C/min in these measurements.

4.2.5. Fourier transform infrared spectroscopy

FT IR spectra of the stereoregular PVA films with about 25 μm in thickness were recorded on a Nicolet 520 FT IR spectrometer in the wave number range of 4000-500 cm^{-1}. Fast Fourier transforms were conducted after the accumulation of 32 scans.

4.2.6. Solid-state ^{13}C NMR spectroscopy

Cross polarization/magic angle spinning (CP/MAS) ^{13}C NMR spectroscopy was performed at room temperature on a JEOL JNM-FX200

spectrometer under a static magnetic field of 4.7 T. ^{1}H and ^{13}C radio-frequency field strengths $\gamma B_1/2\pi$ were 69 kHz in the CP process, whereas the ^{1}H field strength was reduced to 59 kHz for the dipolar decoupling. The CP contact time and MAS rate were set to 1 ms and 3.5 kHz, respectively. A MAS rotor with an O-ring seal[19,20] was employed not to allow each dried sample to adsorb atmospheric moisture during NMR measurements. The detailed procedure of the solid-state NMR measurements was almost the same as described in the previous papers.[20-25]

4.3. Results and Discussion

4.3.1. Characterization of stereoregular PVAs

The triad tacticities of HI-PVAs determined by solution-state ^{1}H NMR spectroscopy are listed in Table 4-1. For reference, the tacticities of LI-PVA derived from poly*t*BVE, A-PVA derived from poly(vinyl acetate), and S-PVA derived from poly(vinyl pivalate) are also listed in this table. Here, these results can be evaluated in the same way as previously reported[26,27] on the basis of the simple stereoregular polymerization mechanism. When δ is defined as the persistence probability that an attacking monomer gives the same configuration (diad *meso*, *m*) as that of the last monomer residue, the following equations hold:

$$f_{mm} = \delta^2$$
$$f_{mr} = 2\delta(1 - \delta) \tag{1}$$
$$f_{rr} = (1 - \delta)^2$$

Table 4-1. The characterization of the stereoregular PVA samples.

Sample	Tacticity in triad			Tacticity in diad		$P_v{}^a$	T_m (°C)	ΔH (kJ mol^{-1})	$T_d{}^b$ (°C)
	mm	*mr*	*rr*	*m*	*r*				
HI-PVA1	0.791	0.189	0.020	0.886	0.114	3540	246.8	3.87	287
HI-PVA2	0.788	0.189	0.023	0.883	0.117	6800	248.8	3.79	280
HI-PVA3	0.781	0.189	0.030	0.876	0.124	23800	246.3	3.50	267
HI-PVA4	0.762	0.206	0.032	0.865	0.135	4800	243.8	2.89	260
LI-PVA1	0.634	0.295	0.071	0.782	0.218	9300	222.3	2.41	239
LI-PVA2	0.421	0.397	0.183	0.619	0.281	3450	212.0	-	186
A-PVA	0.220	0.050	0.280	0.470	0.530	1750	224.7	3.41	233
S-PVA	0.140	0.480	0.380	0.380	0.620	1700	247.1	4.31	247

[a] viscosity-average degree of polymerization. [b] 5 wt% loss temperature determined by TGA.

where f_{mm}, f_{mr}, and f_{rr} are the mole fractions of the *mm, mr,* and *rr* sequences, respectively. The observed δ values were obtained from the f_{mm} values determined by solution-state ^{1}H NMR using Eq.1 and the relationship between δ and the mole fraction (*P*) of each triad tacticity is shown in Figure 4-1. Here, solid lines are the theoretical results calculated by Eq.1.

As is clearly seen, the observed results are in good agreement with the theoretical ones for each triad tacticity in the wide range of δ including the higher values newly obtained in this work. This fact suggests that the growing chain end and its penultimate unit may admit the statistically random addition reaction of the monomer irrespective of the tacticity of the chain end. The diad tacticities calculated by using Eq.1 are also listed in Table 4-1.

4.3.2. Thermal properties

As previously reported,[10,11] HI-PVAs are further richer in isotacticity than the PVA samples derived from polyVOSi[8,9] whose isotacticity was the highest of all isotactic PVAs so far. We have first studied thermal behavior of HI- PVAs. Figure 4-2 shows DSC thermograms measured for several stereoregular PVA samples at a heating rate of 10 °C/min. The melting temperature (T_m) determined as an endothermic peak top and the heat of melting (ΔH) estimated from the integrated intensity of the endothermic curve are also listed in Table 4-1 for each sample. The HI-PVA sample shows a rather sharper melting curve and a higher melting
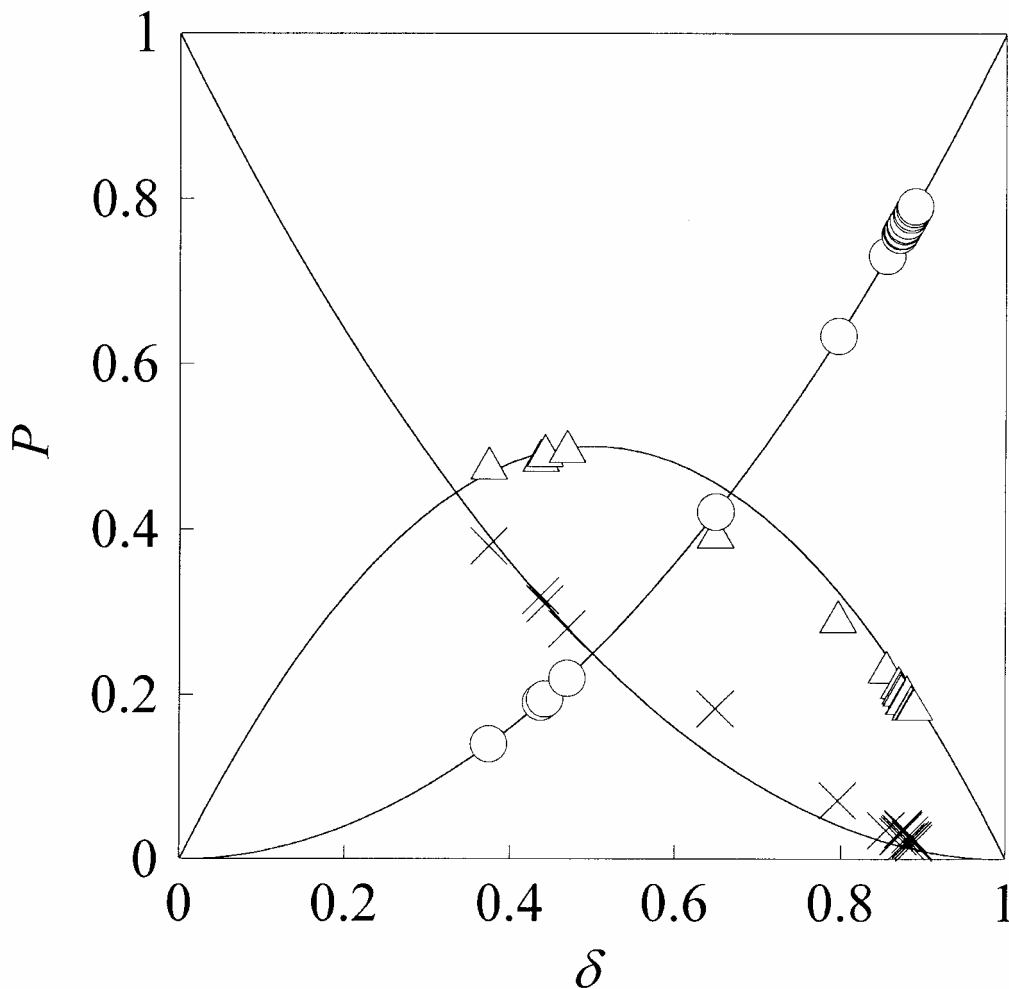
Figure 4-1.　Relationship between the fraction of *meso* diad (δ) and the probability (P) of the *mm* (circle), *mr* (triangle), or *rr* (cross) sequences for different stereoregular PVA samples.　The solid curves indicate the theoretical values calculated by the Bovey's model.[27]
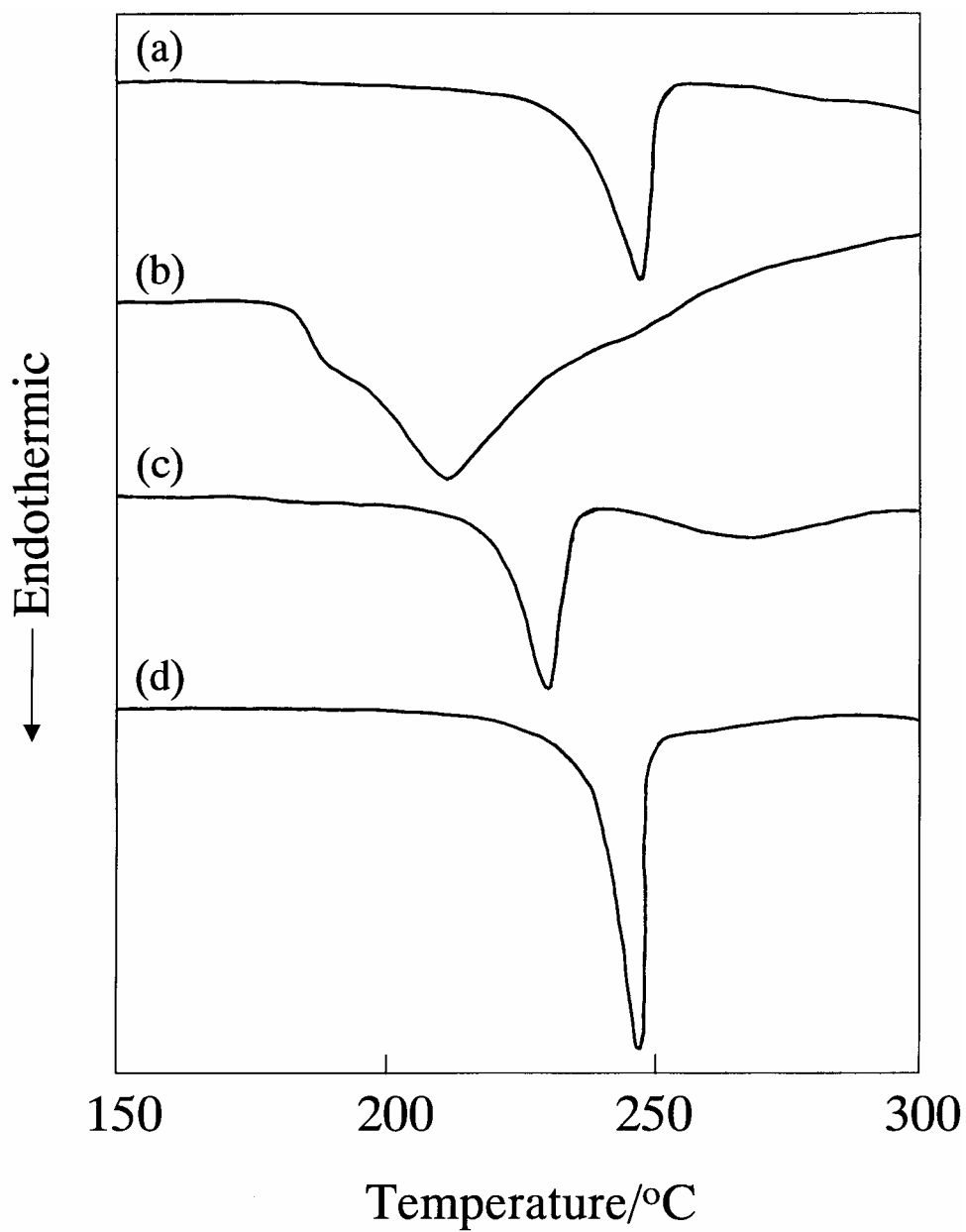
Figure 4-2. DSC thermograms of different stereoregular PVA samples: (a) HI-PVA (f_{mm}=0.78), (b) LI-PVA (f_{mm}=0.42), (c) A-PVA, (d) S-PVA.

temperature similarly to the cases of S-PVA compared to A-PVA or LI-PVA. In contrast to the HI-PVA samples, it is difficult to determine the heat of melting (DH) for the LI-PVA samples because of its broad melting endothermic curve. This may be due to low heat stability of this sample, as shown later by TGA measurements. On the other hand, the glass-rubber transition cannot be clearly observed in each case in Figure 4-2 but it should be noted here that the peak temperature of tan δ, which may correspond to the glass transition temperature estimated by dynamic viscoelastic measurements, was not significantly influenced by the difference in stereoregularity. The details of dynamic viscoelastic behavior of the stereoregular PVA samples are described in chapter 6.

In Figure 4-3, the T_m values determined by DSC are plotted against the *mm* fractions for the stereoregular PVAs. It is clearly found that the T_m greatly depends on the *mm* fraction and a marked minimum appears at f_{mm} =~0.50. The cause of the appearance of the minimum at f_{mm}=~0.50 will be discussed later after the detailed structural characterization is completed by solid-state ^{13}C NMR spectroscopy. Interestingly, the T_m of one of HI-PVAs is the highest of all PVA samples including S-PVAs. Here, A-PVAs show the T_m values ranging from 225 to 240°C as seen in Figure 4-3. Such a somewhat wide distribution in T_m among these samples may be due to the differences in molecular weight or in a small amount of residual water.

A similar remarkable dependence on the *mm* fraction is also obtained from the observed enthalpy for the same stereoregular PVA samples, as shown in Figure 4-4. It should be noted that a clear minimum appears
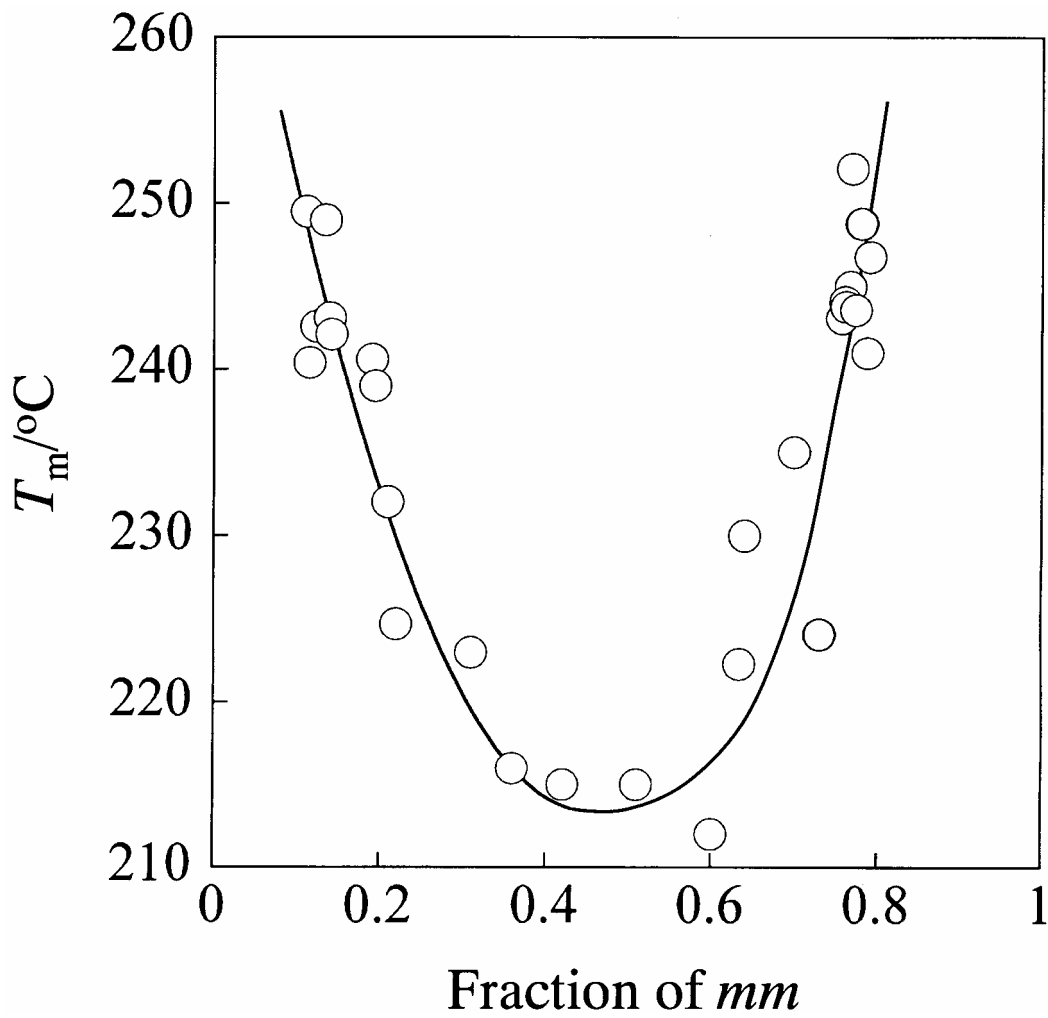
Figure 4-3. Relationship between the *mm* fraction and the melting temperature (T_m) for different stereoregular PVA samples.

also at the *mm* fraction of about 0.50 in this case. In general, the degrees of crystallinity of A-PVA and S-PVA can be determined from the ΔH values obtained in the DSC measurements by assuming $\Delta H_c =6.87$ kJ mol^{-1} for the 100 % crystals[28] irrespective of the stereoregularity. However, the same DH_c value may not be used for the HI-PVA samples because the crystal structure of HI-PVA significantly differs from that of A-PVA or S-PVA.[10] Here, the apparent degrees of crystallinity were determined for HI-PVA by using the same ΔH_c because no determination of ΔH_c has not yet been made for these polymers. The apparent degrees of crystallinity thus obtained were shown against the right vertical axis in Figure 4-4, for reference.

4.3.3. Thermal decomposition

TGA curves of the stereoregular PVA samples are shown in Figure 4-5. As clearly seen in this figure, the first weight loss process for A-PVA (dotted line) occurs at 220 - 275 °C, followed by a further weight loss at 300 - 350 °C, leaving a residue of approximately 15 wt% at 400 °C. In contrast, the major weight loss of HI-PVA (bold line) takes place at 270 - 350 °C, leaving a residue of about 20 wt% at 400 °C. The 5 wt% loss temperature T_d which is defined as the temperature where the 5% weight loss occurs is also listed for each sample in Table 4-1. This table indicates that the order of the T_d is HI-PVA > S-PVA > A-PVA > LI-PVA. This order well corresponds to the order of T_m and thus HI-PVA has also the highest heat stability of all PVAs.

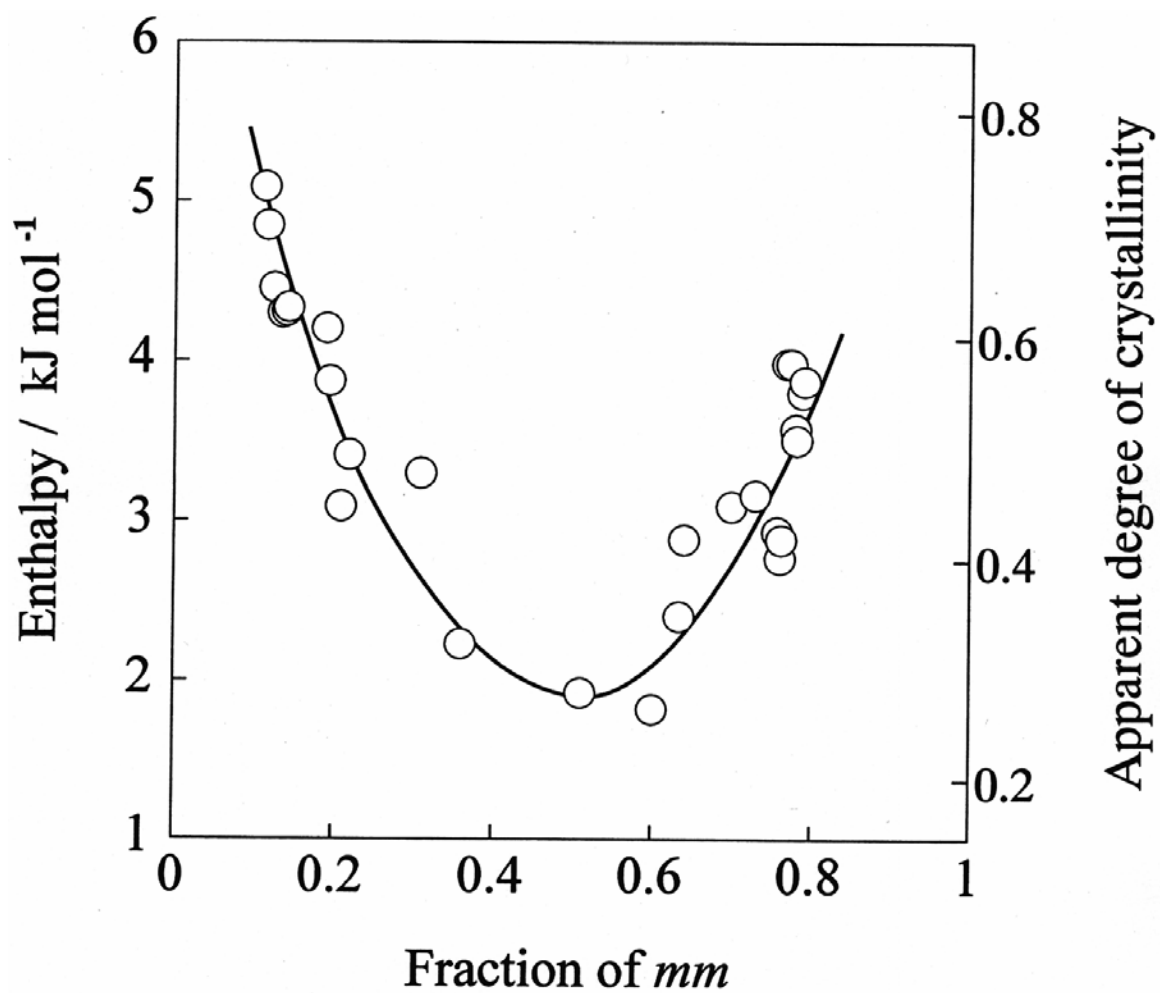According to the previous studies of the thermal decomposition of

Figure 4-4.   Relationship between the *mm* fraction and the enthalpy Δ*H* for melting and the apparent degree of crystallinity estimated from Δ*H* for different stereoregular PVA samples.
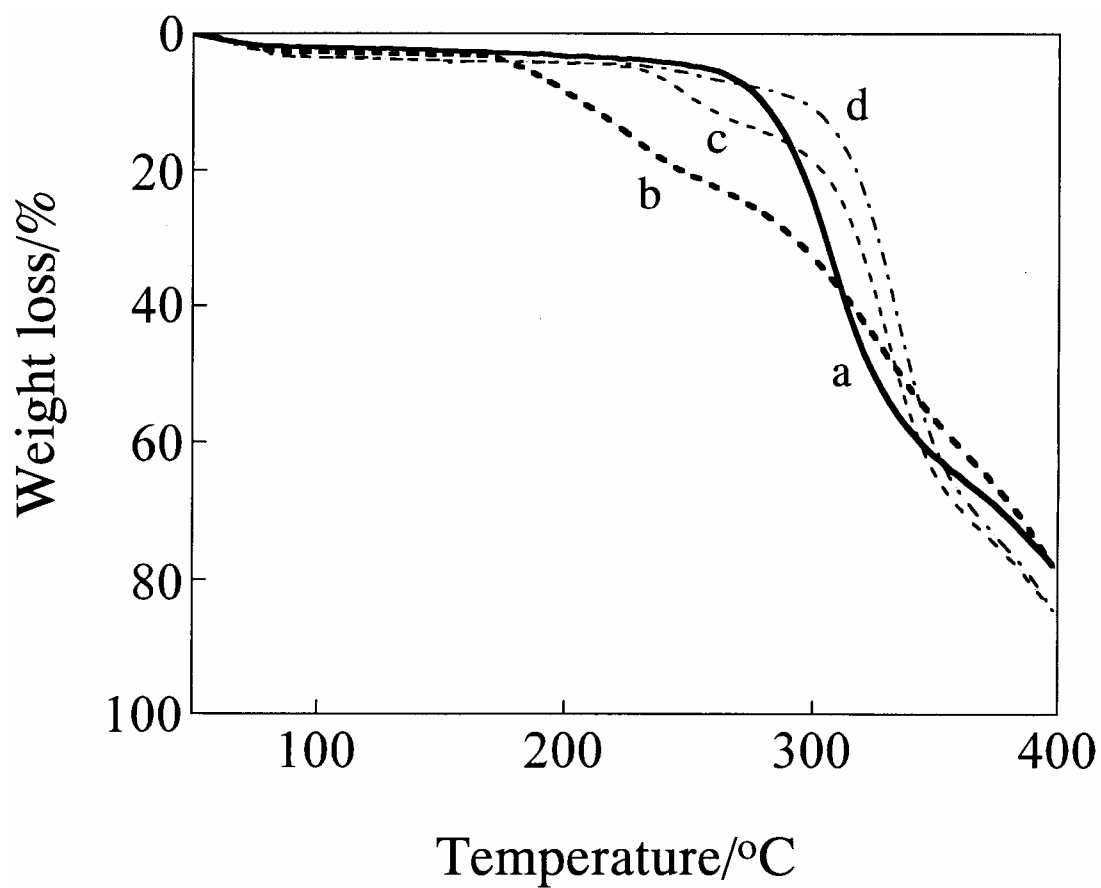
Figure 4-5. TGA thermograms of different stereoregular PVA samples: (a) HI-PVA (f_{mm}=0.78), (b) LI-PVA (f_{mm}=0.42), (c) A-PVA, (d) S-PVA.

A-PVA,[29] the major pyrolysis product is water, which is produced by the elimination of the OH groups, and water begins to evolve at lower temperatures than the other degradation products such as aldehydes, ketones and benzene derivatives. Therefore, the initial weight loss should be due to the elimination of water for all PVA samples, and such elimination will preferably occur in the molten state of each PVA sample.

The second weight loss clearly observed for A-PVA and S-PVA in Figure 5-5 should be due to other degradation products such as aldehydes and ketones. However, this process is not clear for HI-PVA and such different behavior may be due to the difference in the chain-end structure in each polymer. More detailed experiments will be made in future including the characterization of the chain ends by considering the termination reaction during the polymerization.

4.3.4. FT IR spectra

Figure 4-6 shows FT IR spectra of the stereoregular PVA samples. Remarkable intensity changes with the change in stereoregularity are observed for the 916 cm^{-1} and 849 cm^{-1} bands, which are assigned to the CH_2 rocking motion or the skeletal motion and to the stretching of the C-C bond or the skeletal motion of the main chain, respectively.[30] The relationship between the absorbance ratio, D_{916}/D_{849}, of the two bands and the syndiotacticity expressed as r % was already proposed as follows:[1,31]

$$\text{syndiotacticity (r \%)} = (72.4 \pm 1.09) \, (D_{916}/D_{849})^{\,0.43\pm0.006} \tag{2}$$
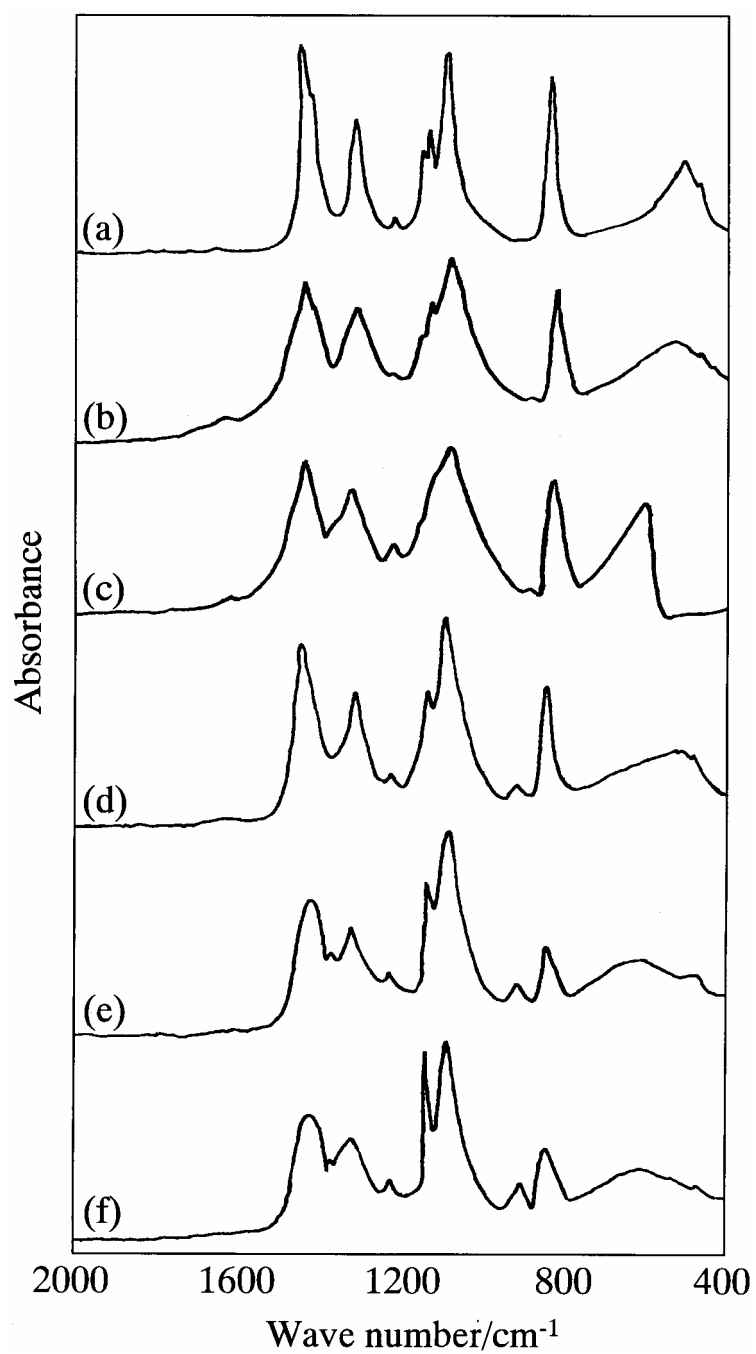
Figure 4-6. FT IR spectra of different stereoregular PVA samples: (a) HI-PVA (f_{mm}=0.78), (b) HI-PVA (f_{mm}=0.67), (c) LI-PVA (f_{mm}=0.64), (d) LI-PVA (f_{mm}=0.42), (e) A-PVA, (f) S-PVA.

In Figure 4-7, the D_{916}/D_{849} ratios obtained for our present samples including HI-PVAs are plotted against the m and r fractions. As clearly seen in Figure 4-7, the ratio continuously decreases with increasing r fraction in the whole region including the region for HI-PVA and the r fraction (f_r) is found to be well expressed by the following equation (solid line in the figure):

$$f_r = 0.713 + 0.334 \log(D_{916}/D_{849}) \tag{3}$$

For comparison, the corresponding relation derived from Eq.(4) is also depicted as a dotted line in Figure 4-7. It is found that Eq.(4) does not hold in the present case. One of the causes for the discordance may be that the syndiotacticity (r %) in Eq.(4) was determined by using the CH_3 proton resonance lines of PVAc in solution. Namely, the tacticity determination seems not to be carried out in a fully high precision because of the low resolution of the CH_3 resonance lines.[1,32] In contrast, the triad tacticity can be determined much more precisely by using the OH triplets[17] observed by ^{1}H NMR measurements of PVA in DMSO-d_6 and this method was used to obtain the f_r values shown in Figure 4-7. Another remark is that the intensity of the 916 cm^{-1} band tends to be somewhat affected by the crystallization of PVA.[1,33] Since HI-PVAs have much higher degrees of crystallinity than the isotacticity-rich PVA samples used for the derivation of Eq.(2), some complicated effect of crystallinity may be included in the relationship between the f_r and D_{916}/D_{849} shown in Figure 4-7.
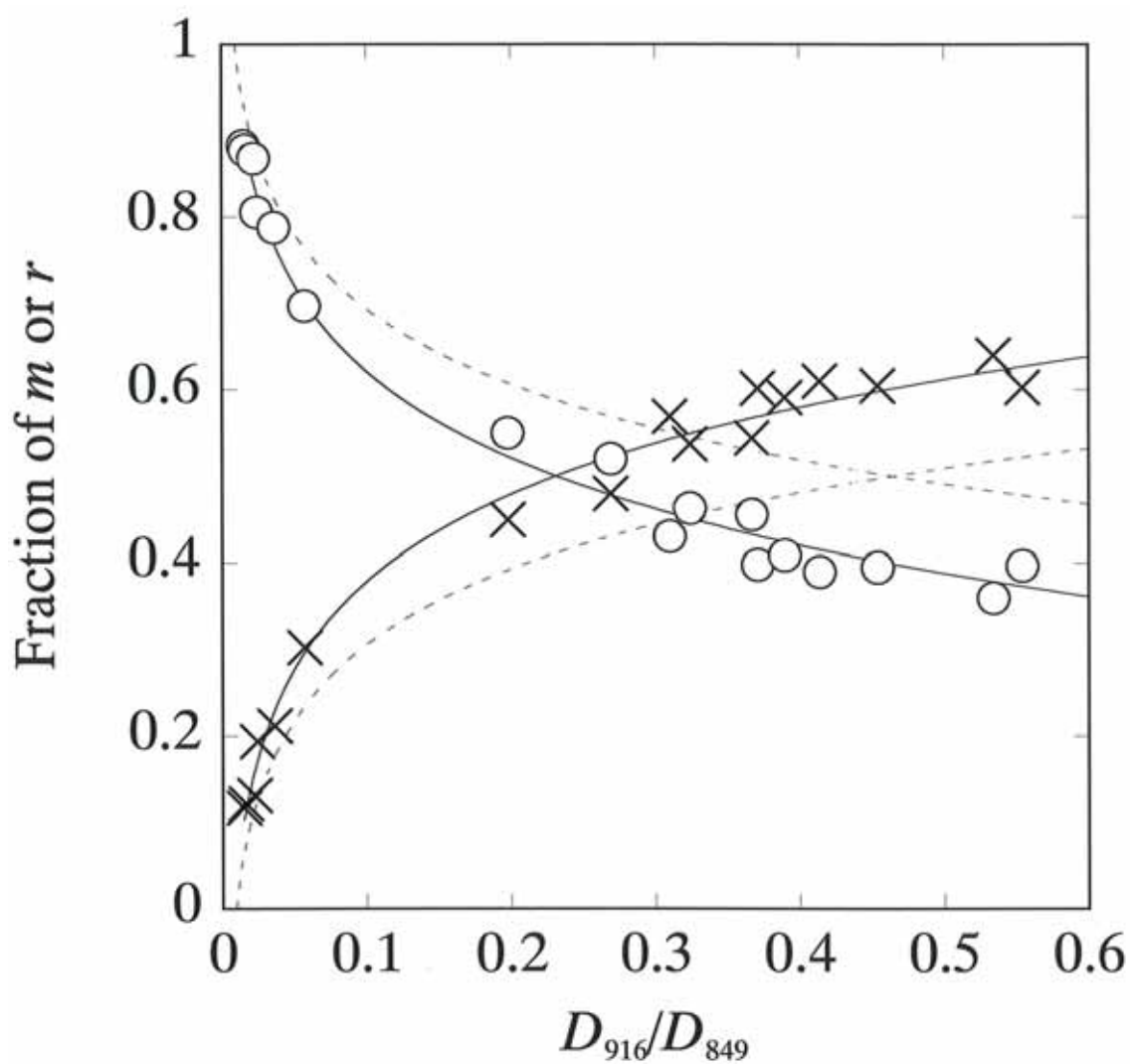
Figure 4-7. Relationship between the fraction of the *meso* diad (circle) or the *racemo* diad (cross) and the D_{916}/D_{849} ratio for different stereoregular PVA samples. The broken and solid lines indicate the values calculated by using Eqs.(2) and (3), respectively.

Another remarkable spectral change in the stereoregular PVAs is observed for the band at 1140 - 1150 cm^{-1} in Figure 4-6. This band is assigned to the C-C stretching vibration in the crystals, which is coupled with the C-O stretching, or to the O-C-C symmetric stretching vibration ascribed to the skeletal vibration of the atactic or syndiotactic part.[30,32] The intensity of the band was found to depend on the crystallinity[33] and, in accord with such previous finding, an intensity increase of the band is observed in S-PVA having higher crystallinity. Moreover, the band is hardly observed for the HI-PVA (f_{mm}=0.67) sample, probably because the crystallinity is very low in this sample as shown in Figure 4-4.

In contrast, a new band appears at about 1165 cm^{-1} for HI-PVA and another band that may correspond to the original band is also observed at a slightly higher wave number in Figure 4-6. This fact is due to the formation of another type of crystal form observed for HI-PVA.[10-12] Murahashi et al. also observed such two bands for their isotactic PVA derived from polyVOSi but the intensities were very weak because of the low crystallinity.[31] In Figure 4-8, the wave numbers of the crystalline bands appearing at 1140 – 1160 cm^{-1} are plotted against the *mm* fraction for all PVA samples used in this work. An evident boundary between the ordinary and new crystal forms is found to exist at the *mm* fraction of about 0.55. This value seems to agree with the value that gives the lowest crystallinity of PVA as shown in Figure 4-4.

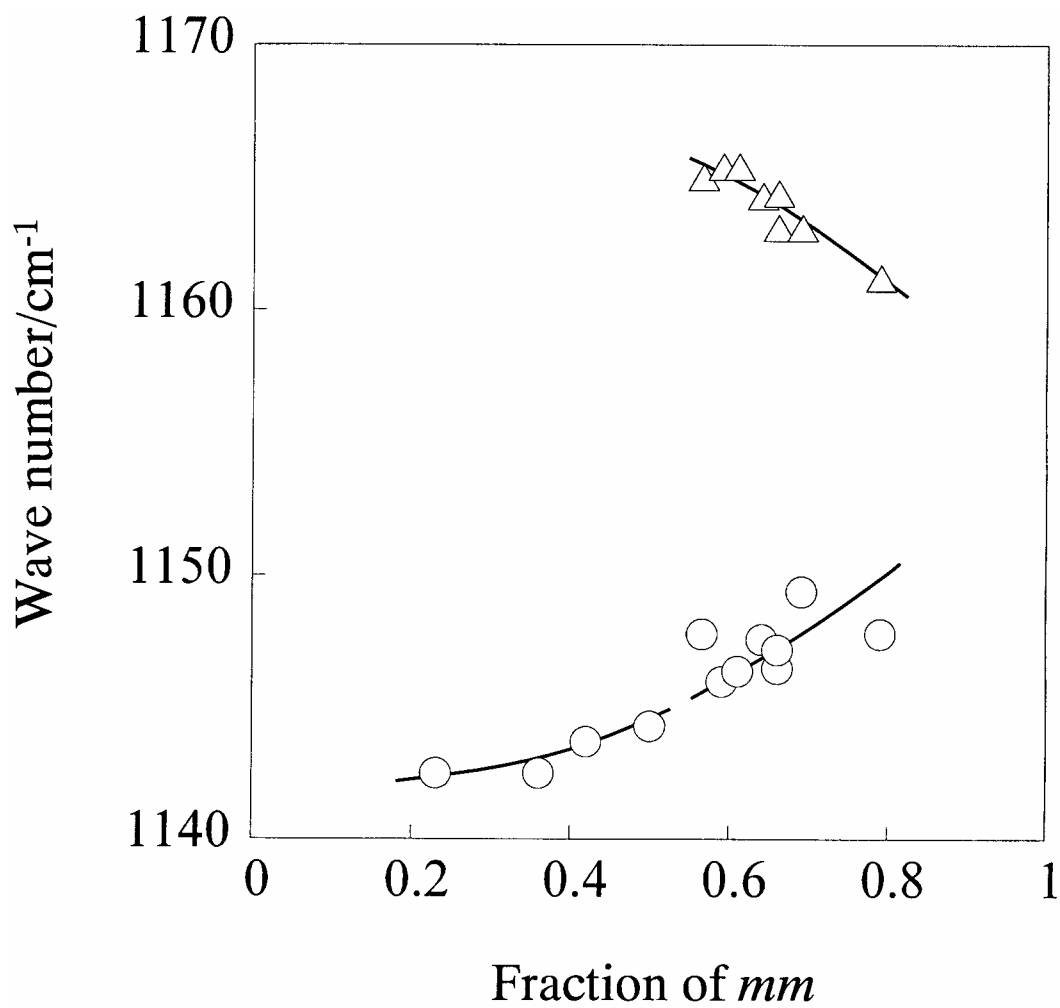### 4.3.5. CP/MAS ^{13}C NMR characterization

Figure 4-8. Relationship between the *mm* fraction and the wave number of the crystalline band for different stereoregular PVA samples.

Since the stereoregularity dependence of the physical properties of PVA may be closely related to inter- and intramolecular hydrogen bonding, it is very important to characterize such hydrogen bonding for the stereoregular PVAs in detail.   As previously reported,[34-40] CP/MAS ^{13}C NMR spectroscopy is very powerful in characterizing the structure of the crystalline and noncrystalline regions of semi-crystalline polymers.   In the case of the crystalline component of solid A-PVA samples, the CH resonance line splits into a triplet due to the formation of 2, 1, and 0 intramolecular hydrogen bond(s) in the triad sequences having the all-*trans* conformation.[20-25] As for the noncrystalline component, the characterization becomes more complicated because of the effects of the *gauche* conformation and it may be successful when the statistical treatment will be allowable for the formation of intramolecular hydrogen bonding and for the generation of the *gauche* conformation.[23-25] Here, we apply the CP/MAS ^{13}C NMR analysis established for A-PVA[20-25] to the highly isotactic PVA samples.

Figure 4-9 shows CP/MAS ^{13}C NMR spectra measured at room temperature for the PVA samples with different tacticities.   As expected, the CH resonance lines basically split into three constituent lines in the respective samples and the relative intensities are greatly altered depending on the tacticity. To separate the contributions from the crystalline and noncrystalline regions, ^{13}C spin-lattice relaxation behavior was measured at room temperature for each sample by the CPT1 pulse sequence as reported previously.[20-22,24,25] In accord with the results of the different A-PVA
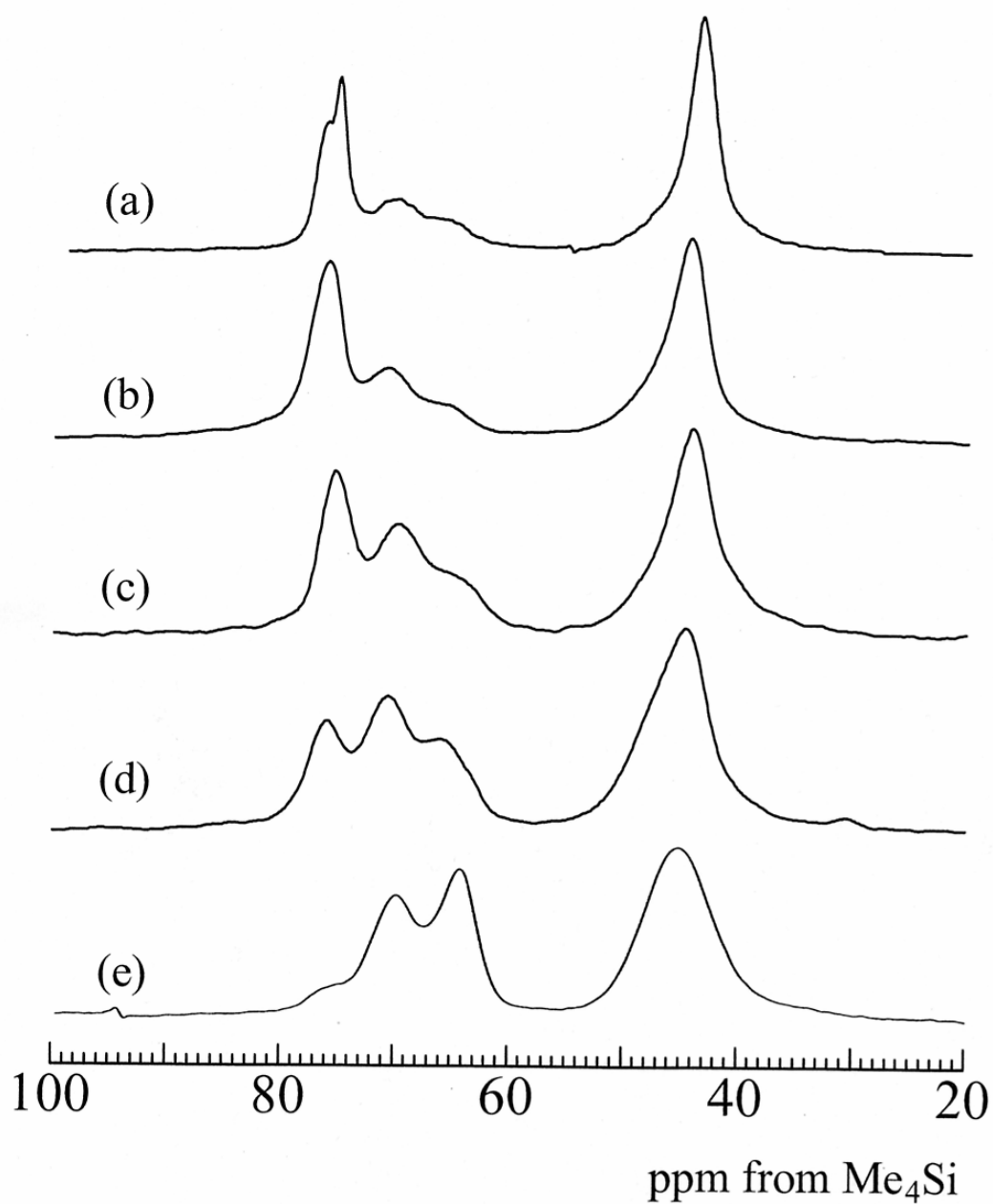
Figure 4-9. CP/MAS ^{13}C NMR spectra measured at room temperature for different stereoregular PVA samples: (a) HI-PVA (f_{mm}=0.79), (b) HI-PVA (f_{mm}=0.70), (c) LI-PVA (f_{mm}=0.59), (d) LI-PVA (f_{mm}=0.50), (e) A-PVA.

samples,[20-22,24,25] it was also found that there exist two components with different T_{1C} values for each sample. Since longer T_{1C} implies less molecular mobility for solid PVA under the present experimental condition, the components having a longer and shorter T_{1C} should be assigned to the crystalline and noncrystalline components, respectively, as the cases of A-PVA. [20-22,24,25]

Figure 4-10 shows a plot of the T_{1C} values of the crystalline components thus obtained for the CH lines as a function of the *mm* fraction.　In good accord with the cases of T_m and crystallinity shown in Figures 4-3 and 4-4, a clear minimum of the T_{1C} is also observed at an *mm* fraction of about 0.40. The *mm* fraction giving the T_{1C} minimum is somewhat lower than the corresponding fractions for T_m and crystallinity, probably suggesting that the T_{1C} may be affected not only by the crystallite size but also by the disordering extent of the structure. It should be, therefore, noted that the crystalline component may be more disordered in the sample with an *mm* fraction of about 0.40.　In contrast, the T_{1C} value of the HI-PVA sample having the highest *mm* fraction is as high as about 260 s, which is much higher than that of A-PVA or S-PVA.　This fact suggests that the crystalline chains of the HI-PVA may be much more rigid than those of S-PVA probably due to the successive formation of intramolecular hydrogen bonding since the crystallite size may be not significantly different from that of S-PVA.

As for the noncrystalline component, the T_{1C} value was found to be less than about 10 s for each sample regardless of the *mm* fraction.　Since the
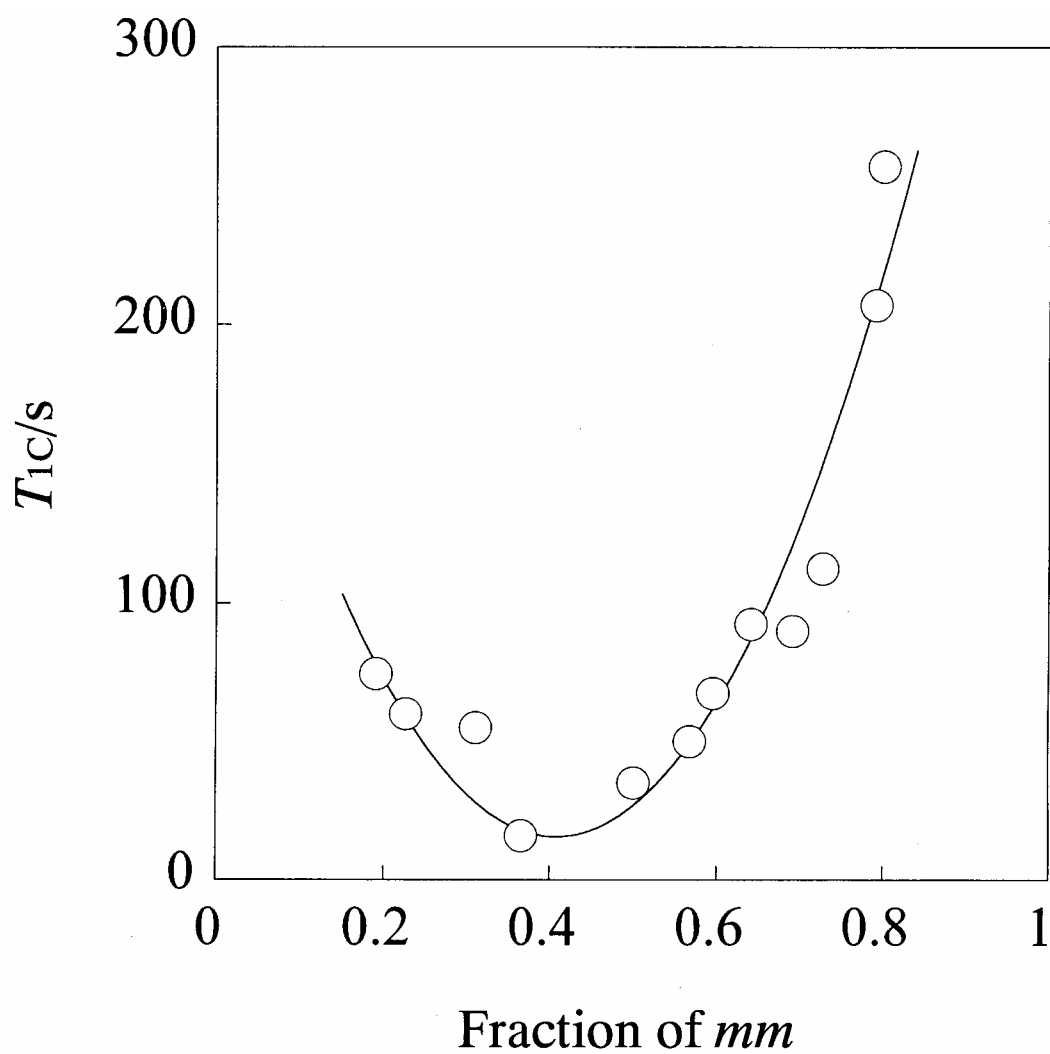
Figure 4-10. Relationship between the fraction of the mm sequence and the ^{13}C spin-lattice relaxation time (T_{1C}) for the crystalline component of different stereoregular PVA samples.

[13]C magnetization observed by the CPT1 pulse sequence[41] exponentially decays with increasing relaxation delay time τ, a certain resonance line disappears by setting the τ to a value larger than 5 times of the T_{1C} of the line. Using this fact, the T_{1C}–filtered spectrum of the crystalline component was selectively measured for each sample by the CPT1 pulse sequence with $\tau = 40\text{-}50$ s in the same way as for A-PVA.[20-22,24,25]

Figure 4-11 shows the spectra of the crystalline components thus obtained for the PVA samples shown in Figure 4-9. As already reported,[20-25] the CH resonance line of the crystalline component of A-PVA splits into three lines designated as lines I, II, and III, which are assigned to the CH carbons that are, respectively, associated with two, one, and no intramolecular hydrogen bond(s) in the triad sequences with the all-*trans* conformation. Interestingly, the relative intensity of line I is markedly increased with increasing *mm* fraction and only line I is observed for HI-PVAs having the *mm* fractions higher than 0.70. The latter fact seems to imply that the crystalline component of HI-PVA may be composed of the *mm* sequences having intramolecular hydrogen bonded OH groups. However, the degrees of crystallinity are at least as high as 0.4-0.5 for these samples as shown in Figure 4-4 and it must be, therefore, impossible to produce the crystalline chains composed of only the *m* units because of such a low *mm* fraction as 0.7.

Figure 4-12 shows two model PVA sequences composed of the *mmrmm* unit. The one shown in Figure 4-12(a) adopts the all-*trans* conformation and, therefore, intramolecular hydrogen bonding is not formed only in the *r*
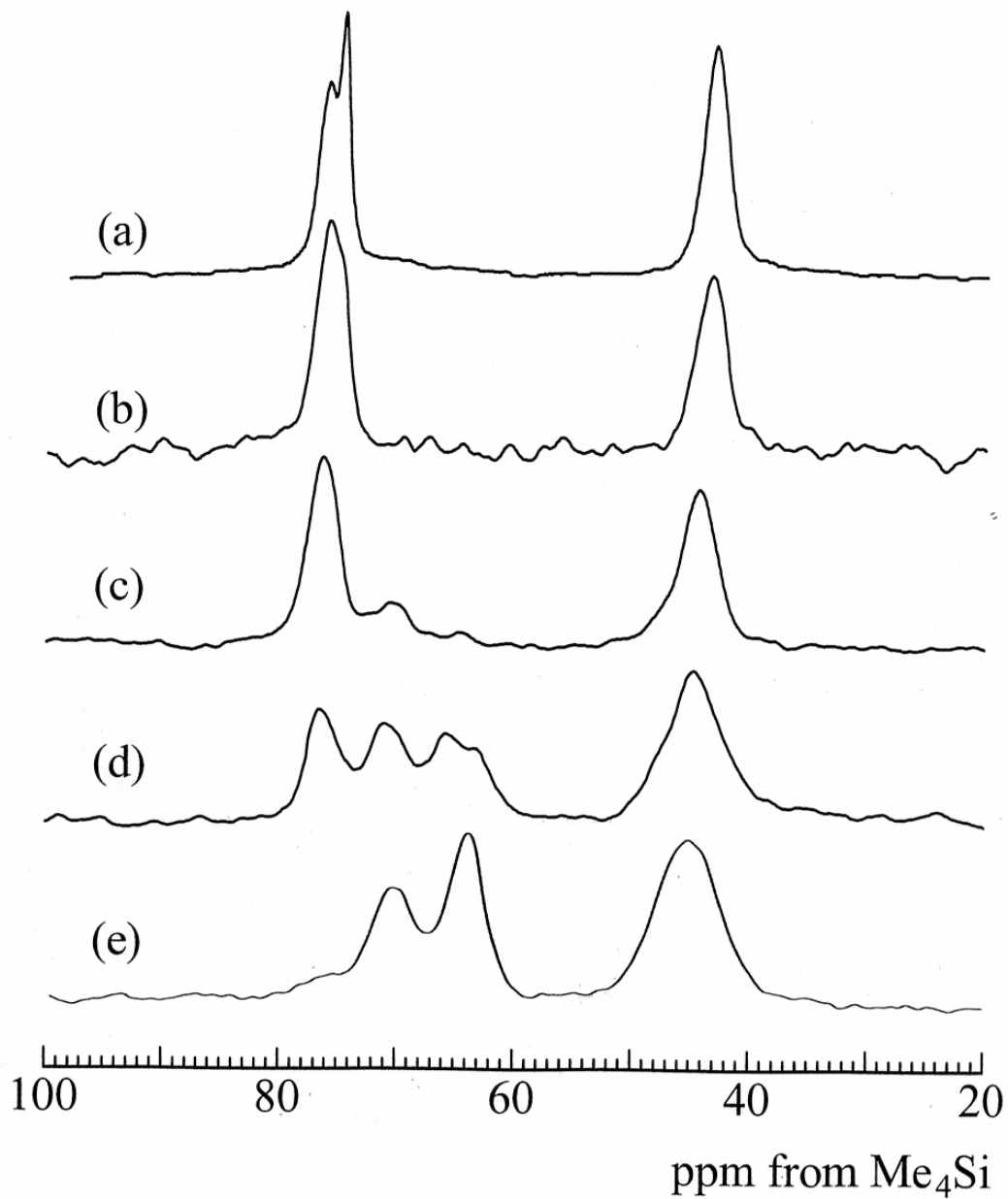
Figure 4-11. CP/MAS ^{13}C NMR spectra of the crystalline component of different stereoregular PVA samples : (a) HI-PVA (f_{mm}=0.79), (b) HI-PVA (f_{mm}=0.70), (c) LI-PVA (f_{mm}=0.59), (d) LI-PVA (f_{mm}=0.50), (e) A-PVA.

unit. In contrast, when the *gauche*$^+$ conformation is introduced to the CH-CH$_2$ bond in the *r* unit as shown in Figure 4-12(b), the same type of intramolecular hydrogen bonding is allowed to form even in the *r* unit. This fact seems to support the preferential appearance of line I for the crystalline component of HI-PVA, although a prominent kink of the molecular chain axis is produced by the introduction of the *gauche* conformation as already pointed out.[42] Moreover, such a kink will be readily cancelled out by the introduction of the *gauche*$^-$ conformation as a pair at another position along the chain.[42] However, when some amounts of the *gauche* conformations are introduced, the so-called *γ-gauche* effect[43] should induce about 5 ppm upfield shift for the CH$_2$ and CH carbons compared to the case of the *trans* conformation. Since such upfield shifts are not actually observed for the CH and CH$_2$ resonance lines as seen in Figure 4-11, normal types of *gauche* conformations should not be introduced in the crystalline region for HI-PVA although intramolecular hydrogen bonding must be really formed for all OH groups.

One possible way to overcome such difficulties is to set each torsion angle for each C-C bond to appropriate values that are not greatly deviated from the equilibrium value, 180 °, at the *trans* conformation so as to allow to form intramolecular hydrogen bonding even in the *r* units. The distributions in the torsion angle may be reasonably narrow and each chain must adopt a slightly helical structure with a considerably long period. Since the CH line designated as line I splits into two lines for HI-PVA as seen in Figure 4-11, two types of the helical structures may be produced in
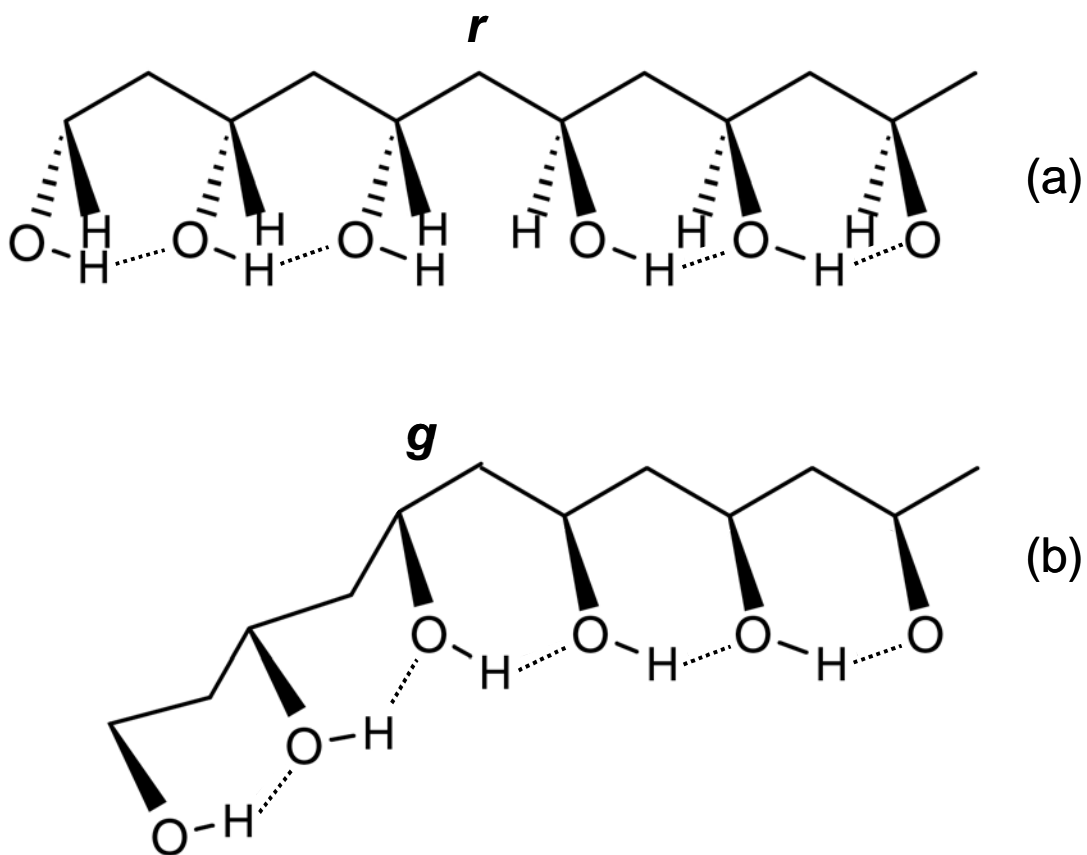
Figure 4-12.   Schematic representations of intramolecular hydrogen bonding forming for the *mmrmm* sequence with different conformations: (a) all-*trans* conformation, (b) disordered conformation containing *gauche* (*g*) in the *r* unit.

the crystalline region probably depending on the probability of the *r* units appearing along each chain. Moreover, an appreciable upfield shift observed for line I with increasing *mm* fraction suggests the decrease in the strength of intramolecular hydrogen bonding, which may be induced by the increase in the O···O distance due to the deviation from the *trans* conformation. An actual helical structure will be explicitly created by computer simulations for a single PVA chain or an assembly of the chains particularly by considering the formation of intramolecular hydrogen bonding for each OH group in near future.

The integrated fractions of lines I, II and III for the crystalline component, which were obtained by the lineshape analysis,[20-25] are plotted against the *mm* fraction in Figure 4-13.   Both of the integrated fractions of lines I and III are found to continuously change with the change of the *mm* fraction although their changes seem almost symmetric.   In contrast, the fraction of line II has a maximum at the *mm* fraction of about 0.4, which well corresponds to the *mm* fractions giving the minima of T_m, degree of crystallinity, and T_{1C} shown in Figures 4-3, 4-4, and 4-10, respectively. This fact suggests that the introduction of the *mr* units may induce significant disordering of the regular formation of intermolecular or intramolecular hydrogen bonding for the syndiotactic or isotactic sequences, respectively.   However, in such a case, the maximum of line II would appear at the *mm* fraction of 0.25, which corresponds to the maximum *mr* fraction of 0.50. The cause of the deviation of the *mm* fraction giving the maximum of line II from 0.25 to about 0.4 may be due to the fact that the
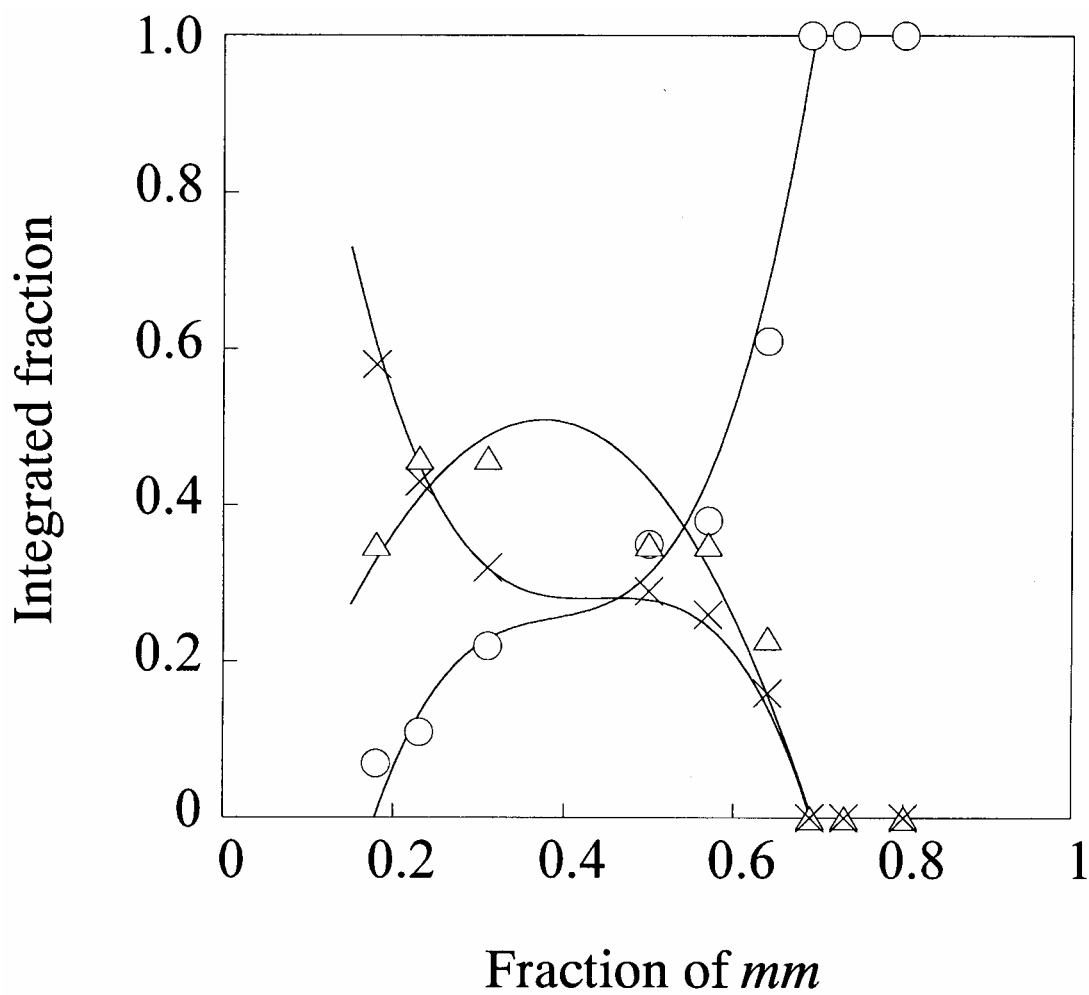
Figure 4-13. Relationships between the *mm* fraction and the integrated fractions of line I (circle), II (triangle) and III (cross) for the crystalline components of stereoregular PVA samples.

probability f_a of the formation of intramolecular hydrogen bonding in the *m* units will be less than 1.0.   In fact, f_a was estimated 0.56 and 0.85 for the crystalline and noncrystalline components of A-PVA, respectively.[25] Moreover, the deviation will become larger since the f_a value must be decreased with decreasing *mm* fraction.   It should be, therefore, concluded that the basic properties of stereoregular PVAs are mainly dominated by the formation or disordering of intermolecular and intramolecular hydrogen bonding in the polymer chains.

4.4. Conclusions

We have characterized the structure, hydrogen bonding and some basic physical properties as a function of the *mm* fraction for different stereoregular PVA films including highly isotactic PVAs, which were successfully synthesized by evaluation of the polymerization recently, by using different analytical methods, and obtained the following conclusions:

(1) It has been confirmed that the triad tacticities are well interpreted in terms of the Bovey's statistical model in the wide range of tacticity.   This fact suggests that the growing chain end and its penultimate unit may admit the statistically random addition reaction of the monomer irrespective of the difference in the polymerization methods used in this work.

(2) T_m, degree of crystallinity, and T_{1C} of the crystalline component have their own minima at the *mm* fraction of 0.4 - 0.5, implying that the decrease in crystallite size and the structural disordering may most significantly occur at this *mm* fraction.

(3) The appearance of a new crystalline band at about 1160 cm^{-1} in the FT IR spectra has reconfirmed the formation of a new type of crystal structure for isotacticity-rich PVA having the *mm* fractions higher than about 0.55, in good accord with the results previously obtained by wide-angle X-ray diffractometry. The relationship between the absorbance ratio, D_{916}/D_{849}, of the two bands and the syndiotacticity has been revised on the basis of the results of HI-PVA.

(4) The relative intensity for line I of the CH resonance line, which is assigned to the CH carbons associated with the formation of two intramolecular hydrogen bondings, is markedly increased with increasing *mm* fraction for the crystalline component and only line I is observed for HI-PVAs having the *mm* fractions higher than 0.70. This fact suggests that intramolecular hydrogen bonding is formed for all OH groups in the crystalline region for the HI-PVAs along the chains that contain some number of the *r* units and the respective chains may adopt a slightly helical structure with a considerably long period to allow the formation of such successive intramolecular hydrogen bonding.

(5) The lineshape analysis of the CH resonance lines of the crystalline components for the different stereoregular PVAs has revealed that the integrated fraction for line II, which is assigned to the CH carbons associated with one intramolecular hydrogen bonding in the *mm* or *mr* units, has a maximum at the *mm* fraction of about 0.4. Since this *mm* fraction well corresponds to the *mm* fraction giving the minima of T_m, degree of crystallinity and T_{1C}, it should be concluded that the disordering due to the

introduction of irregular hydrogen bonding into successive intramolecular or intermolecular hydrogen bonding along each chain may induce the decreases in these physical values relating to the crystallinity.

References

(1) Fujii, K. *J. Polym. Sci., Part D* **1971**, 5, 431.

(2) Finch, C. A. *Polyvinyl Alcohol-Developments*; John Wiley & Sons: New York, **1992**; Chapters 9 and 10.

(3) Finch, C. A. *Polyvinyl Alcohol*; John Wiley & Sons: New York, **1973**; Chapters 6 and 10.

(4) Murahasi, S.; Yuki, H.; Sano, T., Yonemura, U.; Tadokoro, T.; Chatani, Y. *J. Polym. Sci.* **1962**, 62, S77.

(5) Yuki, H.; Hatada, K.; Oda, K.; Kinoshita, Murahashi, S.; Ono, K.; Ito, Y. *J. Polym. Sci., Part A-1* **1969**, 7, 1517.

(6) Okamura, S.; Kodama, T.; Higashimura, T. *Makromol. Chem.* **1962**, 53, 180.

(7) Higashimura, T.; Suzuki, K.; Okamura, S. *Makromol. Chem.* **1965**, 86, 259.

(8) Murahashi, S.; Nozakura, S.; and Sumi, M. *J. Polym. Sci. Part B* **1965**, 3, 245.

(9) Murahashi, S.; Nozakura, S.; Sumi, M.; Yuki, H.; Hatada, K. *J. Polym. Sci., Polym. Lett. Ed.* **1966**, 4, 65; *Kobunshi Kagaku* **1966**, 23, 550.

(10) Ohgi, H.; Sato, T. *Macromolecules* **1993**, 26, 559.

(11) Ohgi, H.; Sato, T. *Macromolecules* **1999**, 8, 2403.

(12) Ohgi, H.; Sato, T. *Polymer* **2002**, 43, 3829.

(13) Horii, F.; Hu, S.; Deguchi, K.; Sugisawa, H.; Ohgi, H.; Sato, T. *Macromolecules* **1996**, 29, 3330.

(14) Yamamoto, T.; Yoda, S.; Takase, H.; Sangen. O.; Fukae. R.; Kamachi, M.; Sato, T. *Polym. J.* **1991**, 23, 185.

(15) Finch, C. A. *Polyvinyl Alcohol-Developments*; John Wiley & Sons: New York, **1992**, p. 757.

(16) Nakajima, A. *Kobunshi Kagaku* **1949**, 6, 451.

(17) Moritani, T.; Kuruma, I.; Shibatani, K.; Fujiwara, Y. *Macromolecules* **1972**, 5, 577.

(18) DeMember, J. R.; Haas, H. C.; MacDonald, R. L. *J. Polym. Sci., Polym. Lett. Ed.* **1972**, 10, 385.

(19) Horii, F.; Hirai, A.; Kitamaru, R.; Sakurada. I. *Cellulose Chem. Technol.* **1985**, 19, 513.

(20) Horii, F.; Hu, S.; Ito, T.; Odani, H.; Kitamaru, R.; Matsuzawa, S.; Yamaura, K. *Polymer* **1992,** 33, 2299.

(21) Hu, S.; Horii, F.; Odani, H.; Narukawa, H.; Akiyama, A.; Kajitani, K. *Kobunshi Ronbunshu* **1992**, 49, 361.

(22) Hu, S.; Tsuji, M.; Horii, F. *Polymer* **1994**, 35, 2516.

(23) Masuda, K.; Horii, F. *Macromolecules* **1998**, 31, 5810.

(24) Masuda, K.; Kaji, H.; Horii, F. *Polym. J.* **1999**, 31, 105.

(25) Masuda, K.; Kaji, H.; Horii, F. *J. Polym. Sci., Part B: Polym. Phys.* **2000**, 38, 1060.

(26) Ouchi, M.; Kamigaito, M.; Sawamoto, M. *J. Polym. Sci. Part A* **2001**,

39, 1060.

(27) Bovey, F. A.; Tiers, G. V. D. *J. Polym. Sci.* **1960**, 44, 173.

(28) Tubbs, R. K. *J. Polym. Sci.* **1965**, 3, 4181.

(29) Holland, B. J.; Hay, J. N. *Polymer* **2001**, 42, 6775 and references therein.

(30) Cooney, T. F.; Wang, L.; Sharma, S. K.; Gauldie, R. W.; Montana, A. J. *J. Polym. Sci.: Part B: Polym. Phys.* **1994,** 32, 1163 and references therein.

(31) Murahashi, S. *Pure Appl. Chem.* **1967**, 15, 435 and references therein.

(32) Sugiura, K.; Hashimoto, M.; Matsuzawa, S.; Yamaura, K. *J. Appl. Polym. Sci.* **2001**, 82, 1291 and references therein.

(33) Fujii, K.; Fujiwara Y.; Brownstein, S. *Prepr. 17th Polym. Symp. (Matsuyama, Japan)* **1968**, 1111.

(34) Tsuji, H.; Horii, F.; Nakagawa, M.; Ikada, Y.; Odani, H.; Kitamaru, R.; *Macromolecules* **1992**, *25*, 4114.

(35) Ishida, H.; Kaji, H.; Horii, F., *Macromolecules* **1997**, *30*, 5799.

(36) Kuwabara, K.; Kaji, H.; Horii, F.; Bassett, D. C.; Olley, R. H., *Macromolecules* **1997**, *30*, 7516.

(37) Kuwabara, K.; Kaji, H.; Horii, F. *Macromolecules* **2000**, *33*, 4453.

(38) Ohira, Y.; Horii, F.; Nakaoki, T. *Macromolecules* **2000**, *33*, 5566.

(39) Ohira, Y.; Horii, F.; Nakaoki, T. *Macromolecules* **2001**, *34*, 1655.

(40) Murakami, M.; Ishida, H.; Miyazaki, M.; Kaji, H.; Horii, F. *Macromolecules*, **2003**, 36, 4160.

(41) Torchia, D. A. *J. Magn. Reson*. **1978**, 30, 613.

(42) Assender, H. E.;Windle, A. H. *Polymer*, **1998**, 39, 4303.

(43) Tonelli, A. E. *NMR Spectroscopy and Polymer Microstructure: The Conformational Connection*; VCH: New York, 1989.

Chapter 5

Solid-State ^{13}C NMR Investigation of the Structure and Hydrogen Bonding for Stereoregular Poly(vinyl alcohol) Films in the Hydrated State

5.1. Introduction

As described in Chapter 2, we studied the cationic polymerization of *t*BVE with boron trifluoride diethyl etherate (BF$_3$·OEt$_2$) and successfully prepared the PVAs having the highest isotacticity so far reported.[1-12]   We found interesting features of these highly isotactic PVAs (HI-PVAs) being different from those of LI-PVA and ordinary atactic PVA (A-PVA).[10,13,14] In particular, as described in Chapter 4, we compared the melting temperatures T_m, degrees of crystallinity χ_c, and ^{13}C spin-lattice relaxation times T_{1C} of the crystalline components for PVA samples with different tacticities (including HI-PVA) to find that these physical quantities show clear minima at the *mm* fraction (f_{mm}) of 0.4-0.5 when plotted against the *mm* fraction.[14]   This result suggests that the structural disordering associated with the decrease in the crystallinity occurs most significantly in this *mm* range.   In relation to these minima, FT IR spectroscopy confirmed the formation of the new crystal form for HI-PVAs with f_{mm}>0.55 and solid-state ^{13}C NMR spectroscopy revealed that all OH groups are allowed to form successive intramolecular hydrogen bonding along the respective

104

chains in the crystalline region for HI-PVAs with f_{mm}>0.7.

As described above, the solid-state ^{13}C NMR analyses are powerful for the characterization of hydrogen bonding of PVA in the solid state.　On the other hand, the characterization of hydrogen bonding in the hydrated state of PVA should be also very important, because the characteristic properties and functions of some application of PVA, e.g., hydrogels, may greatly depend on their hydrogen-bonded states.　In a previous paper,[15] the hydration process and resulting hydrogen bonding for A-PVA films have been investigated by the solid-state ^{13}C NMR analysis.　It was found that there were three components with different T_{1C} values assigned to the crystalline, less mobile, and mobile components in the hydrated A-PVA films.　In the crystalline component, the probability f_a of the formation of intramolecular hydrogen bonding is significantly increased by the addition of water.　In the less mobile component, two types of hydrogen bonds are found to still remain even in the presence of water but the *gauche* fraction greatly increases compared to the case in the dried state due to breaking of hydrogen bonding, and the mobile component is subjected to rapid exchanges among different conformations and hydrogen bonds.　Moreover, the analysis of the mole fractions of the *mm*, *mr*, and *rr* sequences obtained for the mobile component indicates that the different triad structural units are almost equally distributed in the crystalline and noncrystalline regions for A-PVA.

In this chapter, we apply similar ^{13}C NMR analyses to the characterization of the structure and hydrogen bonding for the hydrated

HI-PVA and syndiotactic PVA (S-PVA) films. We also investigate the possibility of the partitioning of the different triad sequences into the crystalline and noncrystalline regions in these samples by selectively measuring the triad tacticities for the mobile components that are produced by swelling with water. The clarification of such partitioning is very important to understand the molecular motion in the noncrystalline region for stereoregular PVA samples in relation to the triad tacticity.[16]

5.2. Experimental Section

5.2.1. Preparation of stereoregular PVAs

HI-PVA was synthesized by the procedure which is described in Chapter 2. The commercially available A-PVA derived from poly(vinyl acetate) and syndiotacticitiy-rich PVA (S-PVA) derived from poly(vinyl pivalate) were also used as reference samples.

5.2.2. Stereoregularities of PVA samples

The stereoregularity of PVA samples was determined from solution-state ^{1}H NMR spectroscopy on the basis of the methods reported previously.[18,19] The triad tacticities are as follows: HI-PVA (f_{mm}=0.78, f_{mr}=0.20, f_{rr}=0.03), A-PVA (0.23, 0.50, 0.27), S-PVA (0.14, 0.48, 0.38).

5.2.3. Preparation and hydration of PVA films

Each PVA films were prepared by the same procedure which is described in Chapter 4. The respective films were further subjected to annealing at

200 and 40 °C for 10 min under vacuum, respectively. Hydrated stereoregular PVA films for solid-state ^{13}C NMR measurements were prepared by soaking the annealed PVA films in distilled water for 24 hr, gently pressed with filter papers, and then packed into the MAS rotor with an O-ring seal to avoid the loss of water during NMR measurements.[20,21] The water contents were about 0.72g-water/g-PVA for the hydrated HI-PVA films and about 0.80g-water/g-PVA for the hydrated S-PVA films.

5.2.4. Solid-state ^{13}C NMR spectroscopy

Cross polarization/magic angle spinning (CP/MAS) ^{13}C NMR spectroscopy was performed by the same procedure which is described in Chapter 4. The detailed procedure of the solid-state ^{13}C NMR measurements was almost the same as described in the previous papers.[15,20-26]

5.3. Results and Discussion
5.3.1. Structure and hydrogen bonding of the hydrated films

Figure 5-1a shows a fully relaxed dipolar decoupling (DD)/MAS ^{13}C NMR spectrum measured for the hydrated S-PVA films with a water content of 0.80g-H_2O/g-PVA by the $\pi/4$ single sequence with a pulse delay time of 50 s. A sharp triplet is clearly observed for the CH resonance line and the constituent lines are assigned to the CH carbons in the *mm*, *mr* and *rr* triad sequences in the order of decreasing chemical shift value. These lines appear as a highly mobile component which is produced in the
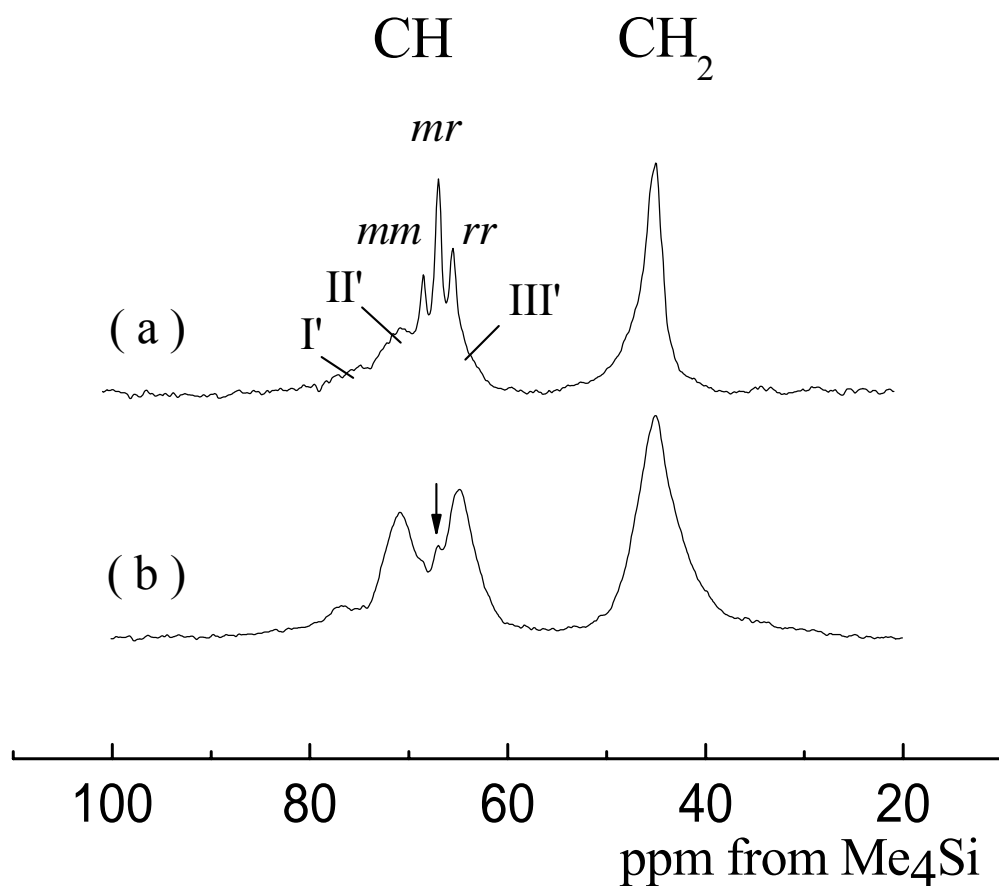
Figure 5-1. High-resolution solid-state ^{13}C NMR spectra of the hydrated S-PVA films: (a) Fully relaxed DD/MAS ^{13}C NMR spectrum obtained by the $\pi/4$ single sequence with a pulse delay time of 50 s, (b) CP/MAS ^{13}C NMR spectrum measured at a CP contact time of 0.8 ms. The arrow indicates the small contribution from the *mr* sequences.

noncrystalline region by the addition of water. As already reported for solid PVA samples,[14,15,21-26] the CH resonance line splits into three lines, lines I', II' and III', which are mainly composed of the contributions from lines I, II and III in the spectrum of the crystalline component. These latter lines are, respectively, assigned to the CH carbons that are associated with two, one and no intramolecular hydrogen bond(s) in the triad sequences with the all-*trans* conformation. Lines I' and II' are also observed in this S-PVA sample but line III' may be superposed on the contribution from the mobile component. In contrast, lines I', II' and III' are evidently observed in the CP/MAS ^{13}C NMR spectrum as shown in Figure 5-1b because the CP efficiency is much higher for the components with less molecular mobility. As for the mobile component, only a small peak as indicated by an arrow appears in this spectrum, which is ascribed to the CH carbons in the *mr* sequence. From these spectra, it is found that there are at least two components with different molecular mobilities in the hydrated S-PVA films, being in good agreement with the case for the hydrated A-PVA films.[15]

Figure 5-2a shows a fully relaxed DD/MAS ^{13}C NMR spectrum of the hydrated HI-PVA films with a water content of 0.72g-H_2O/g-PVA obtained by the $\pi/4$ single sequence with a pulse delay time of 50 s. Three lines assigned to the CH carbons in the *mm, mr* and *rr* triad sequences are also clearly observed for the CH resonance line and their relative intensities are greatly different from those for S-PVA shown in Figure 5-1a as a result of high isotacticity of HI-PVA. However, only one line that corresponds to
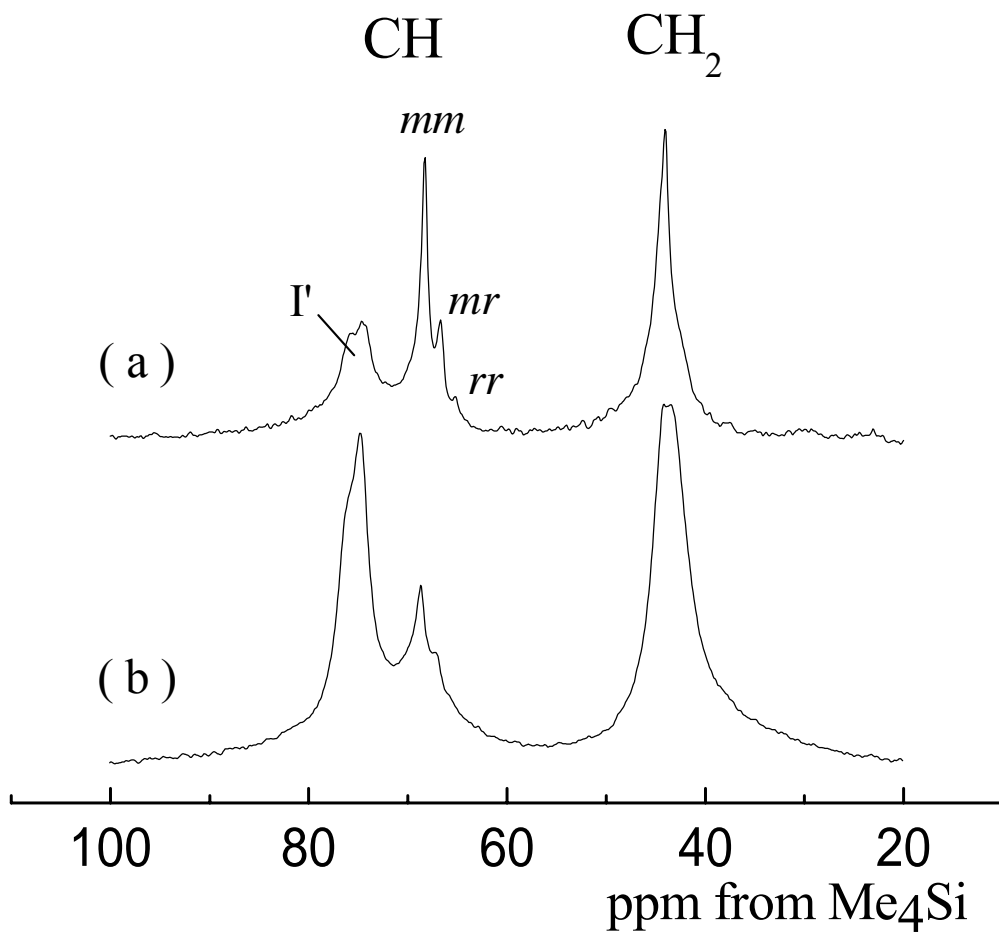
Figure 5-2. High-resolution solid-state ^{13}C NMR spectra of the hydrated HI-PVA films: (a) Fully relaxed DD/MAS ^{13}C NMR spectrum obtained by the $\pi/4$ single sequence with a pulse delay time of 50 s, (b) CP/MAS ^{13}C NMR spectrum.

line I' can be observed in this sample, and this line splits into two lines in good accord with the spectrum for the dried HI-PVA sample, reflecting the features of the crystal structure of HI-PVA.[14] It is still difficult to recognize the contributions from lines II' and III' even in the CP/MAS spectrum shown in Figure 5-2b probably due to their low mass fractions as indicated in detail later.

To obtain detailed information about the different components probably included in the hydrated stereoregular PVA films, the T_{1C} relaxation behavior has been measured for these samples at room temperature by the saturation recovery pulse sequence modified for solid-state measurements.[27,28] Figure 5-3 shows the saturation recovery process of the integrated intensities of the whole CH line over the region from 55 to 85 ppm for the hydrated S-PVA films as a function of the delay time (τ) for the T_{1C} relaxation. It is clearly found by the computer-aided least-squares method that the saturation recovery curve, indicated as open squares, is composed of three components with different T_{1C} values that are designated by dotted lines. The component with the largest T_{1C} value (21.2 s) should be assigned to the crystalline component, because a larger T_{1C} value implies less molecular mobility under the present experimental condition. The component with the smallest T_{1C} value (0.095 s) can be readily assigned to the mobile component in the noncrystalline region because this component corresponds to the sharp CH triplet appearing at shorter relaxation delay times. In addition, the component with the medium T_{1C} value (1.42 s) is referred to as the less mobile component according to a previously reported
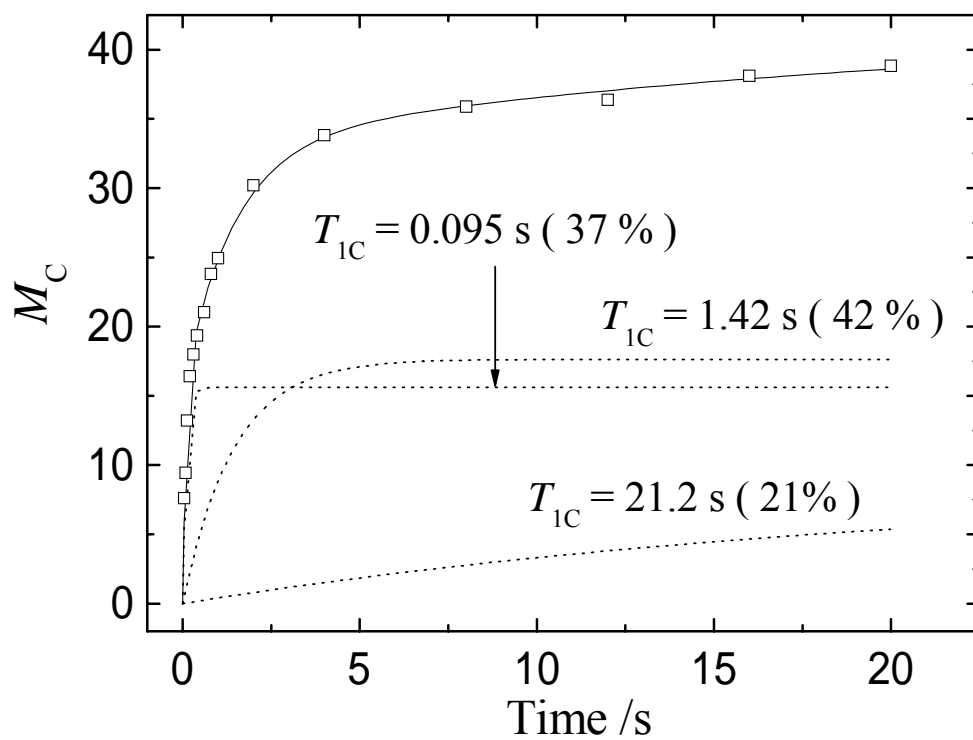
111

Figure 5-3. The saturation recovery process of the integrated intensity for the CH resonance line of the hydrated S-PVA films as a function of the T_{1C} delay time.

paper.[15]   Since the integrated intensity is plotted against the τ value in Figure 5-3, the mass fractions of the respective components, which are shown in parentheses in the figure, are also obtained by this T_{1C} analysis. The degree of crystallinity, which is estimated as mass fraction of the largest T_{1C} component, is 0.21 in this hydrated sample, while the mass fractions of the mobile and less mobile components are as considerably high as 0.37 and 0.42, respectively.

In Figure 5-4, the saturation recovery process is also shown for the integrated intensity of the CH resonance line for the hydrated HI-PVA films. Similar three components with different T_{1C} values are evidently observed in this sample; the crystalline (T_{1C}=19.6s), less mobile (T_{1C}=1.1s), and mobile (T_{1C}=0.063s) components in good accord with the results for the hydrated A- and S-PVA samples.   The degree of crystallinity is found to be as rather high as 0.41 in HI-PVA, whereas the mass fraction of the mobile component remains still high as 0.44.   The T_{1C} values of the CH and CH_2 resonance lines thus obtained for different hydrated PVA films including A-PVA are summarized in Table 5-1.   For comparison, the corresponding T_{1C} values are also listed for the dried stereoregular PVA films in Table 5-1.

The very small T_{1C} values for the mobile component appearing in all stereoregular PVA samples shown in Table 5-1 are due to enhanced molecular motion probably allowed by the occurrence of the rapid exchange among the hydrogen-bonded and free OH groups that are induced by the hydration in the noncrystalline region.   The T_{1C} values of the
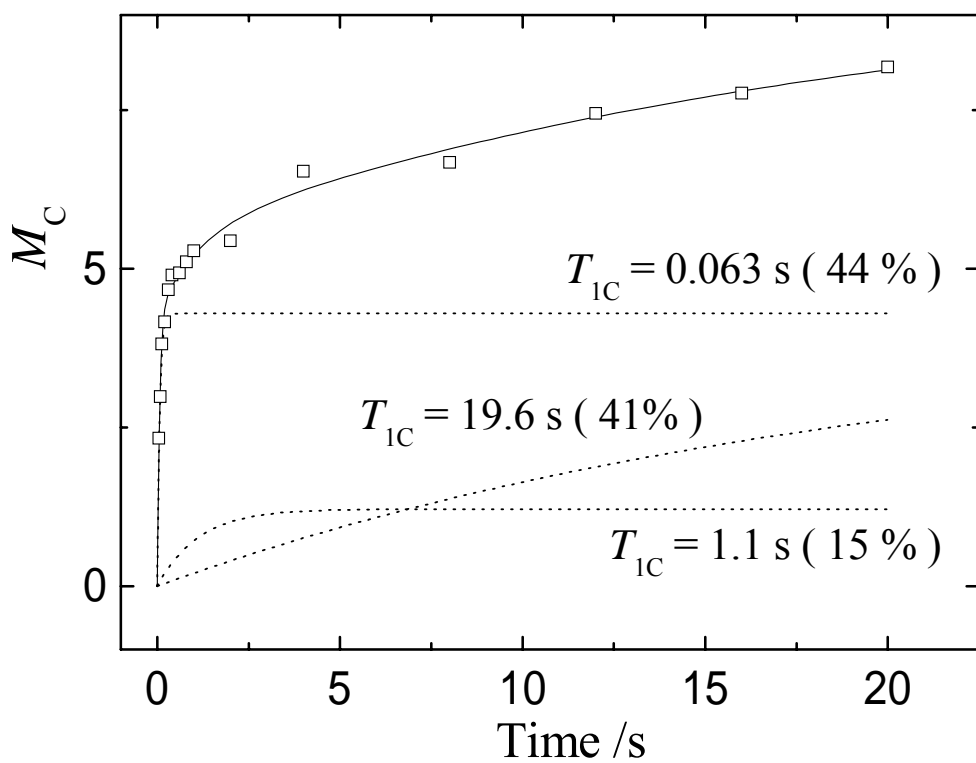
Figure 5-4. The saturation recovery process of the integrated intensity for the CH resonance line of the hydrated HI-PVA films as a function of the T_{1C} delay time.

Table 5-1. ^{13}C spin-lattice relaxation times of the respective resonance lines for the stereoregular PVA films measured at room temperature.

Samples	T_{1C} / s			
	CH			CH$_2$
	I'	II'	III'	
Hydrated[a]				
HI-PVA	19.6(0.41), 1.1(0.15), 0.063(0.44)			23.2(0.35), 1.3(0.25), 0.090(0.40)
A-PVA[b]	10.3(0.35), 1.0(0.24), 0.04(0.41)			--[e]
S-PVA	21.2(0.21), 1.42(0.42), 0.095(0.37)			11.2(0.22), 0.59(0.35), 0.067(0.43)[f]
Dried[c]				
HI-PVA	41.1, 6.1	--[e]	--[e]	39.8, 4.5
A-PVA[d]	56.3, 7.2, -	59.5, 15.4, 4.7	65.2, 14.7, 3.4	65.1, 12.4, 1.9
S-PVA	--[e]	36.5, 3.8	56.7, 5.0	43.7, 4.0

[a] Obtained by the saturation recovery method. [b] Previously obtained.[15] [c] Obtained by the CPT1 method.[30] [d] Previously obtained.[26] [e] not estimated. [f] The values in parentheses are the mass fractions of the respective components with different T_{1C} values.

crystalline components for the hydrated HI-PVA and S-PVA samples are also found to decrease to about half values of the dried samples, indicating enhancement in molecular mobility even in the crystalline region by the hydration. It should be also noted that the T_{1C} value for the hydrated A-PVA greatly decreases to 10.3s from about 60s for the dried sample. These results suggest that the crystalline chains of HI-PVA and S-PVA may be much more rigid than those of A-PVA even in the hydrated state because strong intramolecular or intermolecular hydrogen bonding may be successively formed along the chains for HI-PVA or for S-PVA, respectively. In fact, the CH resonance lines ascribed for the formation of these hydrogen bondings are clearly confirmed for the crystalline components in the hydrated HI-PVA and S-PVA samples as shown later in Figures 5-5 and 5-6.

On the basis of the T_{1C} measurements shown in Figures 5-3 and 5-4, the high-resolution ^{13}C NMR spectra of the respective components can be separately recorded mainly by using the T_{1C} filtering method. Namely, the spectra of the crystalline and mobile components were selectively obtained by the CPT1 pulse sequence with τ=10s and by the saturation recovery pulse sequence with τ=0.6ms, respectively.[30] Moreover, the spectrum of the less mobile component was recorded by subtracting the spectrum of the crystalline component from the spectrum measured by the CPT1 pulse sequence with τ=1s. Figure 5-5 shows the CH resonance lines for the crystalline, less mobile and mobile components thus obtained for the hydrated S-PVA films. The results of the line shape analyses are also
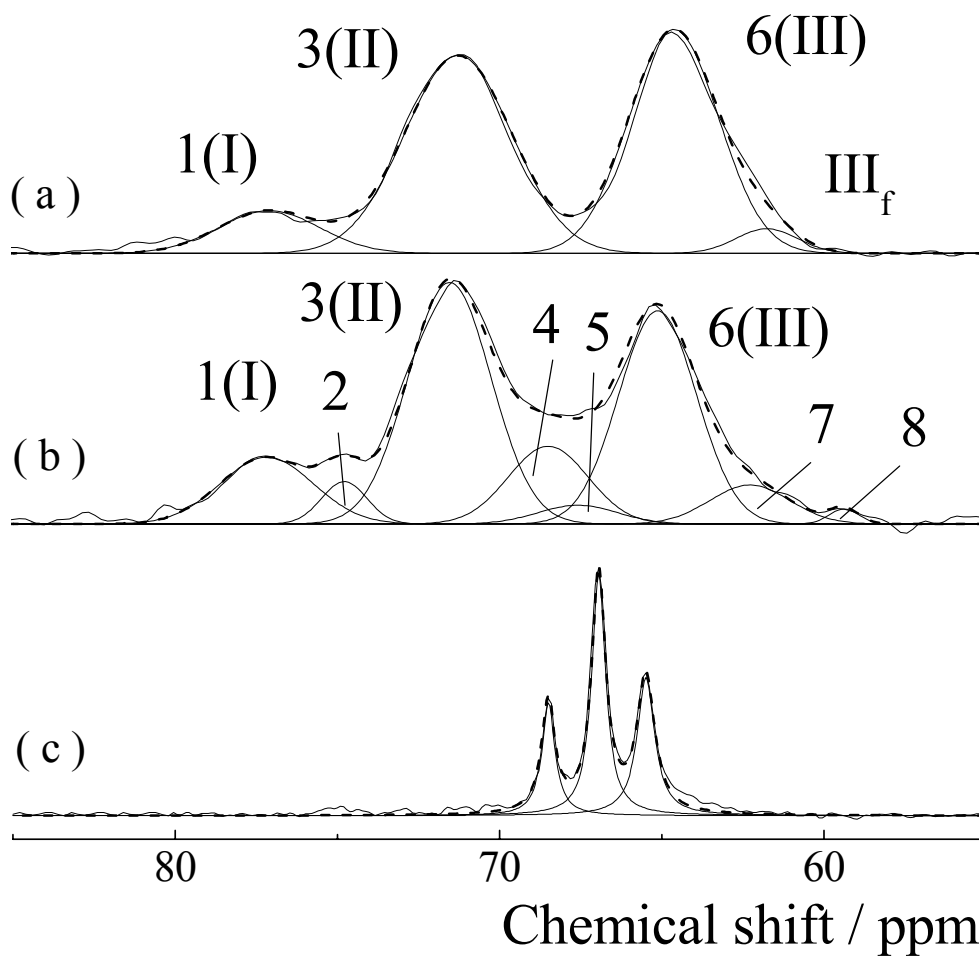
Figure 5-5. High-resolution solid-state ^{13}C NMR spectra of the different components measured for the hydrated S-PVA films at room temperature: (a) crystalline, (b) less mobile, (c) mobile.

shown for each component in this figure. Here, each constituent line was assumed to be a Gaussian for the crystalline and less mobile components according to the method that was originally established for the frozen PVA solutions,[24] and successfully applied to different solid PVA samples.[14,15,26,29] In contrast, three Lorentzian curves were assumed for the triplet of the mobile component. The composite curve designated as a broken line is in good accord with the observed curve depicted by solid line in each component. As for the crystalline component shown in Figure 5-5a, lines I, II and III that correspond to constituent lines 1, 3 and 6 in that line shape analysis,[24] are also clearly observed in the hydrated state as expected for the chains with all-*trans* conformation. In addition, a minor Gaussian contribution referred to as III$_f$ is found to exist in the most upfield region. This contribution should be assigned to the CH carbons associated with the OH groups free from any hydrogen bonding as already reported for the hydrated A-PVA samples.[15,21]

A similar line shape analysis was successfully applied to the less mobile component as shown in Figure 5-5b. Interestingly, the main contributions are also lines I, II and III in this component and additional smaller lines 2, 4, 5, 7 and 8 appear as a result of the introduction of the *gauche* conformations. This fact indicates that the fraction of the *trans* conformation is considerably high in this component probably because this component may form the transitional (or interfacial) region that locates between the highly chain-oriented crystalline region and the conformationally randomized amorphous region. Accordingly, the low

molecular mobility of this component induced by the addition of water may be mainly due to the restriction in conformation in the interfacial region. In contrast, the mobile component is subjected to enhanced random motion like the chains in the dissolved state, leading to the observation of the triplet ascribed to the *mm*, *mr* and *rr* sequences as shown in Figure 5-5c. The respective triad fractions were determined from the integrated intensities obtained by the line shape analysis and discussed in detail later.

Figure 5-6 shows the ^{13}C NMR spectra of similar three components separately obtained for the hydrated HI-PVA films by almost the same method used for the hydrated S-PVA sample. As shown in Figure 5-6a, only line I is observed in the crystalline component in good accord with the case of the dried films.[14] This result also suggests that all OH groups are allowed to form successive intramolecular hydrogen bonding along the respective chains in the crystalline region even for the hydrated sample. Since these chains should contain some amount of *r* units even in the crystalline region, a slightly helical structure with a considerably long period may be adopted by them as previously pointed out for the dried sample.[14] Moreover, splitting of line I into two lines also suggests the existence of two types of the helical structures that may be produced in the crystalline region probably depending on the probability of the *r* units appearing along each chain.[14]

As for the less mobile component shown in Figure 5-6b, the CH resonance line seems very similar to that of the crystalline component including the splitting, though additional minor contributions are also
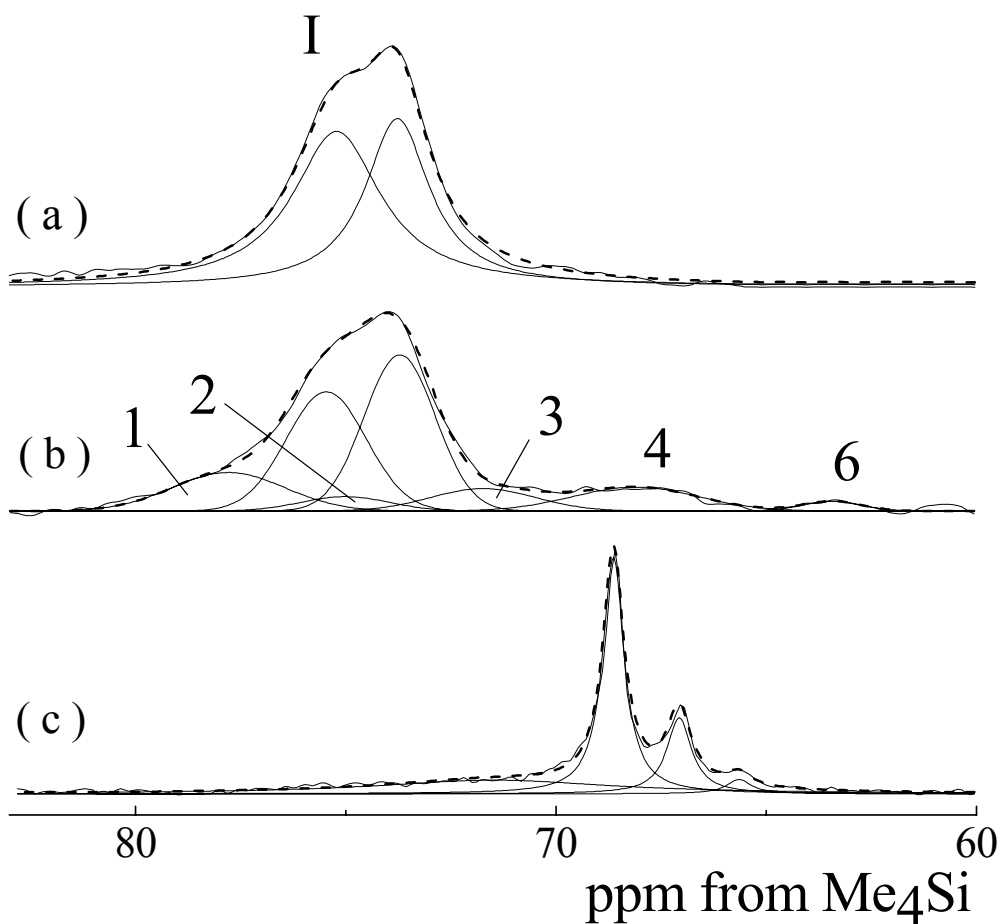
Figure 5-6. High-resolution solid-state ^{13}C NMR spectra of the different components measured for the hydrated HI-PVA films at room temperature: (a) crystalline, (b) less mobile, (c) mobile. The broad Lorentzian contribution at the downfield side is assigned to the less mobile component partially relaxed due to the relatively small T_{1C} value.

observed in the downfield and upfield sides. Therefore, the line shape analysis was made by additionally introducing two contributions corresponding to the two lines in the crystalline component. However, Gaussian curves were assumed for these two lines in the less mobile component whereas Lorentzian curves were employed for the crystalline component. The composite curve indicated by the broken curve is also in good agreement with the observed curve depicted by the solid line in this case. This result indicates that almost the same slightly helical structure should be formed in the interfacial region and the successive formation of strong intramolecular hydrogen bonding allows the formation of such a helical structure even in the hydrated state. It is also highly plausible to assume that the helical structure may be gradually disordered along each chain with increasing distance from the surface of the crystallite by the introduction of the *gauche* conformation and the breaking of successive intramolecular hydrogen bonding as a result of the solvation of water molecules. Finally, the chain segments are completely randomized in conformation and hydrogen bonding to contribute to the mobile component, which is observed as a triplet shown in Figure 5-6c.

Figure 5-7 shows the experimental integrated intensities (solid histograms) for the 9 constituent lines obtained for the crystalline and less mobile components of the hydrated S-PVA films by the line shape analysis shown in Figure 5-5 and statistically calculated intensities (open histograms) that were obtained so as to fit the experimental intensities by the least-squares method. Here, the calculated intensities were obtained

(a) crystalline

$f_t = 1.00$

$f_a = 0.85$

Intensity

Constituent lines

(b) less mobile

$f_t = 0.91$

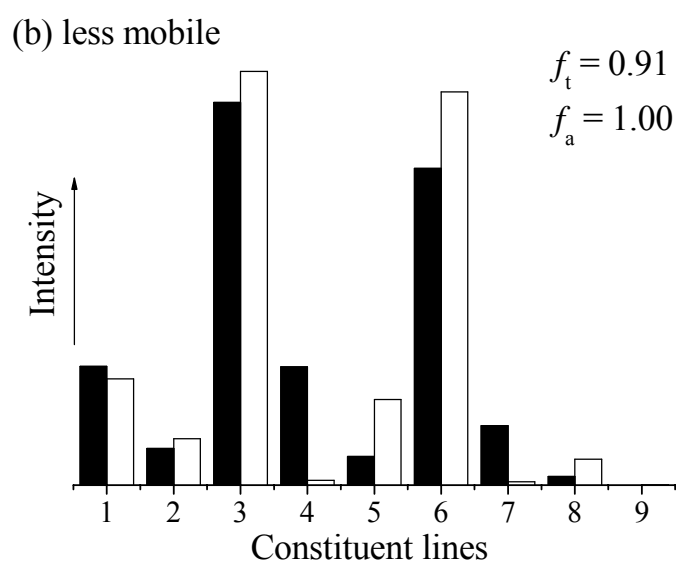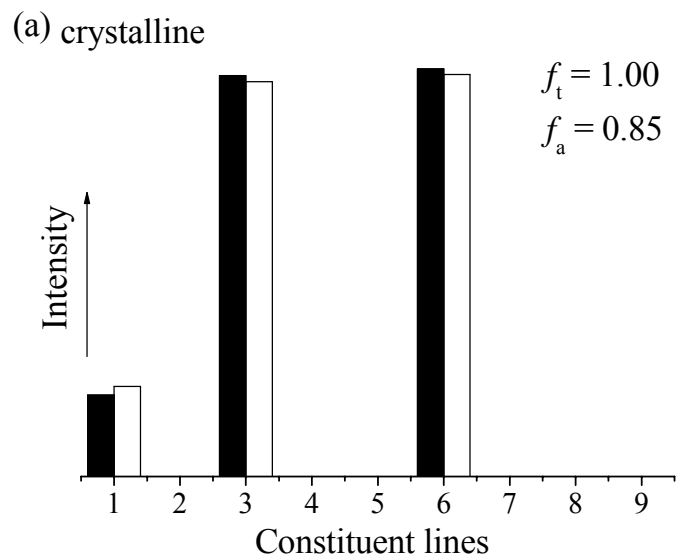$f_a = 1.00$

Intensity

Constituent lines

Figure 5-7. Histograms for the observed and calculated relative intensities of the nine constituent lines of each component for the hydrated S-PVA films: (a) crystalline, (b) less mobile.

by using the equations previously derived by assuming the statistical occurrence of the *trans* and *gauche* conformations in the respective C-C bonds as well as the statistical formation of intramolecular and intermolecular hydrogen bonding in the possible successive two OH groups in the *m* or *r* units along the chain.[15]   In this case, it was also assumed that almost no preferential partitioning of the *mm*, *mr* and *rr* sequences may occur in the crystalline and noncrystalline regions.   This assumption is found to be reasonably held in the PVA samples used in this work as described later in detail.   The calculated intensities are in good accord with the experimental intensities for both crystalline and less mobile components as shown in Figure 5-7.   From these statistical treatments, we can determine the optimal probabilities f_t and f_a for the occurrence of the *trans* conformation in each C-C bond and for the formation of intramolecular hydrogen bonding in the possible *m* or *r* units as indicated in Figure 5-7.[15]

The f_t and f_a values obtained for the crystalline and noncrystalline components in different stereoregular PVA samples including the dried samples are listed in Table 5-2.   However, the statistical treatment to obtain these values could not be applied to the noncrystalline or less mobile component for the hydrated and dried HI-PVA films and also for the hydrated A-PVA films probably because the chains may not adopt completely statistical structure in conformation and hydrogen bonding in these components.   As already pointed out, the f_a value is 1.0 for the crystalline component of the hydrated or dried HI-PVA films because all

123

Table 5-2. The f_t and f_a values for different components of hydrated and dried stereoregular PVA films.

Samples	Crystalline		Noncrystalline	
	f_t	f_a	f_t	f_a
HI-PVA[a]				
Hydrated	1.0	1.0	-	-
Dried	1.0	1.0	-	-
A-PVA[b]				
Hydrated	1.0	0.84	-	-
Dried	1.0	0.67	0.92	0.97
S-PVA[a]				
Hydrated	1.0	0.85	$(0.91)^c$	$(1.0)^c$
Dried	1.0	0.80	0.82	1.0

[a] This work. [b] Previously obtained.[15] [c] The less mobile component.

OH groups form intramolecular hydrogen bonding irrespective of the m or r units keeping the almost all-*trans* conformation. Such a characteristic structure may be allowed by adopting a slightly helical chain structure and seems not to be significantly influenced by the hydration. The f_a values are still as large as 0.67 and 0.85 for the crystalline components in the dried A-PVA and S-PVA films, respectively. In particular, the intramolecular hydrogen bonding tends to form at a higher probability for the two OH groups in the m units in the high syndiotactic chains. Moreover, the increase in f_a by the hydration in these crystalline components indicates that water may promote the formation of the intramolecular hydrogen bonding in the m units by breaking the intermolecular hydrogen bonding. This fact also implies that small amount of water molecules can penetrate into the crystalline region, as separately confirmed by the H-D exchange of the OH groups in the crystalline region observed by the immersion of the A-PVA films in D_2O.[15] In addition, such changes in hydrogen bonding will also induce the enhanced molecular motion as indicated by the decrease in T_{1C} for the hydrated films as shown in Table 5-1.

As for the noncrystalline components, the f_a values further increase to almost 1.0 for the dried A-PVA and S-PVA films. This indicates that the intramolecular hydrogen bonding is energetically more stable than the intermolecular hydrogen bonding in the m or r units in the dried noncrystalline region. It should be also noted that such features of hydrogen bonding seems to be also kept in the less mobile component for S-PVA that is produced by the hydration. Moreover, the increase in f_t

value to 0.91 for the less mobile component clearly supports that this component should be ascribed to the contribution from the interfacial region locating between the highly chain-oriented crystalline region and completely conformationally randomized amorphous region.

5.3.2. Partitioning of the *mm*, *mr* and *rr* units in the crystalline and noncrystalline regions

As described in Chapter 6, dynamic viscoelasticities of different stereoregular PVA films were investigated to elucidate the effect of the stereoregularity on the molecular motion of the PVA chains.[16]   The local twisting motion (β_a dispersion) and micro-Brownian motion (α_a dispersion) of the respective chains in the noncrystalline region were found to occur at almost the same temperatures for the PVA films having various stereoregularities (f_{mm}=0.14-0.78).   Such *mm*-insensitivity of the α_a and β_a dispersions is a somewhat great surprise because the stereoregularity would affect the mobility of the noncrystalline chains.   One possible origin of the insensitivity may be the enrichment of the stereoregular units (either *m* or *r* units) of the PVA chains in the crystalline region and the resulting reduction in the difference of the stereoregularities in the noncrystalline region of the PVA samples.   To examine this possibility, we estimated the mole fractions of the *mm, mr* and *rr* sequences for the mobile components that are produced in the stereoregular PVA films by swelling with water as described above.

The mole fractions of the *mm, mr* and *rr* sequences of the mobile

Table 5-3. Comparison between the triad tacticities for the mobile components that are produced in different stereoregular PVA films by the addition of water and their total values.

Samples		Triad tacticity		
		mm	*mr*	*rr*
HI-PVA	Total[b]	0.78	0.20	0.03
	Mobile[c]	0.70	0.26	0.04
A-PVA[a]	Total[b]	0.23	0.50	0.27
	Mobile[c]	0.24	0.50	0.26
S-PVA	Total[b]	0.14	0.48	0.38
	Mobile[c]	0.21	0.46	0.33

[a] Previously obtained.[15] [b] Determined in solution by ^{1}H NMR spectroscopy as described in the experimental section. [c] Determined for the mobile component that is produced in each sample by swelling with water as described in the text.

127

components determined for the hydrated HI-PVA and S-PVA films are summarized in Table 5-3 together with the results for the hydrated A-PVA films previously obtained.[15]   Here, the total values of the triad tacticities, which were determined in solution by ^{1}H NMR spectroscopy as described in the experimental section, are also shown for comparison.   A slight decrease in the *mm* fraction is found to occur for the mobile component in the HI-PVA films as a result of small increases in *mr* and *rr* fractions.   A similar slight decrease in the *rr* fraction and a compensating increase in the *mm* fraction are also observed for the mobile component in the S-PVA films. In contrast, no appreciable changes in triad tacticities are found to occur for the mobile component in the A-PVA films.   These facts indicate that a very small level of preferential partitioning of the *mm* or *rr* units tends to be, respectively, induced in the crystalline region in the highly isotactic or syndiotactic PVA films whereas almost no preferential partitioning should occur in the atactic PVA films.   Nevertheless, it should be strongly pointed out that the mole fractions of the triad tacticites for the mobile components are not greatly different from the respective total values even in the HI-PVA and S-PVA films.   Namely, appreciable reductions of the stereoregularity in the mobile components, which would be assumed to induce the *mm*-insensitivity of the α_a and β_a dispersions as described above, are not confirmed in these PVA samples.   It is, therefore, concluded that the local twisting or the micro-Brownian motion, which is respectively associated with the β_a or α_a dispersion, is not significantly influenced by the stereoregularity in the PVA samples.   One possible origin of the

mm-insensitivity of the molecular motions in the noncrystalline region may be the existence of the strong intramolecular and intermolecular hydrogen bondings in the PVA films.   These hydrogen bondings may make obscure the effect of the stereoregulality on the molecular mobility of PVA chains. More detailed characterization of the molecular motion in the stereoregular PVA samples will be made in relation to hydrogen bonding mainly by solid-state ^{13}C NMR in future.

5.4. Conclusions

We have investigated the structure and hydrogen bonding for the hydrated stereoregular PVA films by solid-state ^{13}C NMR analyses, and obtained the following conclusions:

(1) Solid-state ^{13}C NMR analyses for the hydrated S-PVA and HI-PVA films reveal that there are three components with different T_{1C} values, the crystalline, less mobile, and mobile components, being in good agreement with the case for the hydrated A-PVA films.   The evaluation of the T_{1C} values of the crystalline components for the hydrated films suggests that the crystalline chains of S-PVA and HI-PVA may be much rigid than those of A-PVA even in the hydrated state because strong intermolecular and intramolecular hydrogen bonding may be successively formed along the chains for S-PVA and HI-PVA, respectively.

(2) The line shape analysis of the CH resonance line for the crystalline component reveals that lines I, II, and III are clearly observed in the hydrated S-PVA films as expected for the chains with all-*trans*

conformation. In addition, a minor Gaussian contribution referred to as III$_f$, which is assigned to the CH carbons combined to the OH groups free from hydrogen bonding, is found to exist in the most upfield region. For the hydrated HI-PVA films, only line I of the CH resonance line is observed in the crystalline component in good accord with the case of the dried films. This result suggests that all OH groups are allowed to form successive intramolecular hydrogen bonding along the chains that contain some r units and the respective chains may adopt a slightly helical structure in the crystalline region. Moreover, splitting of line I into two lines implies the existence of two types of the helical structures that may be produced in the crystalline region probably depending on the probability of the r units appearing along each chain.

(3) As for the less mobile components, the line shapes of CH resonance lines for the hydrated S-PVA and HI-PVA films are, respectively, similar to those of their crystalline components, though such similarity is not clearly observed for the hydrated A-PVA films. These results indicate that almost the same structure (all-*trans* conformation for S-PVA, or slightly helical structure for HI-PVA) should be mainly formed in the interfacial region because of the successive formation of strong intermolecular or intramolecular hydrogen bonding for S-PVA or HI-PVA, respectively, even in the hydrated state. In contrast, the mobile components for the hydrated S-PVA and HI-PVA films are subjected to enhanced random motion like the chains in the dissolved state, leading to the observation of the triplet ascribed to the *mm*, *mr* and *rr* sequences.

130

(4) In the crystalline component, the probabilities f_a of the formation of intramolecular hydrogen bonding for the hydrated and dried HI-PVA films are 1.0, and these values seem not to be significantly influenced by the hydration.   For the S-PVA or A-PVA samples, the increases in f_a values by the hydration in these crystalline components are observed.   These results indicate that water may promote the formation of the intramolecular hydrogen bonding in the *m* units by breaking the intermolecular hydrogen bonding.

(5) The mole fractions of the *mm, mr* and *rr* sequences for the mobile components are found not to greatly differ from the overall triad tacticities even for the HI-PVA and S-PVA films.   It is, therefore, concluded that the local twisting or the micro-Brownian motion is not significantly influenced by the stereoregularity in the noncrystalline region of the PVA samples.

References

(1)   Fujii, K. *J. Polym. Sci., Part D* **1971**, 5, 431.

(2)   Finch, C. A. *Polyvinyl Alcohol-Developments*; John Wiley & Sons: New York, **1992**; Chapters 9 and 10.

(3)   Finch, C. A. *Polyvinyl Alcohol*; John Wiley & Sons: New York, **1973**; Chapters 6 and 10.

(4)   Murahasi, S.; Yuki, H.; Sano, T., Yonemura, U.; Tadokoro, T.; Chatani, Y. *J. Polym. Sci.* **1962**, 62, S77.

(5)   Yuki, H.; Hatada, K.; Oda, K.; Kinoshita, Murahashi, S.; Ono, K.; Ito, Y. *J. Polym. Sci., Part A-1* **1969**, 7, 1517.

(6) Okamura, S.; Kodama, T.; Higashimura, T. *Makromol. Chem.* **1962**, 53, 180.

(7) Higashimura, T.; Suzuki, K.; Okamura, S. *Makromol. Chem.* **1965**, 86, 259.

(8) Murahashi, S.; Nozakura, S.; and Sumi, M. *J. Polym. Sci. Part B* **1965**, 3, 245.

(9) Murahashi, S.; Nozakura, S.; Sumi, M.; Yuki, H.; Hatada, K. *J. Polym. Sci., Polym. Lett. Ed.* **1966**, 4, 65; *Kobunshi Kagaku* **1966**, 23, 550.

(10) Ohgi, H.; Sato, T. *Macromolecules* **1993**, 26, 559.

(11) Ohgi, H.; Sato, T. *Macromolecules* **1999**, 8, 2403.

(12) Ohgi, H.; Sato, T. *Polymer* **2002**, 43, 3829.

(13) Horii, F.; Hu, S.; Deguchi, K.; Sugisawa, H.; Ohgi, H.; Sato, T. *Macromolecules* **1996**, 29, 3330.

(14) Ohgi, H.; Sato, T.; Hu, S.; Horii, F. *Polymer* **2006**, 47,1324.

(15) Masuda, K.; Kaji, H.; Horii, F. *Polym J* **2001**, 33, 356.

(16) Ohgi, H.; Sato, T.; Watanabe, H.; Horii, F. *Polym J* **2006**, 38, 1055.

(17) Yamamoto, T.; Yoda, S.; Takase, H.; Sangen, O.; Fukae, R.; Kamachi, M.; Sato, T. *Polymer J* **1991**, 23, 185.

(18) Moritani, T.; Kuruma, I.; Shibatani, K.; Fujiwara, Y *Macromolecules* **1972**, 5, 577.

(19) DeMember, JR.; Haas, HC.; MacDonald, RL. *J Polym Sci, Polym Lett Ed* **1972**, 10, 385.

(20) Horii, F.; Hirai, A.; Kitamaru, R.; Sakurada, I. *Cellulose Chem Technol* **1985**, 19, 513.

(21) Horii, F.; Hu, S.; Ito, T.; Odani, H.; Kitamaru, R.; Matsuzawa, S.; Yamaura, K. *Polymer* **1992**, 33, 2299.

(22) Hu, S.; Horii, F.; Odani, H.; Narukawa, H.; Akiyama, A.; Kajitani, K. *Kobunshi Ronbunshu* **1992**, 49, 361.

(23) Hu, S.; Tsuji, M.; Horii, F. *Polymer* **1994**, 35, 2516.

(24) Masuda, K.; Horii, F. *Macromolecules* **1998**, 31, 5810.

(25) Masuda, K.; Kaji, H.; Horii, F. *Polymer J* **1999,** 31, 105.

(26) Masuda, K.; Kaji, H.; Horii, F. *J Polym Sci, Part B, Polym Phys* **2000**, 38, 1060.

(27) Kitamaru, R.; Horii, F.; Murayama, K. *Macromolecules* **1986**, 19, 636.

(28) Hirai, A.; Horii, F.; Kitamaru, R.; Fatou, JG.; Bello, A. *Macromolecules* **1990**, 23, 2913.

(29) Yang, H.; Hu, S.; Horii, F.; Endo, R.; Hayashi, T. *Polymer* **2006,** 47, 1995.

(30) Torchia, DA. *J Magn Reson* **1978**, 30, 613.

Chapter 6

Viscoelastic Behavior of Highly Isotactic Poly(vinyl alcohol) Films

6.1. Introduction

As reported in Chapter 4, we found interesting features of the highly isotactic PVAs (HI-PVAs) being different from those of LI-PVA and ordinary atactic PVA (A-PVA).   In particular, we compared the melting temperatures T_m, degrees of crystallinity χ_c, and ^{13}C spin-lattice relaxation times T_{1C} of the crystalline components for PVA samples with different tacticities (including HI-PVA) to find that these physical quantities show clear minima at the mole fraction of mm (f_{mm}) of 0.4-0.5 when plotted against f_{mm}.   We also investigated the structure and hydrogen bonding for the hydrated state of the stereoregular PVA by high-resolution solid-state ^{13}C NMR spectroscopy, as reported in Chapter 5.   It was found by the ^{13}C spin-lattice relaxation analysis that there exist three components with different T_{1C} values assigned to the crystalline, less mobile, and mobile components for the hydrated HI-PVA films.   The line shape analysis indicates that a slightly helical structure, which is probably allowed by the formation of the successive intramolecular hydrogen bondings along the chains in the crystalline region, seems not to undergo any significant change by the hydration for HI-PVA.

It is of our interest to elucidate the effect of the stereoregularity on the

motion of the PVA chains in addition to the above structural features. This motion can be conveniently examined through dynamic viscoelastic behavior. Indeed, Nagai et al.[15] examined this behavior for A-PVA, S-PVA and LI-PVA and found that the decrease of the dynamic Young's modulus E' (at 138 Hz) at high temperatures is larger in the order, S-PVA > A-PVA > LI-PVA. However, the viscoelastic behavior of the HI-PVA with mm fractions higher than 0.70 has not yet been investigated, and the effect of the stereoregularity on this behavior and underlying chain motion has not been fully elucidated. Thus, we have synthesized HI-PVAs having higher mm values from poly$t$BVE and compared their behavior with that of A-PVA (f_{mm}=0.22) and S-PVA (f_{mm}=0.14). It turned out that the stereoregularity hardly affects the viscoelastic behavior of the noncrystalline component but a significant effect (related to the hydrogen bonding) is observed for the behavior of the crystalline component. Details of these results are reported in this chapter.

6.2. Experimental Section

6.2.1. Preparation of stereoregular PVA samples

HI-PVA was synthesized by the procedure which is described in Chapter 2. The commercially available A-PVA derived from poly(vinyl acetate) and syndiotacticitiy-rich PVA (S-PVA) derived from poly(vinyl pivalate) were also used as reference samples.

The stereoregularity of PVA samples was determined from solution-state ^{1}H NMR spectroscopy on the basis of the methods reported previously.[18,19]

The triad tacticities are as follows: HI-PVA (f_{mm}=0.78, f_{mr}=0.20, f_{rr}=0.03), A-PVA (0.23, 0.50, 0.27), S-PVA (0.14, 0.48, 0.38)..

All physical properties were measured for the PVA films with a thickness of about 100 μm unless otherwise specified. Each PVA films were prepared by the same procedure which is described in Chapter 4. The films were annealed at several temperatures for 30 min.

6.2.2. Dynamic Viscoelasticity

Dynamic storage Young's modulus (E'), loss modulus (E'') and loss tangent (tan δ) were measured at 110Hz with a heating rate of 2 ˚C/min from –50 ˚C to 250 ˚C using a dynamic viscoelastic spectrometer DVE-V4 (Rheology Engineering Co., Ltd.).

6.2.3. Density, Swelling and DSC tests

The densities of PVA films prepared as above were measured with a density gradient tube (Shibayama Kagaku) using a mixture of *n*-heptane and carbon tetrachloride at 25 ˚C.

For the swelling experiment, the PVA films were soaked in water at room temperature for 24 hr to be fully equilibrated in water. The degree of equilibrium swelling, Q, was determined by the following formula : Q = (weight of swollen films – weight of dried films after swelling) / (weight of dried films after swelling).

Differential scanning calorimetry (DSC) thermograms were recorded on 10mg of each PVA films under nitrogen with a Mettler differential scanning

calorimeter. The heat of melting (ΔH) of each film was evaluated from the integrated intensity of the endothermic curve observed in the thermogram.

6.3. Results and Discussion

6.3.1. Overview of behavior of HI-PVA with different heat treatments

Figure 6-1 shows dynamic storage Young's modulus (E') and loss modulus (E'') of HI-PVA films with f_{mm}=0.78 (the highest f_{mm} so far reported) at temperatures from −50 ˚C to 250 ˚C. The corresponding loss tangent (tan δ) is shown in Figure 6-2. The HI-PVA films examined here were annealed for 30 min at different temperatures, 40, 120, and 200 ˚C, and subjected to the viscoelastic test with a heating mode. The degree of crystallinity χ_c of the film increased with an increase of the annealing temperature, as explained later in more detail.

The HI-PVA films exhibit four dispersions referred to as β_a, α_a, β_c, and α_c in the order of increasing temperature, as most clearly noted for tan δ (Figure 6-2). The major dispersion (α_a) observed at around 70 ˚C is attributable to the onset of micro-Brownian motion (i.e., glass transition) of the polymer chains in the non-crystalline region, as judged from the sharpness of the dispersion reflected in the large decrease of E' at around 70 ˚C. The β_a dispersion seen at around −10 ˚C can be assigned to the local twisting motion of non-crystalline chains.[19] The α_c and β_c dispersions, seen at around 140 ˚C and 220 ˚C, occurs at temperatures well above the glass transition temperature and are attributable to the motion in
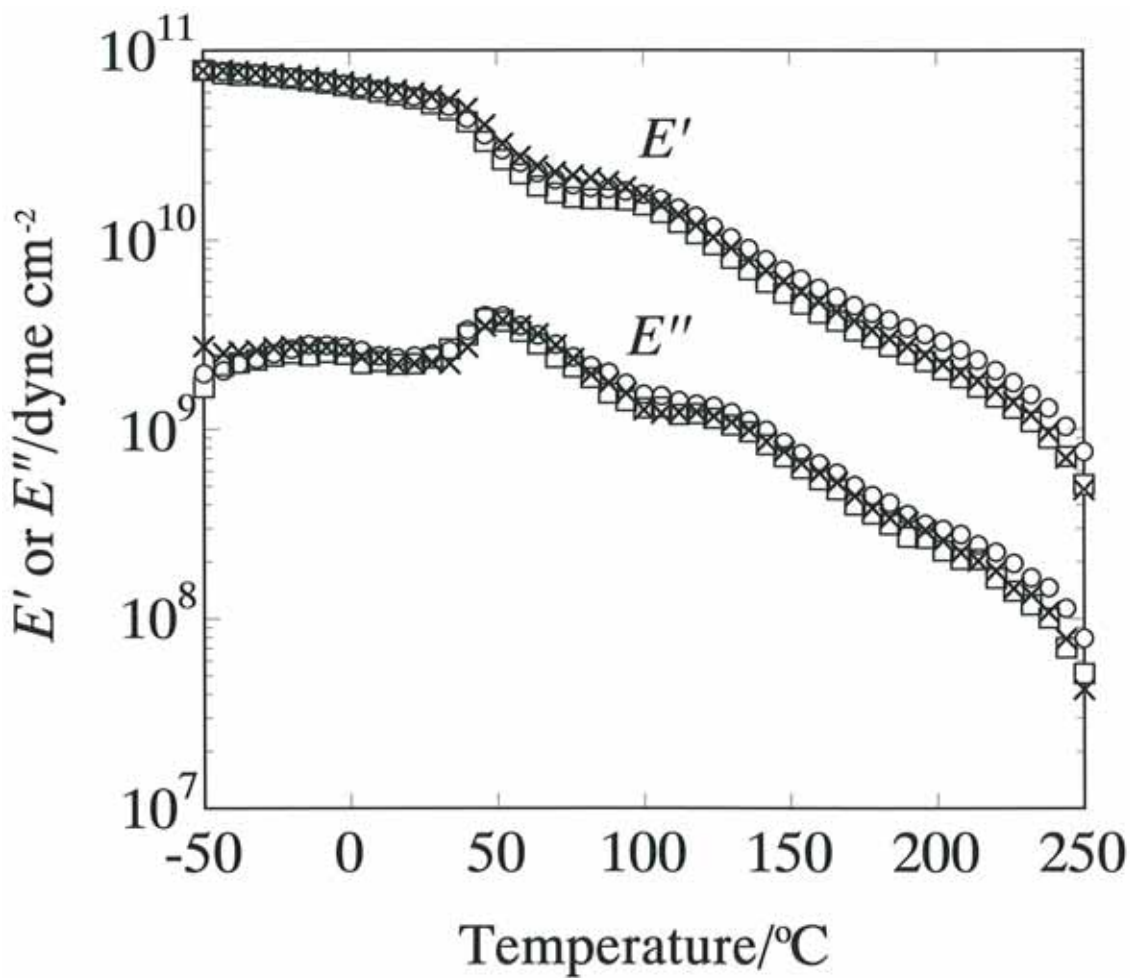
137

Figure 6-1. Temperature dependence of the dynamic storage Young's modulus (E') and loss modulus (E'') of HI-PVA films (f_{mm}=0.78). The annealing temperature is 40 ˚C (circle), 120 ˚C (square) and 200 ˚C (cross).
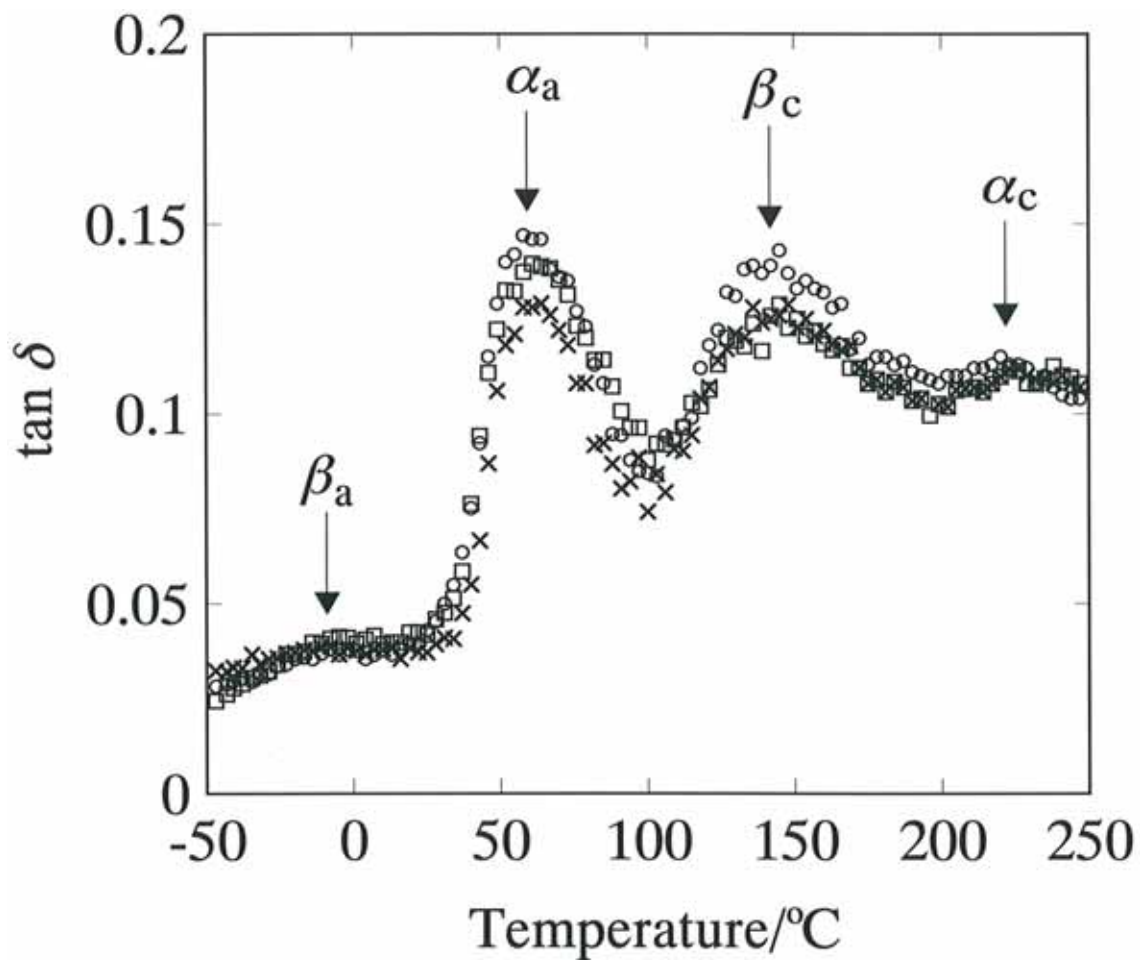
Figure 6-2. Temperature dependence of the loss tangent (tan δ) of HI-PVA films (f_{mm}=0.78). The annealing temperature is 40 ˚C (circle), 120 ˚C (square) and 200 ˚C (cross).

the crystallites.[20-23]

The decrease of E' at around 70 ˚C (Figure 6-1) can be used as a measure of the intensity of the α_a dispersion (glass transition). This decrease becomes smaller on the increase of annealing temperature, which suggests that the content of the noncrystalline component decreases (and thus the degree of crystallinity χ_c increases) on sufficient annealing. (Indeed, the increase of χ_c was confirmed, as explained later for Figure 6-3). At the same time, we note that the dispersion temperatures for all of the β_a, α_a, β_c, and α_c processes hardly change with the annealing. Thus, the mobility of respective HI-PVA chains in the crystalline and noncrystalline regions appears to be insensitive to the change in the degree of crystallinity induced by the annealing.

6.3.2. Density, swelling and thermal behavior of PVAs

Since the viscoelastic behavior of PVA films changes not only with the stereoregularity but also with the crystallinity, the effect of stereoregularity on the behavior can be most clearly examined for films having the same crystallinity. The degree of crystallinity of PVA, χ_c, has been studied by various methods: X-ray diffraction, swelling, density and DSC measurement, etc. Among the various methods, the generally available is the DSC method, and χ_c can be determined from the enthalpy change for melting, ΔH. In this determination, the ΔH_c value for the 100 % crystallinity (ΔH_c=6.87 kJ mol^{-1})[24] is often assumed to be independent of the stereoregularity. However, the crystal structure of HI-PVA differs
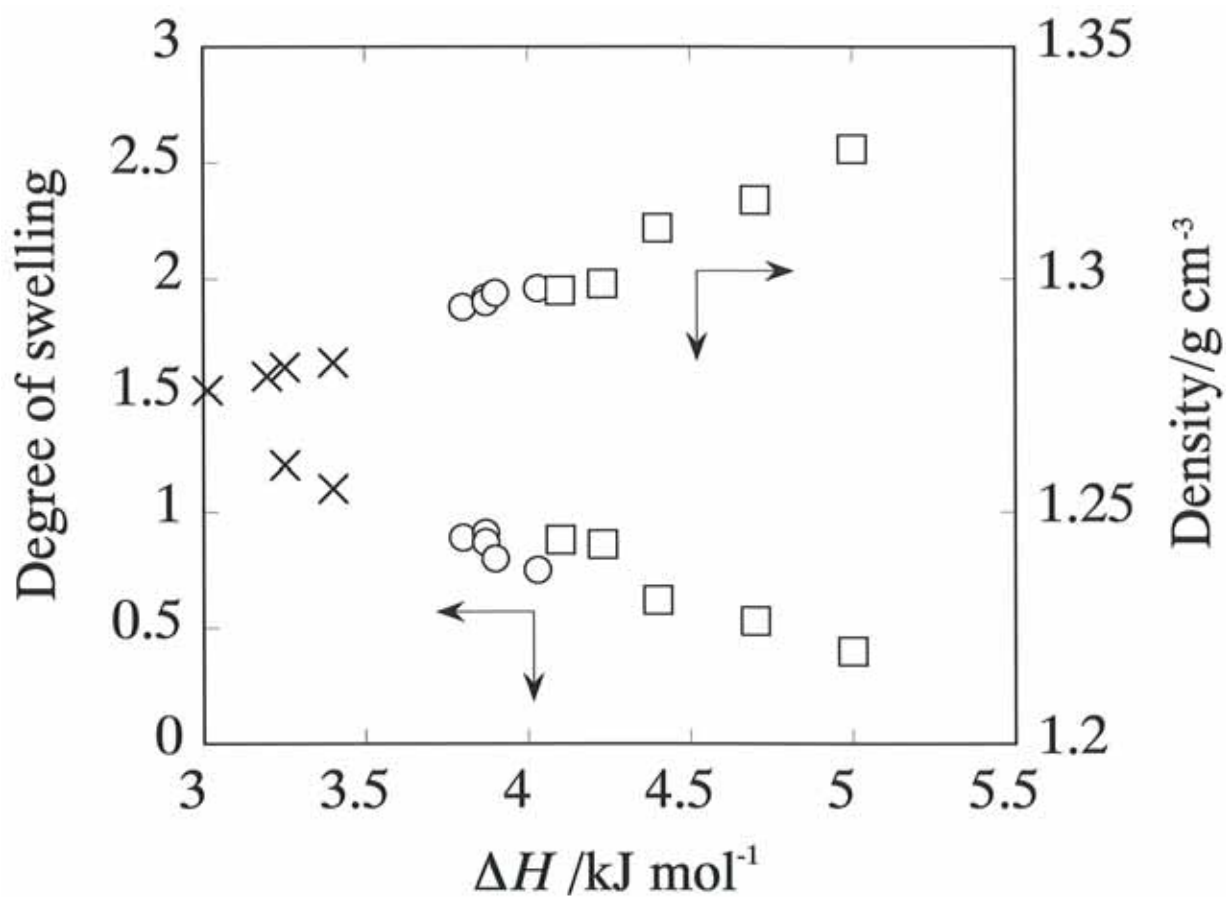
Figure 6-3.   Dependence of the degree of swelling in water and the density on the ΔH

values for HI-PVA (f_{mm}=0.78, circle), A-PVA (f_{mm}=0.22, cross) and S-PVA (f_{mm}=0.14,

square).

from that of S-PVA and A-PVA,[10] and no ΔH_c data have been reported for HI-PVA.

For this problem, we here focus on the density (ρ) and the degree of swelling (Q) of HI-PVA, S-PVA, and A-PVA films in water. For HI-PVA (f_{mm}=0.78), A-PVA (f_{mm}=0.22), and S-PVA (f_{mm}=0.14) films being annealed at several different temperatures and thus having different χ_c values, we measured the ρ, Q and ΔH values from the density, swelling and DSC measurements. In Figure 6-3, the ρ and Q values are plotted against the ΔH. For the PVAs with different stereoregularities, ρ and Q exhibit a universal, almost linear dependence on ΔH. These results suggest that the ΔH_c value for the 100% crystallinity is almost same for the HI-PVA, S-PVA, and A-PVA films. In the absence of more detailed information for χ_c, this chapter utilizes the ΔH data and the *mm*-independent ΔH_c value to estimate χ_c of HI-PVA films. The width of the scatter in the plots in Figure 6-3 suggests that the accuracy of this estimate is better than $\pm$ 10 %.

6.3.3. Comparison of HI-PVA, S-PVA, and A-PVA films

Figure 6-4 shows a comparison of the temperature dependence of the E' and E'' for HI-PVA film (ΔH=4.03 kJ cm^{-1}; annealed at 200 ˚C), S-PVA film (ΔH=4.08 kJ cm^{-1}; annealed at 40 ˚C), and A-PVA film (ΔH=3.40 kJ cm^{-1}; annealed at 200 ˚C). The corresponding tan δ is shown in Figure 6-5. The degree of crystallinity χ_c, determined satisfactorily from the ΔH value as explained in the previous section, is almost identical for the HI-PVA and S-PVA films (χ_c=0.59) but somewhat smaller for the A-PVA
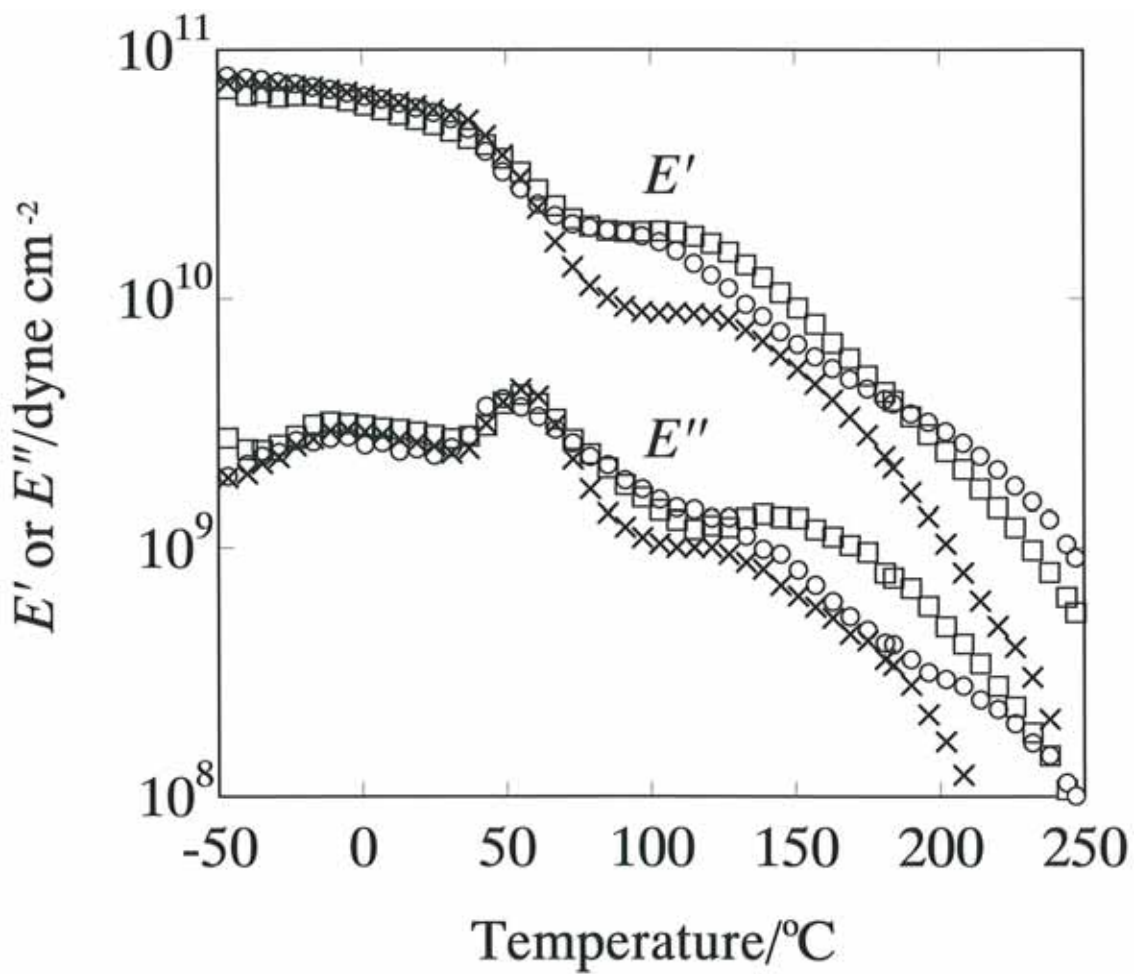
Figure 6-4.　Temperature dependence of the dynamic storage Young's modulus (E') and loss modulus (E'') of HI-PVA (χ_c=0.59, circle), A-PVA (χ_c =0.49, cross) and S-PVA (χ_c =0.59, square).
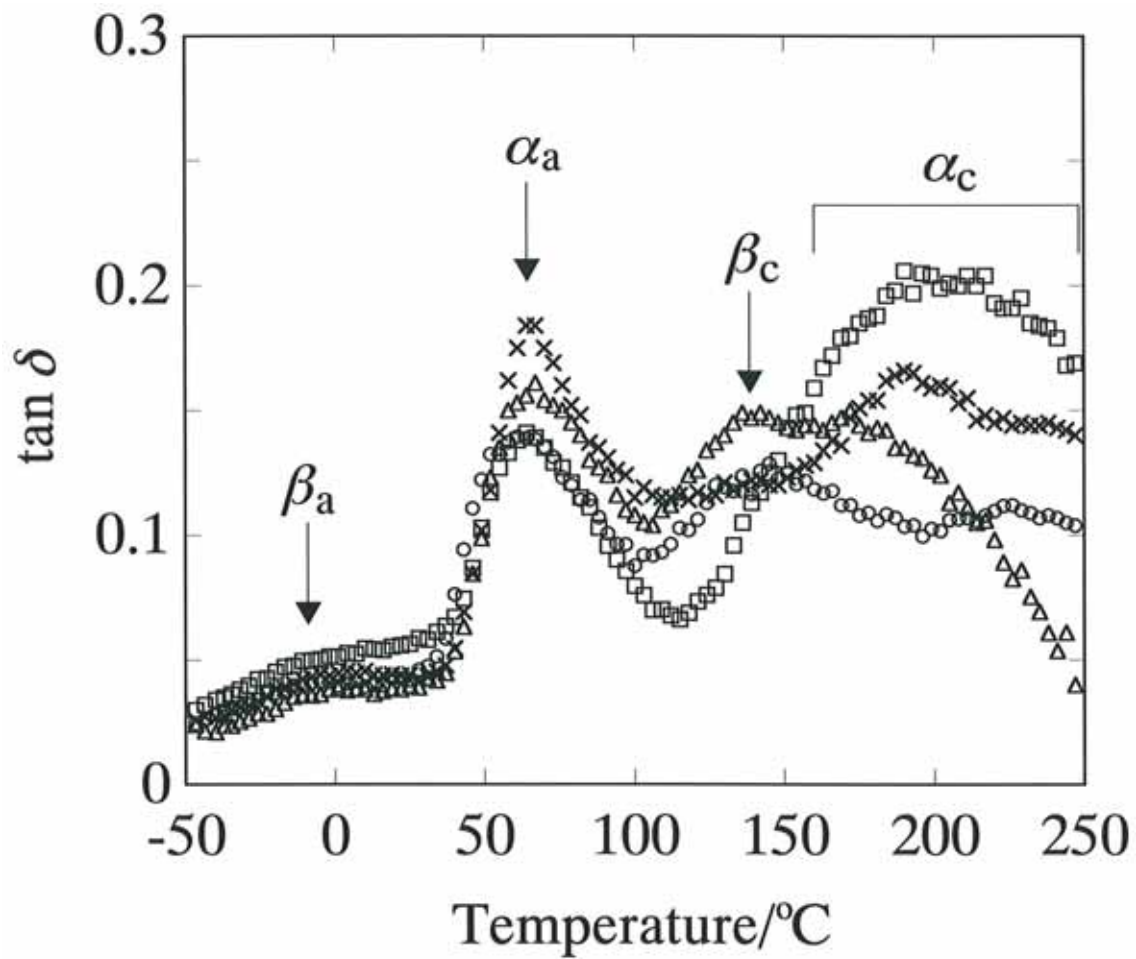
Figure 6-5. Temperature dependence of the loss tangent (tan δ) of HI-PVA (χ_c =0.59; circle), LI-PVA (χ_c~0.3; triangle), A-PVA (χ_c=0.49; cross) and S-PVA (χ_c=0.59; square).

film (χ_c=0.49).   We can keep this point in our mind to relate the data in Figures 6-4 and 6-5 to the difference in the stereoregularity (*mm* value), as discussed below.

As clearly seen in Figures 6-4 and 6-5, the β_a and α_a dispersions occurring at around -10 ˚C and 70 ˚C are nearly the same, in both magnitude (reflected in the decrease of E') and location (noted as the peak temperature for *E"* and/or tan δ), for the HI-PVA and S-PVA films having almost identical χ_c.   For the A-PVA film having a smaller χ_c value, the magnitude of the α_a dispersion is larger but the location of the β_a and α_a dispersions are the same compared to the HI-PVA and S-PVA films.

To clarify the effect of the stereoregularity on the non-crystalline chain motions of PVA, the tan δ data for LI-PVA film (f_{mm}=0.44 and χ_c~0.3; annealed at 200 ˚C) are also shown in Figure 6-5.   The degree of crystallinity of this LI-PVA film, obtained from a DSC measurement (only approximately because of its poor thermal stability at high temperatures as reported in Chapter 4), was χ_c~0.3.   As seen in Figure 6-5, the local twisting motion (seen as the β_a dispersion) and micro-Brownian motion (α_a dispersion) of the respective chains in the noncrystalline region are essentially the same in the PVA films of various stereoregularities (f_{mm}=0.14-0.78).   This behavior is in harmony with the change in the intensity of the α_a dispersion (measured as the decrease of *E'* at around 70˚C) with ΔH (and χ_c) shown in Figure 6-6.   The intensity appears to be almost universally dependent on ΔH (and χ_c) irrespective of the f_{mm} value, suggesting that the noncrystalline chain motion resulting in the α_a
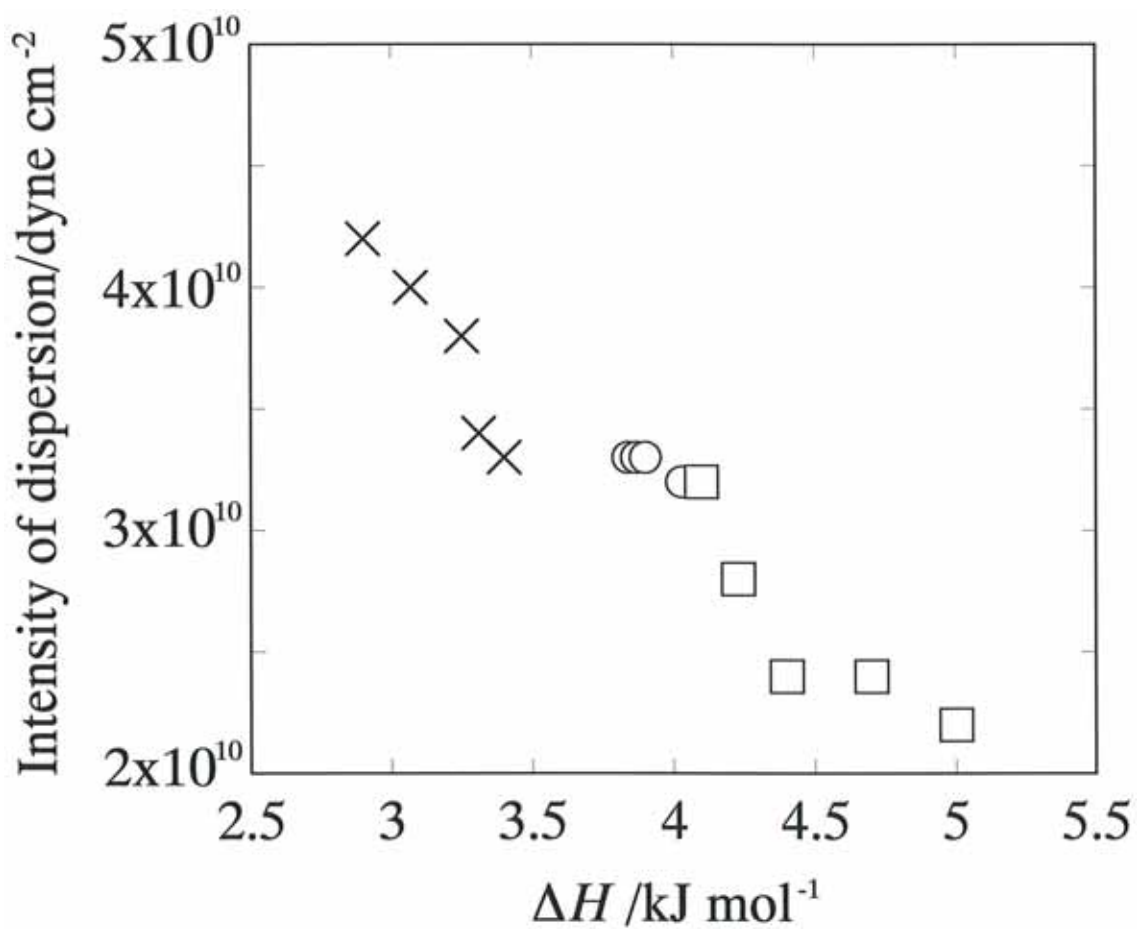
Figure 6-6. Dependence of the α_a dispersion intensity measured as the decrease of E' on the ΔH for HI-PVA (f_{mm}=0.78; circle), A-PVA (f_{mm}=0.22; cross) and S-PVA (f_{mm}=0.14; square).

dispersion is insensitive to the stereoregularity.

The f_{mm}-insensitivity of the α_a and β_a dispersions is rather surprising because the stereoregularity is expected to affect the mobility of the noncrystalline chain.   One possible origin of this insensitivity is the enrichment of the stereoregular sequences (either *m*- or *r*-sequences) of the PVA chains in the crystalline region and the corresponding reduction in the difference of the stereoregularities in the noncrystalline region of the samples.   To examine this possibility, we followed the previous paper[25] to apply the solid-state ^{13}C NMR analysis for the hydrated PVA films to estimate the mole fractions of the *mm, mr,* and *rr* sequences for the mobile component that is produced by swelling with water.   As reported in Chapter 5, however, the mole fractions of the *mm, mr,* and *rr* sequences for the mobile components are found not to greatly differ from the overall triad tacticities even for the HI-PVA and S-PVA films.   These results suggest that the *mm, mr,* and *rr* units should be almost equally distributed in the crystalline and noncrystalline regions for the HI-PVA and S-PVA films, which is in harmony with the result obtained for the A-PVA films.[25]   Thus, the chain motion in the noncrystalline region is insensitive to the stereoregularity therein, and an examination of the origin of this result requires more detailed solid-state ^{13}C NMR experiments.

Now, we turn our attention to the dispersions of the crystalline components observed in Figures 6-4 and 6-5 at temperatures above 100 ˚C. The locations and intensities of these dispersions significantly change with the stereoregularity of the films.   The HI-PVA sample (f_{mm}=0.78) shows

the major crystalline dispersion (β_c) at around 140 ˚C and the side dispersion (α_c) at around 220 ˚C. The LI-PVA sample (f_{mm}=0.44) shows the β_c dispersion at nearly the same temperature but its α_c dispersion emerges at around 180 ˚C (well below $T\alpha_c$ for HI-PVA). For the A-PVA (f_{mm}=0.22) and S-PVA (f_{mm}=0.14) samples, no β_c dispersion is clearly detected and the α_c dispersion emerges at around 195 ˚C and 205 ˚C. These differences can be related to the structural origin(s) of the dispersions, as discussed below.

The β_c dispersion has been related to the transition in the expansion of the crystal[21] or a discontinuous point of the expansion coefficient of PVA.[22] It resulted from a reduction of intermolecular forces in crystals, and this reduction takes place with thermal expansion of the PVA unit cells.[19,21] As previously reported, successive intramolecular hydrogen bonding is formed for all OH groups along the chains in the crystalline region for the HI-PVAs.[14] This perfect intramolecular bonding would in turn weaken the intermolecular bonding and thus enhance the sensitivity of the latter type of bonding to the unit cell expansion. This enhancement appears to result in the clear β_c dispersion seen for HI-PVA. For LI-PVA having a fairly large f_{mm} value (=0.44), the β_c dispersion seems to be clearly resolved for the same reason. In contrast, for S-PVA, the β_c dispersion peak vanishes possibly because the strong intermolecular forces due to syndiotactic regulation[23] (and lack of significant intramolecular hydrogen bonding) hardly changes with the cell expansion. For A-PVA, the lack of the clear β_c dispersion peak can be also attributed to a similarly strong

intermolecular forces as well as to high ordering in crystallites in A-PVA film, the latter resulting from the lamellar thickening on high-temperature annealing (i.e. at 200 ˚C).

Differing from the β_c dispersion, the α_c dispersion is assigned to thermal motion of the chain axis in the crystal lattices.[22,23] Figure 6-5 clearly indicates that the α_c dispersion temperature $T\alpha_c$ decreases in the order of HI-PVA (220 ˚C) > S-PVA (205 ˚C) > A-PVA (195 ˚C) > LI-PVA (180 ˚C). This order, well corresponding to the order of the other physical properties, T_m, χ_c, and T_{1C}, is not in accord to the order of the f_{mm} value. In other words, plots of $T\alpha_c$, T_m, χ_c, and T_{1C} against f_{mm} show minima at f_{mm}=0.4-0.5 (for LI-PVA). This behavior of the physical properties including $T\alpha_c$ suggests that the disordering of the intermolecular and/or intramolecular hydrogen bonding along each PVA chain, being most significant at f_{mm}=0.4-0.5, governs these properties.[14] In particular, the enhancement of the intermolecular bonding on a decrease of f_{mm} below 0.4 (for A-PVA and S-PVA) would naturally reduce the axial mobility of *respective* chains in the crystal lattice, while the enhancement of intramolecular bonding on an increase of f_{mm} above 0.5 (for HI-PVA) would stiffen the chain to reduce the axial mobility. The reduction of the mobility due to these two types of enhancement results in an increase of $T\alpha_c$ thereby possibly giving the order of $T\alpha_c$ explained above.

6.4. Conclusions

We have examined dynamic viscoelasticity of highly isotactic poly(vinyl

alcohol) (HI-PVA, f_{mm}=0.78) in comparison with syndiotactc PVA (S-PVA, f_{mm}=0.14) and atactic PVA (A-PVA, f_{mm}=0.22). The relaxation in the non-crystalline region, the β_a and α_a dispersions reflecting the local twisting motion and micro-Brownian motion of the chains in this region, were nearly the same, in both magnitude and location, for the HI-PVA and S-PVA having an almost identical degree of crystallinity. As reported in Chapter 5, the solid-state ^{13}C NMR experiments revealed that there is no significant enrichment of the stereoregular sequences (neither *m*- or *r*-units) of the PVA chains in the crystalline region for each PVA sample. Thus, the chain motion in the noncrystalline region is insensitive to the stereoregularity therein, and an examination of the origin of this result requires more detailed solid-state ^{13}C NMR experiments.

In contrast, the β_c and α_c dispersions in the crystalline region changed with the stereoregularity. The β_c dispersion (local motion in crystals due to defects) was clearly observed for HI-PVA but not for S-PVA and A-PVA. The α_c dispersion (axial motion of the chain in the crystal lattices) was observed for all PVA films but its temperature increased in the order of HI-PVA > S-PVA > A-PVA, which well corresponded to the order of the melting temperature or ^{13}C spin-lattice relaxation time of these PVAs. These results may be related to a difference of the magnitude of intermolecular and/or intramolecular hydrogen bonding in the crystals of respective PVAs. Specifically, the successive intramolecular bonding in the HI-PVA crystal appears to reduce the magnitude of the intermolecular bonding and stiffen the chain backbone, thereby allowing the chain to

exhibit the β_c motion and increase the α_c dispersion temperature.

References

(1)   Fujii, K. *J. Polym. Sci., Part D* **1971**, 5, 431.

(2)   Finch, C. A. In *Polyvinyl Alcohol*; John Wiley & Sons: New York, **1973**; Chapter 6 and 10.

(3)   Finch, C. A. In *Polyvinyl Alcohol-Developments*; John Wiley & Sons: New York, **1992**; Chapter 9 and 10.

(4)   Murahasi, S.; Yuki, H.; Sano, T., Yonemura, U.; Tadokoro, T.; Chatani, Y. *J. Polym. Sci.* **1962**, 62, S77.

(5)   Yuki, H.; Hatada, K.; Oda, K.; Kinoshita, Murahashi, S.; Ono, K.; Ito, Y. *J. Polym. Sci.* **1969**, Part A-1, 7, 1517.

(6)   Okamura, S.; Kodama, T.; Higashimura, T. *Makromol. Chem.* **1962**, 53, 180.

(7)   Higashimura, T.; Suzuki, K.; Okamura, S. *Makromol. Chem.* **1965**, 86, 259.

(8)   Murahashi, S.; Nozakura, S.; Sumi, M. *J. Polym. Sci.* **1965**, B, 3, 245.

(9)   (a) Murahashi, S.; Nozakura, S.; Sumi, M.; Yuki, H.; Hatada, K. *J. Polym. Sci., Polym. Lett. Ed.* **1966**, 4, 65.
    (b) Murahashi, S.; Nozakura, S.; Sumi, M.; Yuki, H.; Hatada, K. *Kobunshi Kagaku* **1966**, 23, 550.

(10) Ohgi, H.; Sato, T. *Macromolecules* **1993**, 26, 559.

(11) Ohgi, H.; Sato, T. *Macromolecules* **1999**, 8, 2403.

(12) Ohgi, H.; Sato, T. *Polymer* **2002**, 43, 3829.

(13) Horii, F.; Hu, S.; Deguchi, K.; Sugisawa, H.; Ohgi, H.; Sato, T. *Macromolecules* **1996**, 29, 3330.

(14) Ohgi, H.; Sato, T.; Hu, S.; Horii, F. *Polymer* **2006**, 47,1324.

(15) Nagai, A.; Takayanagi, M. *Kogyo Kagaku Zassi* **1965**, 68, 96.

(16) Yamamoto, T.; Yoda, S.; Takase, H.; Sangen, O.; Fukae, R.; Kamachi, M.; Sato, T. *Polymer J* **1991**, 23, 185.

(17) Moritani, T.; Kuruma, I.; Shibatani, K.; Fujiwara, Y *Macromolecules* **1972**, 5, 577.

(18) DeMember, J.R.; Haas, HC.; MacDonald, RL. *J Polym Sci, Polym Lett Ed* **1972**, 10, 385.

(19) Nagai, A.; Takayanagi, M. *Kogyo Kagaku Zassi* **1965**, 68, 836.

(20) Sugiura, K.; Hashimoto, M.; Matsuzawa, S.; Yamaura, K. *J. Applied Polymer Sci.* **2001**, 82, 1291.

(21) Shiraishi, K.; Ishikawa, K.; Miyasaka, K. *Kobunshi Kagaku* **1964**, 21, 588.

(22) Yano, T. *Busseiron Kenkyu* **1956**, 94, 176.

(23) Fukae, R.; Yamamoto, T.; Masago, H.; kawatsuki, N.; Sangen, O.; Kamachi, M. *Sen'i Gakkaishi*, **1997**, 53, 195.

(24) Tubbs, R. K. *J. Polym. Sci.* **1965**, 3, 4181.

(25) Masuda, K.; Kaji, H.; Horii, F. *Polymer J.* **2001**, 33, 356.

(26) Ohgi, H., Yang, H.; Sato, T.; Horii, F. *Polymer* **2007**,48, 3850.

Chapter 7

Investigation of the Complex formation between Highly Isotactic Poly(vinyl alcohol) and Iodine

7.1. Introduction

The complex formation of the PVAs and iodine has been studied from a long time due to its wide range of applications. In particular, PVA films are very suitable for application to polarizers, because they have great ability to form a PVA-iodine complex in the film.[1] Matsuzawa et al. examined this behavior for A-PVA, S-PVA, and LI-PVA, and found that the blue color due to the PVA-iodine complex increased with increasing syndiotacticity of PVA, and LI-PVA showed no color development.[2] However, the complex formation of iodine and PVA with a *mm* fraction (f_{mm}) higher than 0.70 has not yet been investigated.

As described in Chapter 2, we studied the cationic polymerization of *t*BVE in detail and successfully prepared PVAs whose isotacticity is the highest of all the isotacticity-rich PVAs (HI-PVAs) reported so far. In this chapter, we study the complex formation of the HI-PVA (f_{mm}=0.78) with iodine in order to compare it with that for A-PVA (f_{mm}=0.22) and S-PVA (f_{mm}=0.14) in aqueous solutions and in film states.

7.2. Experimental Section

7.2.1. Preparation of stereoregular PVAs

HI-PVA was synthesized by the procedure described in Chapter 2. The commercially available A-PVA derived from poly(vinyl acetate) and syndiotacticitiy-rich PVA (S-PVA) derived from poly(vinyl pivalate) were also used as reference samples to clarify the behavior of the HI-PVA-iodine complexes.

7.2.2. Stereoregularities of PVA samples

The stereoregularity of PVA samples was determined from solution-state ^{1}H NMR spectroscopy on the basis of the methods reported in Chapter 2. The triad tacticities are as follows: HI-PVA (f_{mm}=0.78, f_{mr}=0.20, f_{rr}=0.03), A-PVA (0.23, 0.50, 0.27), and S-PVA (0.14, 0.48, 0.38).

7.2.3. Formation of PVA-iodine complexes

Iodine (I_2), potassium iodide (KI), and boric acid of special grade (Wako Pure Chemicals Industries Co.) were used as received. In the solution state, the mixtures were prepared by adding 2.0 wt% PVA aqueous solution to an I_2-KI aqueous solution containing 2×10^{-3} mol/L iodine and 4×10^{-3} mol/L potassium iodine, and by mixing with various concentrations of boric acid aqueous solutions. Thus the final solutions had a PVA concentration of 0.1 wt%, and I_2/KI concentration of 0.3 mM/0.6 mM with a varying boric acid concentration from 0 to 200 mM. The reaction mixtures maintained at 5 $^{\circ}$C for 5 days. The dissolution of HI-PVA and S-PVA were carried out at 120 $^{\circ}$C in a sealed tube for 2 hr.

7.2.4. Visible Ray and Resonance Raman spectra measurements

Visible light absorption spectra of complex solutions were taken using a Shimazu spectrometer UV-260. The light path length of the cell used was 10 mm. Resonance Raman spectra of the complex solutions were taken using a Jasco NR-1800 Laser Raman spectrophotometer, excited by Ar^+ light of 514.5 nm, 10 mW.

7.2.5. Wide-angle X-ray diffraction measurements

All stereoregular PVA films were prepared by the same procedure described in Chapter 4. The iodinated PVA films for X-ray measurements were prepared by soaking each PVA films in aqueous iodine/potassium iodine solution ($[I_2]/[KI] = 0.01/0.02$ M) at 20 ^{o}C for 5 min. The films removed from the solutions were rinsed with water to remove the solution adhered on the film surface. Then the films were subjected to uniaxial drawing in air up to a draw ratio of 7 for each film. The amount of iodine sorption was determined from the weight difference of a dry film before and after soaking.

All X-ray measurements were carried out at 20 ^{o}C with Ni-filtered and graphite-monochromated Cu-Kα radiation by taking scanning intensity profiles. The X-ray diffraction intensity was measured in a transmission mode using a Rigaku SG-7 diffractometer.

7.3. Results and Discussion

7.3.1. Effect of stereoregularity on the complex formation of PVAs with

iodine

Table 7-1 summarizes the wave length at the visible light absorption maximum, λ_{max}, and the absorbance values at λ_{max} of the color development, which is due to the complex formation, in a solution for different types of srtereoregular PVAs including HI-PVA. In Figure 7-1, the absorbance at λ_{max} of PVA-iodine complexes are plotted against the f_{mm} for stereoregular PVAs. For isotactic PVAs having the f_{mm} higher than 0.44, no color development was observed without boric acid even at low temperatures, as shown in Table 7-1 and Figure 7-1. For A-PVA and S-PVA, the color developments were observed without boric acid, and S-PVA has a higher ability to form complexes as compared to A-PVA. This result agrees with the results of the previous studies reported by Matsuzawa's group.[2,8,9] They showed that the syndiotacticity-rich PVA forms PVA-iodine complexes easier than atactic PVA does, i.e., the syndiotacticity-rich PVAs in solution form complexes with iodine at 30 ^{o}C, whereas the atactic PVA in solution does not form complexes at that temperature. From these results, they concluded that the PVA-iodine complex formation is influenced by the aggregation behavior of PVA molecules in solution. The viscosity of concentrated PVA aqueous solutions increases, and finally gelation occurs due to the formation of intermolecular hydrogen bonding with standing time at lower temperatures; this trend is remarkable for S-PVA.

In contrast to S-PVA or A-PVA, no color change is observed for the HI-PVA solution without boric acid, as shown in Table 7-1. Maeda et al.

reported that S-PVA forms intermolecular hydrogen bonding, whereas isotactic PVA forms intramolecular hydrogen bonding based on an investigation of segment mobility in aqueous solution for stereoregular PVAs using electron spin resonance (ESR).[10] Actually, even at 1 % concentration, an aqueous solution of S-PVA easily forms a gel at 25 $^\circ$C. The minimum A-PVA concentration required to form gel at the same temperature is approximately 5 %, whereas the high concentration (i.e. 10 %) of HI-PVA aqueous solution does not form a gel even at temperatures as low as 5 $^\circ$C in our study.   This indicates that there is no or little intermolecular hydrogen bonding between the HI-PVA molecules in an aqueous solution, and this may be the reason for the lower capability of complex formation between the HI-PVA and iodine as compared to that of A-PVA or S-PVA in solution.

It is well known that the effect of boric acid on PVA-iodine complex formation is important because it remarkably enhances complex formation, and these phenomena are widely used in the production of the polarizer. In Figure 7-1, the absorbances at λ_{max} of PVA-iodine complexes in the presence of boric acid are also plotted against the f_{mm} for all the samples used in this work.   It should be noted that boric acid enhances the color development over a wide range of f_{mm} of PVAs, and such color developments were observed for the HI-PVA having the f_{mm} higher than 0.66 in the presence of boric acid.   Boric acid is believed to form a bridge between PVA chains,[11,12] and this leads to the formation of a complex with iodine easily by the aggregation of PVA molecules in solution.   Figure 7-2

Table 7-1. Absorbances at λ_{max} and absorption maxima λ_{max} of stereoregular PVAs–iodine complexes in aqueous solution.

Samples	*mm* fraction	I[a]		II[b]	
		absorbance	λ_{max}	absorbance	λ_{max}
HI-PVA1	0.79	-	-	2.9	575
HI-PVA2	0.73	-	-	1.9	573
LI-PVA1	0.66	-	-	1.5	570
LI-PVA2	0.44	-	-	-	-
A-PVA	0.22	0.5	600	5.5	666
S-PVA	0.14	1.0	600	7.0	632

[a] [PVA] = 0.1 wt%, [I$_2$] = 0.3 mM, KI = 0.6 mM.

[b] [PVA] = 0.1 wt%, [I$_2$] = 0.3 mM, KI = 0.6 mM, [Boric acid] = 100 mM.
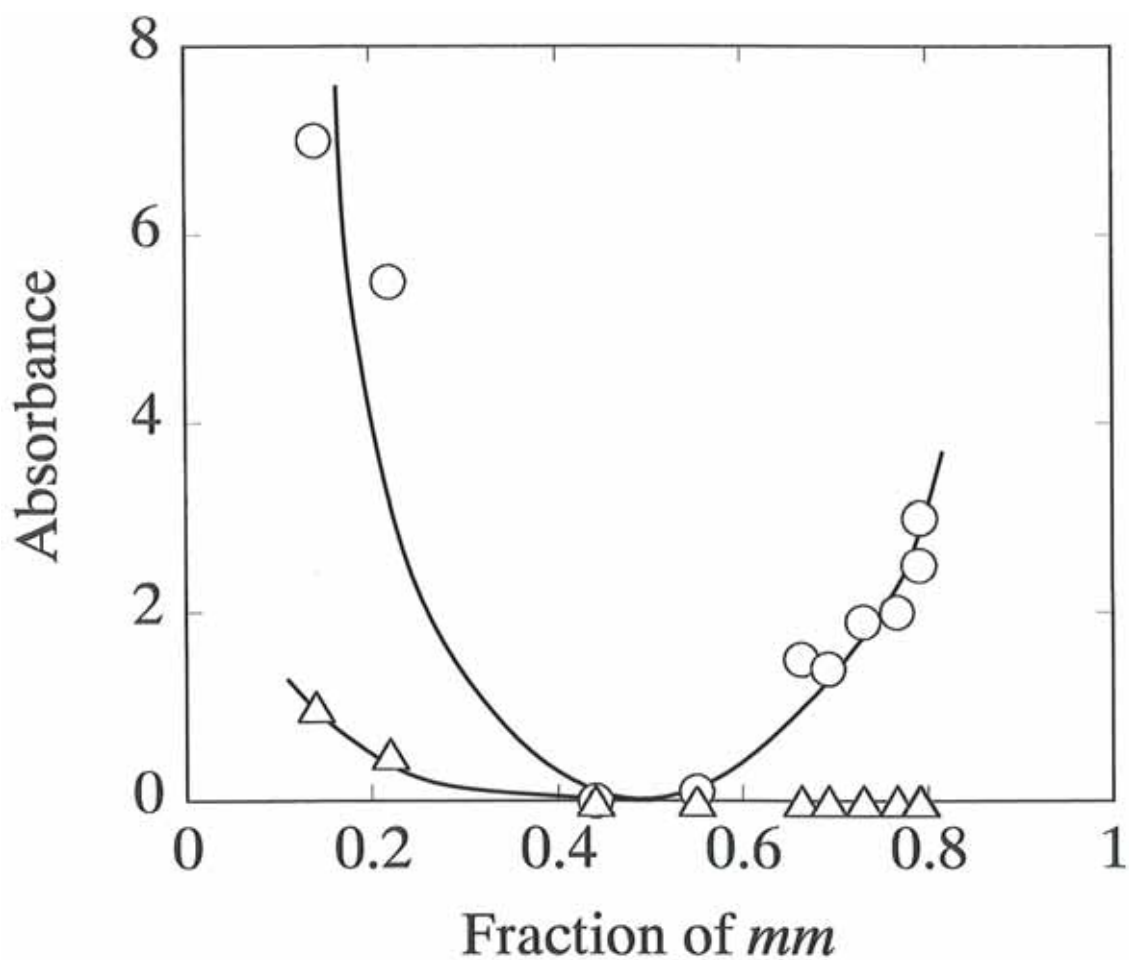
Figure 7-1.　Relationship between the fraction of the *mm* sequence and the absorbance at λ_{max} of PVA-iodine complexes with boric acid (circle) and without boric acid (triangle) in aqueous solution at 5 °C.　[PVA]=0.1 wt%, $[I_2]/[KI]/[H_3BO_3]$=0.3/0.6/100 mM.
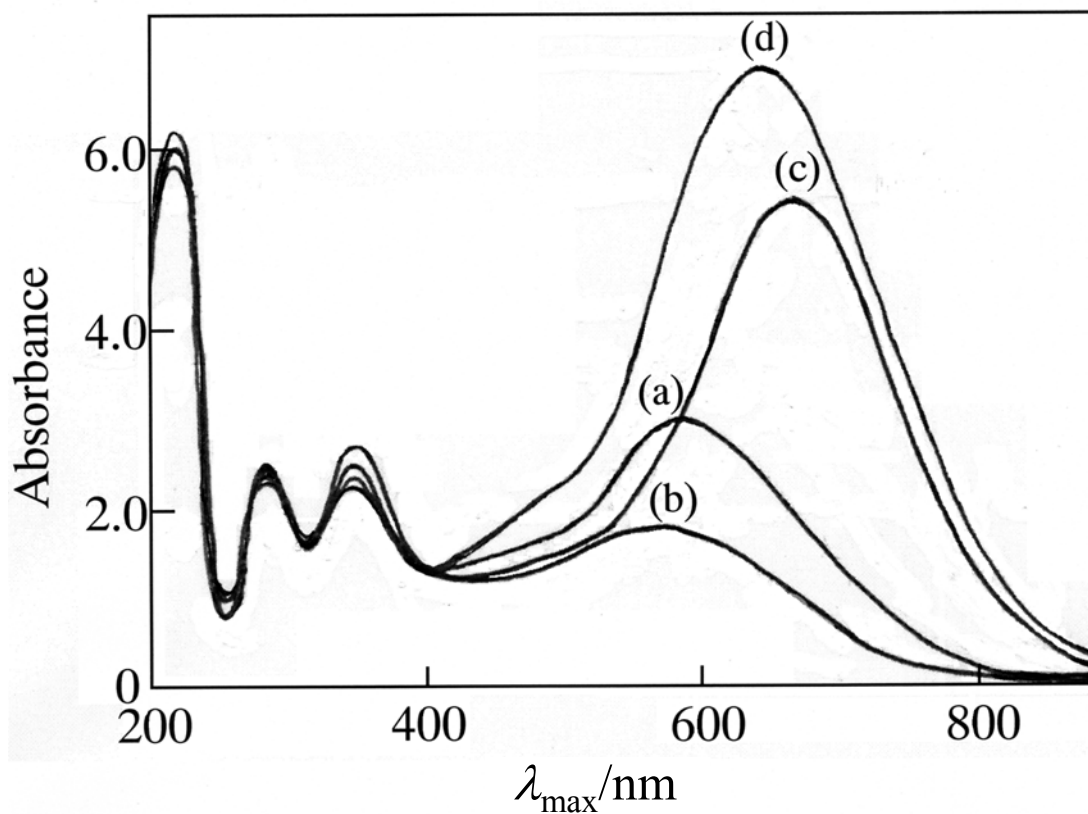
Figure 7-2. Absorption spectra of stereoregular PVA-iodine complexes in aqueous solution for (a) HI-PVA (f_{mm}=0.78), (b) LI-PVA (f_{mm}=0.66), (c) A-PVA (f_{mm}=0.22) and (d) S-PVA (f_{mm}=0.14) at 5 ^{o}C. [PVA]=0.1wt%, [I$_2$]/[KI]/[H$_3$BO$_3$]=0.3/0.6/100mM.

shows the absorption spectra of stereoregular PVA-iodine complexes in aqueous solutions in the presence of boric acid. Each absorption spectrum has two peaks at around 350 nm and at around 600 nm. The former (at 350 nm) has been attributed to polyiodine, I_3^-, and the latter (at 600 nm), I_5^-.[13-16]

It should be noted that the absorbance at λ_{max} of PVA-iodine complexes greatly depends on the f_{mm}, and PVA with f_{mm}=~0.5 shows no color development, as shown in Figure 7-1. These relationships are in good agreement with the case for the physical properties of stereoregular PVAs, i.e., the plots of $T\alpha_c$, T_m, χ_c, and T_{1C} against the f_{mm} show their minima at f_{mm}=0.4–0.5. These results suggest that the disordering of the intermolecular and/or intramolecular hydrogen bonding for each PVA chain, being most significant at f_{mm}=0.4-0.5, governs the formation of PVA-iodine complexes. As described previously, PVA with lower values of f_{mm} (e.g., S-PVA) form the complex with iodine easily because of the aggregation of PVA molecules by the intermolecular hydrogen bonding. On the other hand, PVA molecules with a higher value of f_{mm} (i.e., HI-PVA) aggregate easily in the presence of boric acid because boric acid reacts with a *meso* sequence in the PVA chains selectively.[17] This is probably the reason for the HI-PVAs to form a complex with iodine easily in the presence of boric acid.

The λ_{max} values near 600 nm for stereoregular PVA-iodine complexes are also summarized in Table 7-1. As clearly shown in Table 7-1, the absorption maximum for HI-PVA and iodine complexes changed to a

shorter wavelength than that for S-PVA or A-PVA and iodine complexes. It has been reported that the change in λ_{max} is often accompanied by the change in the amount of complex formed.[13]   The structure of HI-PVA and iodine complexes are discussed later in greater detail.

7.3.2. Effect of the boric acid concentration on the complex formation for stereoregular PVAs

To clarify the effect of the stereoregularity on the complex formation of PVA and iodine, the absorbances at λ_{max} near 600 nm, which has been attributed to I_5^-, are plotted against the concentration of boric acid for the stereoregular PVAs, as shown in Figure 7-3.   The absorbances of the PVA-iodine complex increased with increasing concentration of boric acid for all stereoregular PVAs.   It has been reported that equilibrium is established between I_3^- and I_5^-:[2]

$$I_2 + I_3^- \qquad I_5^- \qquad\qquad (1)$$

The equilibrium shifts to the direction of the increase in I_5^- with increasing boric acid concentration; that is to say, the boric acid accelerates the formation of I_5^-, as seen in the resonance Raman spectra reported by Takamiya's group.[2]

In the range of boric acid concentration from 0–100 mM, the intensity of the S-PVA-iodine complexes is higher than that of the A-PVA-iodine

162

complex. In the range of boric acid concentration over 100 mM, on the *other* hand, the intensity of A-PVA-iodine complex is higher than that of S-PVA-iodine complexes. The boric acid reacts with diols arranged isotactically in the PVA molecules.[17] Therefore, the A-PVA molecules that have more *meso* sequences than the S-PVA aggregate easily in the solution. Further, the aggregation of sequences in PVA molecules is considered to accelerate the production of I_5^-, i.e., the complex. At a fixed boric acid concentration, the absorbance at λ_{max} of the HI-PVA and iodine complexes are found to decrease to approximately half of that for the S-PVA and iodine complexes, as shown in Figure 7-3.

In Figure 7-4, the wavelengths of absorption maxima (λ_{max}) near 600 nm are plotted against the concentration of boric acid for the stereoregular PVAs. It has been reported that the absorption maximum at approximately 600 nm is attributed to the complex with I_5^-.[13,14] For all samples, the λ_{max} values increase with the concentration of boric acid, and the λ_{max} values for HI-PVA are less than that for S-PVA or A-PVA. It has been reported that λ_{max} depends on the structure of the complex, particularly on the number of atoms in polyiodine participating in the complex.[22,24] They reported the effect of the degree of hydration of PVA films on λ_{max} as functions of iodine concentration and temperature, and the λ_{max} value shifts continuously from 520 to 600 nm with increasing degree of hydration, and concluded that a longer complex is formed in the film with higher degree of hydration. As described in greater detail in later sections, the number of iodine atoms and the average size of the polyiodine
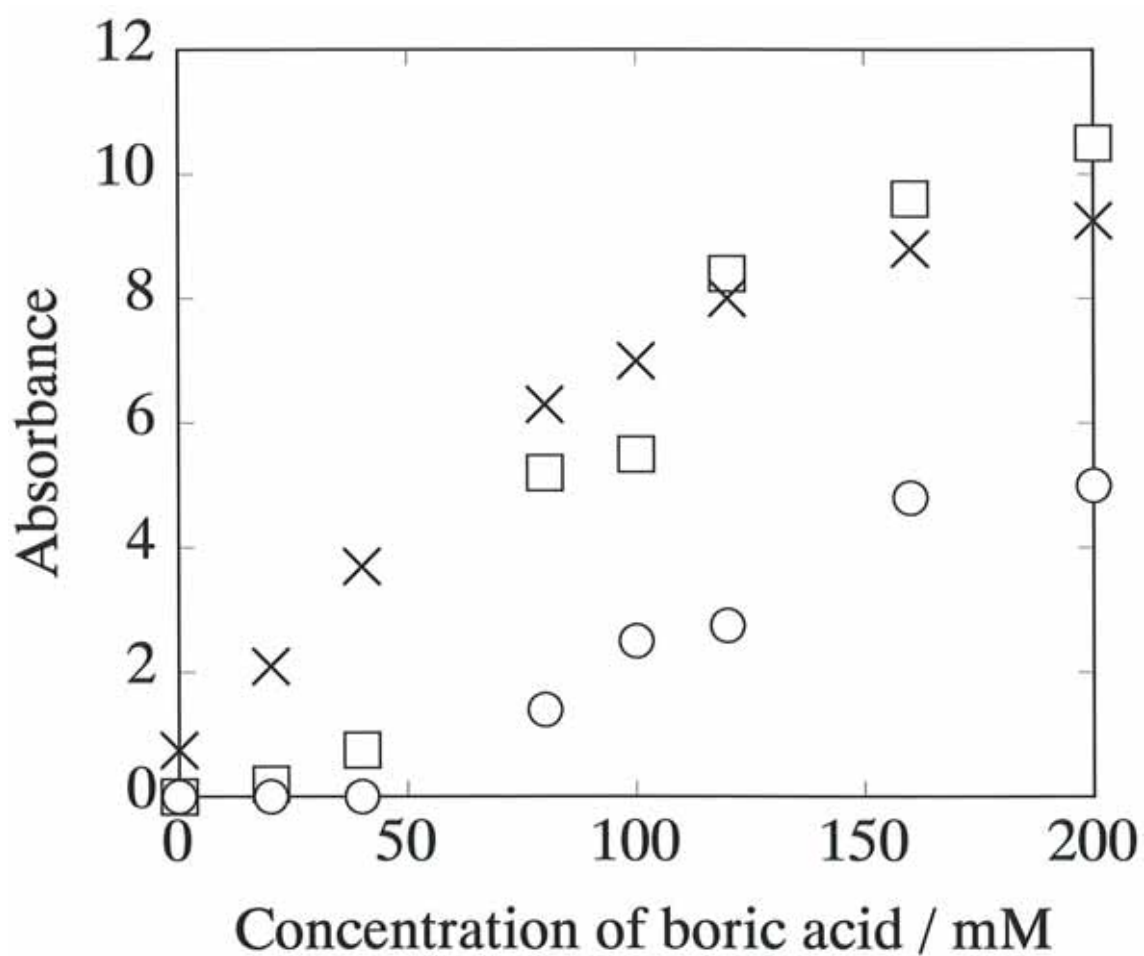
Figure 7-3. Relationship between the concentration of the boric acid and the absorbance at λ_{max} of PVA-iodine complexes in aqueous solution for HI-PVA (f_{mm}=0.78, circle), A-PVA (f_{mm}=0.22, square) and S-PVA (f_{mm}=0.14, cross) at 5 ^{o}C. [PVA]=0.1 wt%, [I$_2$]/[KI]=0.3/0.6 mM.
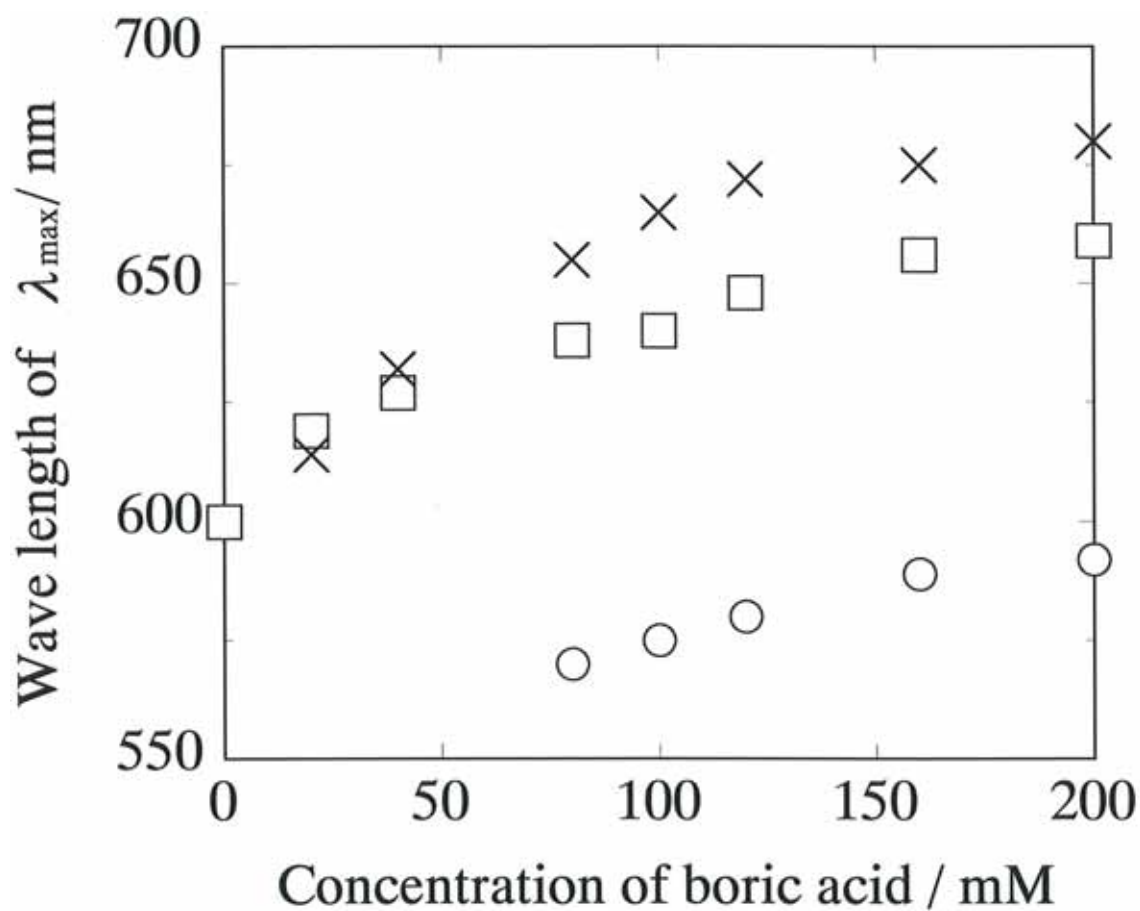
Figure 7-4. Relationship between the concentration of the boric acid and the wave length of λ_{max} of PVA-iodine complexes in aqueous solution for HI-PVA (f_{mm}=0.78, circle), A-PVA (f_{mm}=0.22, square) and S-PVA (f_{mm}=0.14, cross) at 5 $^{\circ}$C. [PVA]=0.1 wt%, [I$_2$]/[KI]=0.3/0.6 mM.

complexes in the HI-PVA films are probably smaller than those for A-PVA films, on the basis of the investigations of X-ray diffraction. This may be related to the difference in λ_{max} in visible absorption. On the basis of the resonance Raman spectroscopy, there are two types of polyiodines, i.e., linear I_5^- and bent complex of I_2 and I_3^-, which may be more unstable than the linear complex, in HI-PVA and iodine complex in solution, and this may be the other reason for the decrease in λ_{max} of Hi-PVA and iodine complexes.

7.3.3. Thermal stability of the stereoregular PVAs and iodine complexes

We studied the temperature dependence of the stability of the PVA-iodine complex using visible ray absorption spectrum. The thermal stability of the complex in the solution was measured as follows: after the PVA and boric acid is dissolved in a solution with a given iodine concentration at 5 ^{o}C until the equilibrium amount of complex is formed, the solution was heated stepwise and maintained at each temperature for 30 min. The relationship between the temperature and relative absorbance at λ_{max}, and the wavelength of λ_{max} of PVA-iodine complexes in an aqueous solution are shown in Figure 7-5 and 7-6, respectively. From Figure 7-5, the amount of complex decreases with increasing temperature for all types of stereoregular PVAs, and the decreasing trend continues until the complex disappears completely at 50 ^{o}C and 65 ^{o}C in the specimens with A-PVA and S-PVA, respectively. It should be noted that under 80 ^{o}C, the
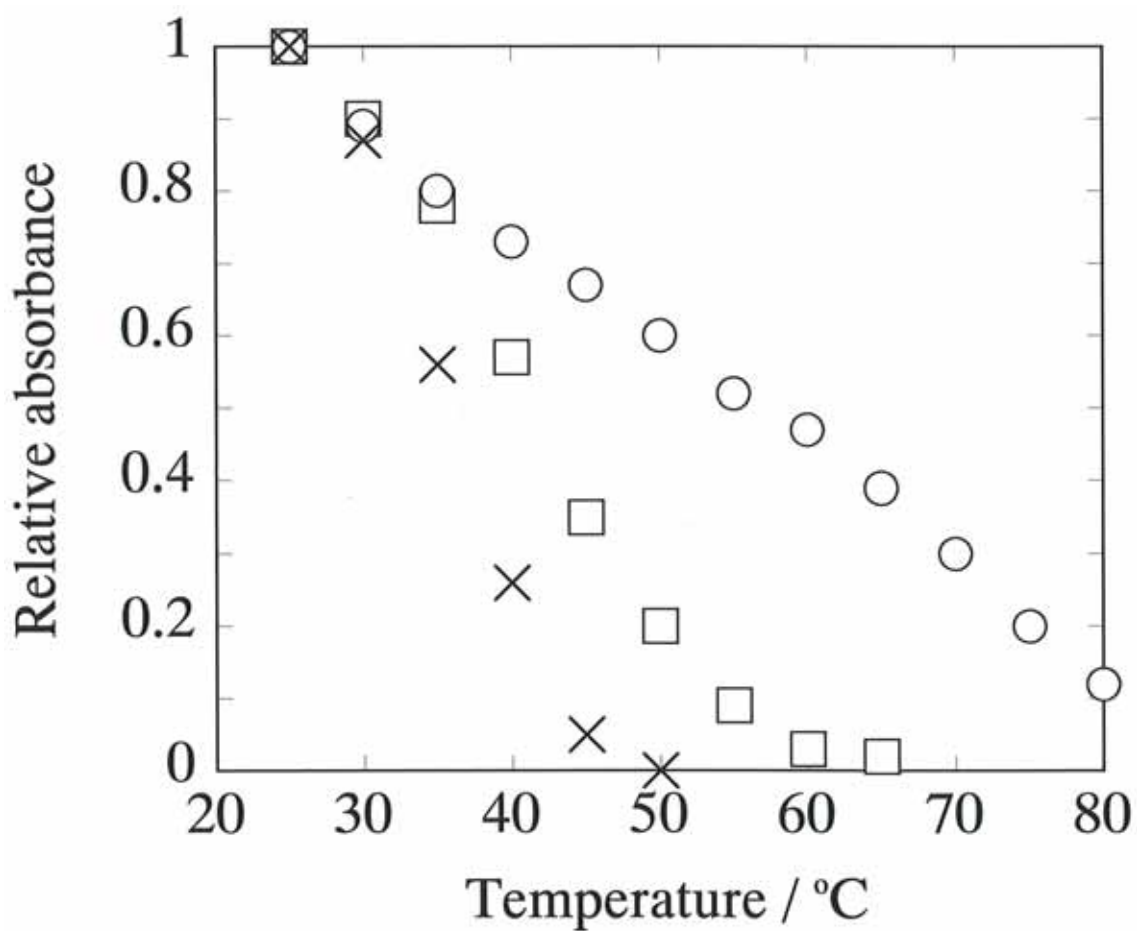
166

Figure 7-5. Relationship between the temperature and the relative absorbance at λ_{max} of PVA-iodine complexes in aqueous solution for HI-PVA (f_{mm}=0.78, circle), A-PVA (f_{mm}=0.22, cross) and S-PVA (f_{mm}=0.14, square).   [PVA]=0.1 wt%, [I$_2$]/[KI]/[H$_3$BO$_3$]=0.3/0.6/100 mM.
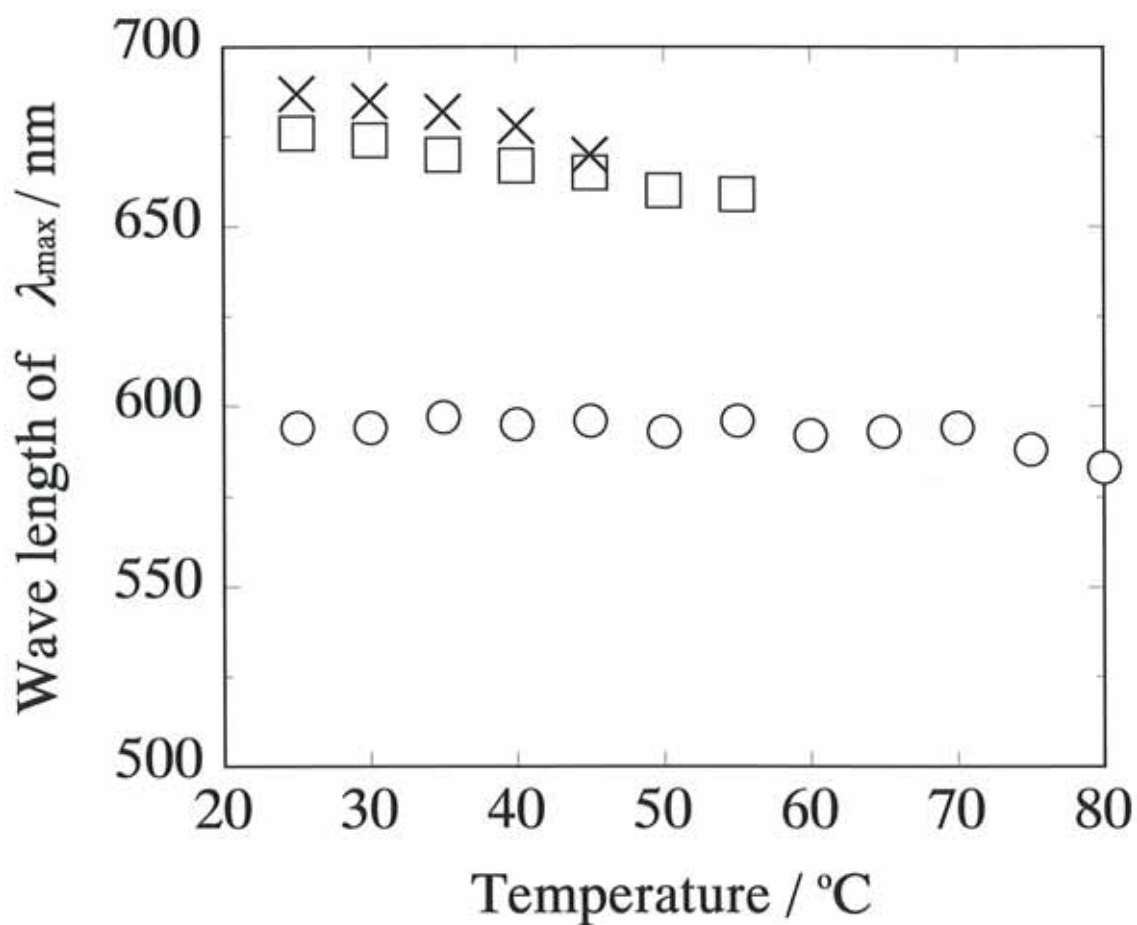
Figure 7-6. Relationship between the temperature and the wave length of λ_{max} of PVA-iodine complexes in aqueous solution for HI-PVA (f_{mm}=0.78, circle), A-PVA (f_{mm}=0.22, cross) and S-PVA (f_{mm}=0.14, square). [PVA]=0.1 wt%, [I$_2$]/[KI]/[H$_3$BO$_3$]=0.3/0.6/100 mM.

blue color of the HI-PVA and iodine complex still remains, and this result means that the thermal stability of the HI-PVA and iodine complex is higher than that of A-PVA or S-PVA.

The mechanism of the crosslink reaction of a borate ion with PVA is believed to be a didiol complexation, which is formed between two diol units in PVA chains and one borate ion.[18]   Matsuzawa et al. studied the reaction of borate ion with isotacticity-rich PVA and compared it with that for atactic PVA, and reported that the equilibrium constants (i.e., K_1 for the monodiol type complex and K_2 for the didiol type) for isotactic PVA were larger than those for atactic PVA at a fixed temperature.[17]   These observations suggest that the order of thermal stability of the PVA-iodine complexes shown in Figure 7-5 may correspond to the order of thermal stability of the aggregation of PVA molecules.   In other words, the aggregation of HI-PVA, which is due to didiol crosslinks, is more thermally stable than that for S-PVA, which is due to intermolecular hydrogen bonding, and the thermal stability of A-PVA molecules is lower than that for HI-PVA or S-PVA.

λ_{max} of the specimens of HI-PVA and iodine remains almost unchanged during heating, as shown in Figure 7-6, which is in contrast to the results that λ_{max} of the complex of A-PVA or S-PVA and iodine decreases gradually with increasing temperature.

7.3.4. Resonance Raman spectroscopy study of the HI-PVA and iodine complexes

As described in the previous section, the λ_{max} values for the HI-PVA and iodine complex with boric acid are smaller than those for S-PVA or A-PVA. It has been reported that the change in λ_{max} is often accompanied by the change in the amount of complex formed.[13] Hence, one possible origin of the decrease in λ_{max} of HI-PVA and iodine complexes may be related to the decrease in I_5^- and increase in I_3^-, for which absorptions appeared at 620 and 510 nm, respectively. The other is that the structure of polyiodine formed in HI-PVA and iodine complex differs from that in A-PVA or S-PVA. To examine these possibilities and to clarify the effect of the stereoregularity of PVA on the complexes with iodine, we studied the structure of polyiodine in the complex with HI-PVA in solution.

Resonance Raman spectroscopy has contributed significantly to the investigation of polyiodines participating in the PVA-iodine complex. Polyiodine identified by Resonance Raman spectroscopy by using a standard material whose polyiodine structure is well established.[19,20] Figure 7-7 shows the resonance Raman spectra of the HI-PVA and iodine complexes with different concentrations of boric acid. The absorption maxima at 162 and 110 cm^{-1}, which is attributed to I_5^- and I_3^-, respectively,[13] are also clearly seen for HI-PVA. It should be noted that a new band appears at approximately 178 cm^{-1} for HI-PVA and iodine complex when the boric acid concentration is low, and this is due to the formation of another type of complex in HI-PVA solution.

Teitelbaum et al. compared the resonance Raman spectrum of starch-iodine with the spectra of various model compounds, and concluded
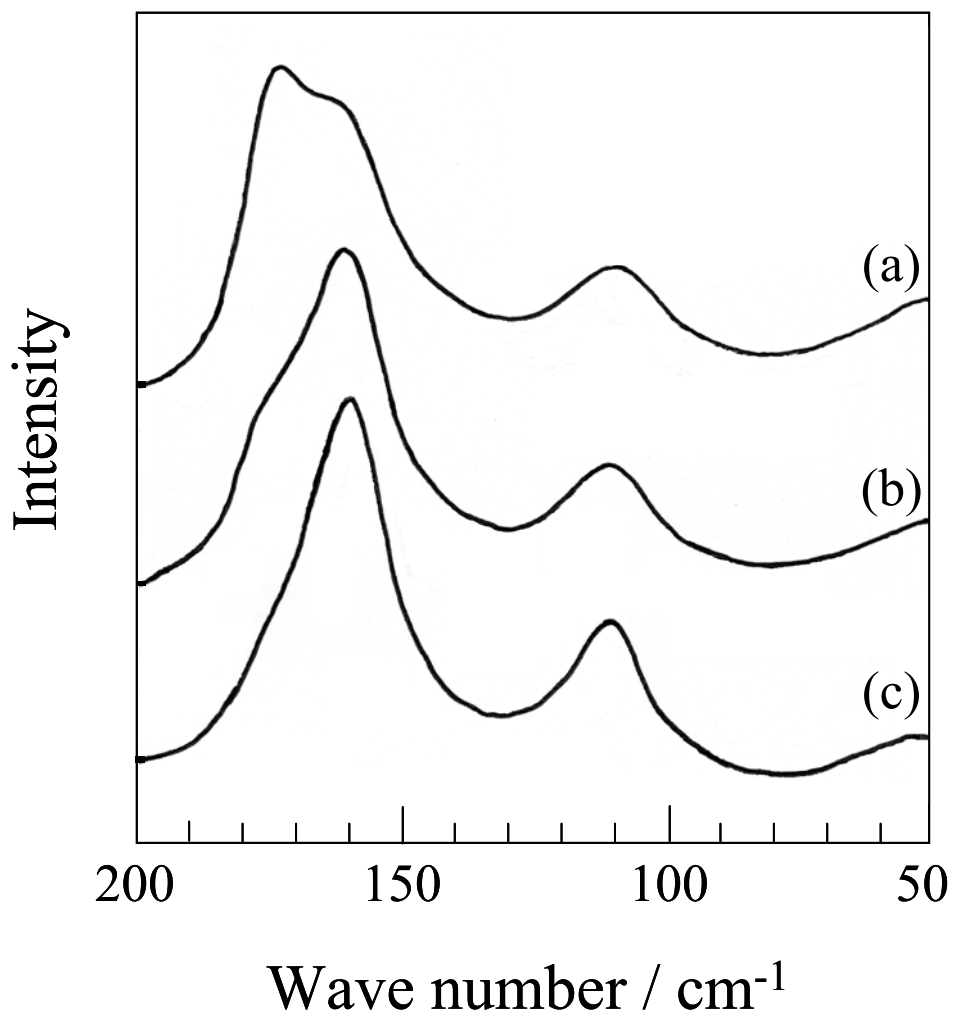
Figure 7-7. Resonance Raman spectra of HI-PVA (f_{mm}=0.78)-iodine complexes in aqueous solution with different concentration of boric acid. (a) [H$_3$BO$_3$]=80 mM, (b) 120 mM, and (c) 200 mM.

that the frequency varies depending on the I_5^- symmetry, and assigned the band at 162 cm^{-1} to linear I_5^- species.[21]   They also reported that the peak corresponding to pentaiodide anion shifts continuously from 162 to 187 cm^{-1} with decreasing bent angle of pentaiodide anion from 180° to 90°. According to their report, the band at 178 cm^{-1} observed in HI-PVA and iodine complexes should be attributed to the pentaiodide anions having distorted combinations of I_2 and I_3^-, which becomes bent at an angle 170°. As clearly seen in Figure 7-7, the intensity of the band at 178 cm^{-1} decreased, whereas the intensity of the band at 162 cm^{-1} increased, with increasing concentration of boric acid.   There are two types of polyiodines, i.e., linear I_5^- and bent complex of I_2 and I_3^-, in HI-PVA and iodine complex in solution, and this may be one of the reasons for the decrease in λ_{max} of HI-PVA and iodine complexes as compared to that of A-PVA or S-PVA.

Several researchers have reported the model of the PVA-iodine complexes in solution, i.e., polyiodine is surrounded by a certain amount of extended PVA molecules in the complex.[2,9,15,23]   The PVA molecules in an aqueous solution becomes easier to associate due to increasing intermolecular hydrogen bonding with increasing content of longer syndiotactic sequences, and iodine molecules enter into the space in the aggregates to form a polyiodine such as I_5^-.   In this model, the PVA molecules participating in a complex are supposed to be fixed by interchain hydrogen bonding without boric acid, or by didiol crosslinks with boric acid.

We believe that the HI-PVA and iodine complexes form basically the

same structure as that for A-PVA or S-PVA, i.e., polyiodine is surrounded by extended PVA molecules.   One of the experimental results supporting the extended conformation for HI-PVA and iodine complex is the acceleration of the complex formation by the chain extension discussed in the later section.   In addition, in Chapter 5, we reported that the HI-PVA molecules should form a slightly helical structure not only in the crystalline region but also in the less mobile region because the successive formation of strong intramolecular hydrogen bonding allows the formation of such a helical structure even in the hydrated state.   These features of hydrogen bonding seem to be also present in the HI-PVA molecules that surround the polyiodine complex.   In other words, the HI-PVA chains probably form a slightly helical conformation rather than a planar zigzag one, which is due to successive intramolecular hydrogen bonding, while each PVA chains aggregate through didiol crosslinking in the presence of boric acid.   When the boric acid concentration is low, the space in the aggregates of HI-PVA chains may be larger than that of A-PVA or S-PVA molecules that aggregate through intermolecular hydrogen bonding, and the polyiodine formed in this space is less restricted.   This is probably the reason that the polyiodine with the HI-PVA molecules forms the unstable bent conformation when the boric acid concentration is low.

7.3.5. Wide-angle X-ray diffraction study of the stereoregular PVAs and iodine complexes

X-ray diffraction measurement has contributed considerably to the

investigation of polyiodine structures directly in PVA films.[22]   According to the previous reports, in practice, we observed that the clear peaks correspond to the polyiodine complex in the undrawn A-PVA films that are immersed in the high iodine concentration, i.e., $[I_2]/[KI]=0.05/0.1$ M. However, for the undrawn HI-PVA films, we cannot observe any peaks corresponding to the polyiodine complex even in iodine concentrations higher than that for the A-PVA films, i.e., $[I_2]/[KI]=0.2/0.4$ M.   Hence, we studied the X-ray diffraction of the drawn PVA films instead of the undrawn films in order to investigate the structure of the polyiodine complex in the HI-PVA films because it is well known that the extension of PVA films remarkably enhances the PVA-iodine complex formation.   The X-ray diffraction diagrams of iodinated drawn PVA films show the existence of linear polyiodides oriented parallel to the draw direction of the films.[22]

   Figure 7-8 shows X-ray meridional (I) and equatorial (II) intensity profiles of the iodinated drawn HI-PVA or A-PVA films.   For the iodinated drawn A-PVA film, a strong and sharp peak appears at about $2\theta = 29$ ^{o} on the meridional intensity profile, as shown in Figure 7-8(I,b), which corresponds to a polyiodine with an interatom period of 0.31 nm as reported previously.[22]   While the broad peak at approximately $2\theta=13.5$ ^{o} on the equatorial profile, as shown in Figure 7-8(II,b), corresponds to a spacing of 0.66 nm, it is probably assigned to the average distance between the polyiodine and the extended PVA chains.   In contrast, for the iodinated drawn HI-PVA film, only weak and broad peaks can be observed at
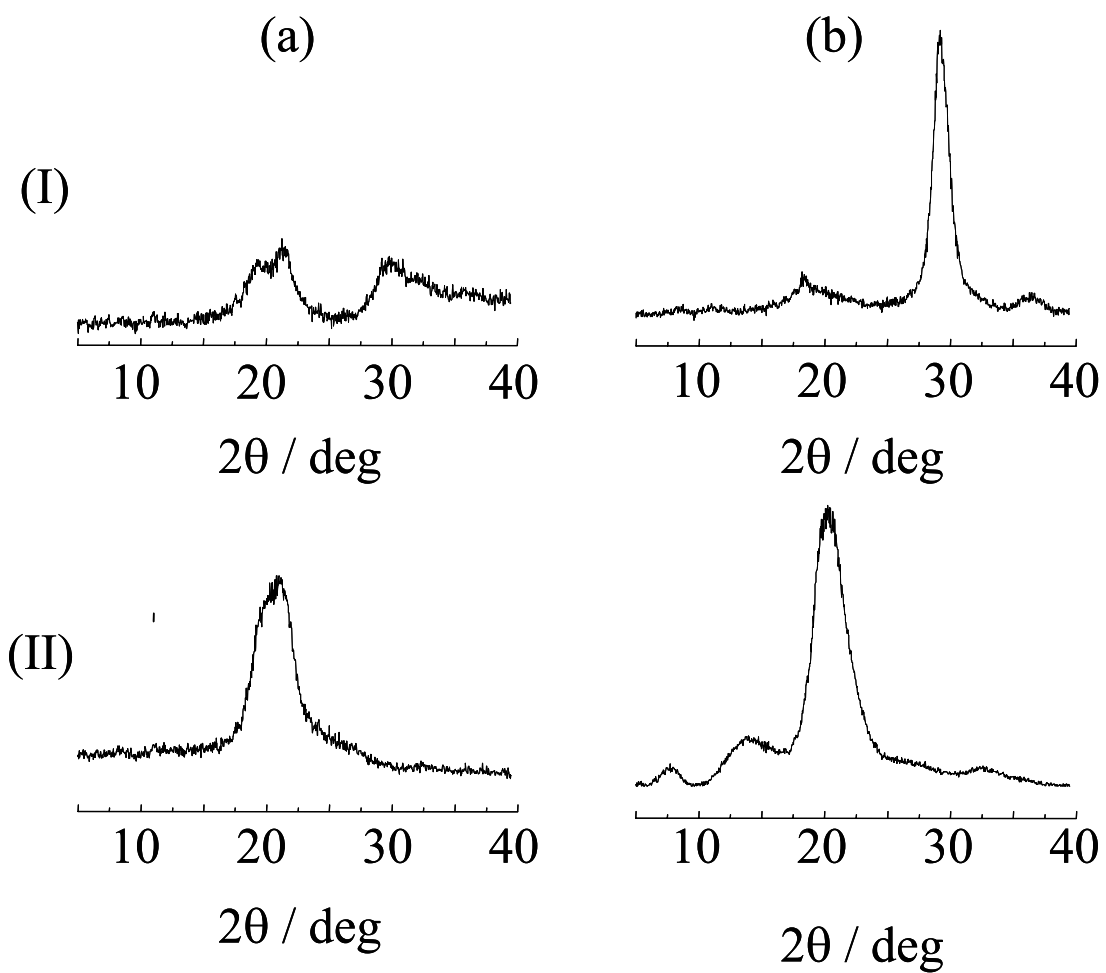
Figure 7-8. X-ray meridiotal (I) and equatorial (II) intensity profiles of iodinated drawn HI-PVA (a) and A-PVA (b) films soaked in an iodine solution ([I$_2$]=0.01 M, [KI]=0.02 M).

approximately $2\theta = 29$ $^{\text{o}}$ on the meridional profile, while no peak appears at approximately $2\theta = 13.5$ $^{\text{o}}$ on the equatorial profile, as shown in Figure 7-8(I,a) and (II,a). This difference implies that the number of iodine atoms and the average size of polyiodine complexes in the HI-PVA films must be smaller, resulting in broader diffraction than that for A-PVA films. These results suggest that the capability of polyiodine complex formation in the HI-PVA films is very low even in an extended mode, which is in agreement with experimental observations for the complex formation in aqueous solution.

Figure 7-9 show the X-ray meridiotal intensity profiles of drawn HI-PVA (a) and A-PVA (b) films soaked in an iodine solution (I) or in water (II). On the profile shown in Figure 7-9(I,b) for the A-PVA film, a peak $2\theta{=}61^{\text{o}}$ corresponds to 0.15 nm, which is the second order reflection of the polyiodine complex, while the peak at $2\theta{=}75.1$ $^{\text{o}}$ corresponding to 0.13 nm is originally assigned to (002) of the PVA crystal lattice. Despite appearance of a strong peak corresponding to polyiodine in the meridianal diffraction, the (002) diffraction characteristic to the A-PVA crystal still remains as it was when drawing in water. In other words, the X-ray diffraction of A-PVA crystals remained without any change after the iodine soaking. This result shows that the iodine sorption and complex formation only take place in the noncrystalline region in A-PVA films under these conditions.

On the other hand, a peak $2\theta{=}61$ $^{\text{o}}$ corresponds to the second order reflection of the polyiodine complex in the HI-PVA film is weak and
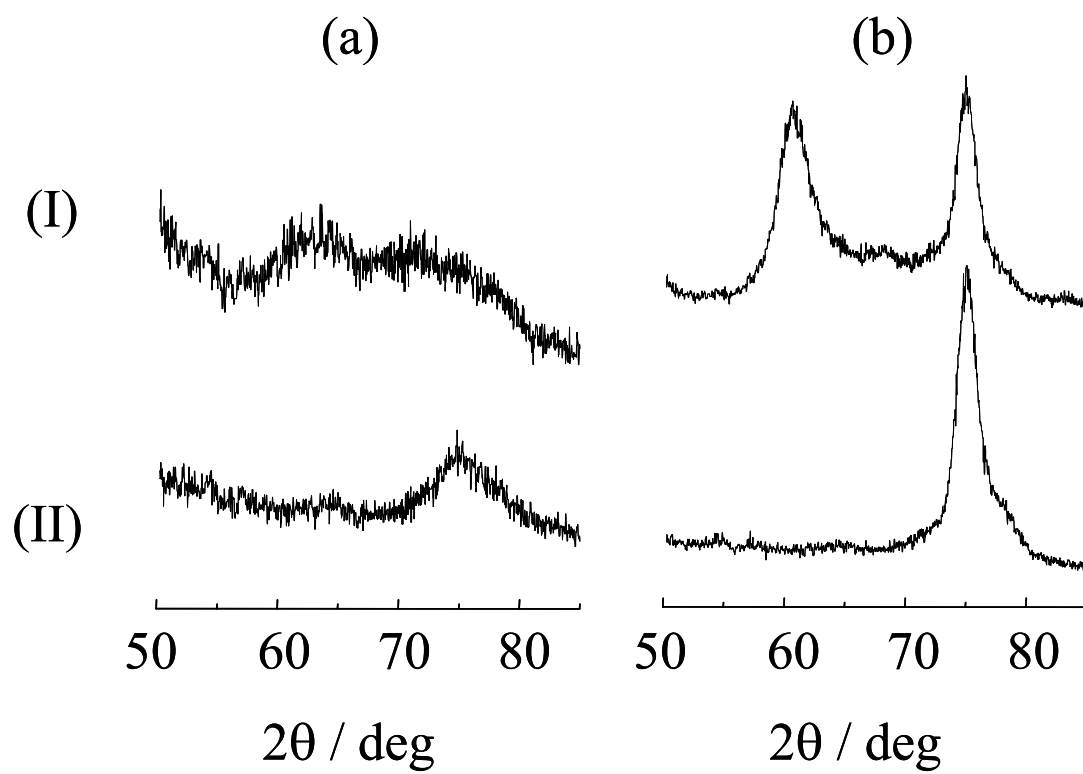
Figure 7-9. X-ray meridiotal intensity profiles of drawn HI-PVA (a) and A-PVA (b) films soaked in an iodine solution (I) or in water (II).

broader than that for the A-PVA film, as shown in Figure 7-9(I,a) and (I,b). It should be noted that a remarkable change of crystal spacing is observed in the iodinated drawn HI-PVA films prepared under the same conditions as A-PVA films. This extraordinary broadening of the peak corresponding to the crystal spacing indicates that the iodine sorption occurs not only in the noncrystalline region but also in the crystalline region in the HI-PVA film. As described in the previous section, HI-PVA molecules form only intramolecular hydrogen bonding; this may be a reason why some of the iodine atoms absorbed can penetrate into the crystalline region and form a complex in the HI-PVA films.

7.4. Conclusions

We have synthesized HI-PVAs having higher f_{mm} values from poly$t$BVE and studied the complex formation with iodine in aqueous solution or in film, and obtained the following conclusions:

(1) Without boric acid, no color change due to the formation of PVA-iodine complex is observed for the HI-PVA solution in contrast to the results for the S-PVA or A-PVA. On the other hand, the boric acid enhances the formation of a complex over a wide range of f_{mm} of PVAs. The absorbance at $\lambda_{\max}$ of PVA-iodine complexes highly depends on the f_{mm}, and PVA with $f_{mm}=\sim0.5$ shows no color development. These results suggest that PVAs with a lower value of f_{mm} (e.g., S-PVA) form the complex with iodine easily because of the aggregation of PVA molecules by the intermolecular hydrogen bonding, while PVA molecules with a

higher value of *mm* fractions (i.e., HI-PVA) aggregate easily in the presence of boric acid because boric acid reacts with the *meso* sequence in the PVA chains selectively.

(2) The absorbance of the PVA-iodine complex increased with increasing concentration of boric acid for all stereoregular PVAs. At a fixed boric acid concentration, the absorbance at λ_{max} of the HI-PVA and iodine complexes are found to decrease to approximately half the values of that for the S-PVA and iodine complexes. For all the samples, the λ_{max} values increase with increasing concentration of boric acid, and the λ_{max} values for the HI-PVA are less than that for S-PVA or A-PVA.

(3) The amount of complex decreases with increasing temperature for all types of stereoregular PVAs, and the decreasing trend continues until the complex disappears completely at 50 ^{o}C and 65 ^{o}C in the specimens with A-PVA and S-PVA, respectively. However, the blue color of the HI-PVA and iodine complex still remains under 80 ^{o}C. The higher thermal stability of the HI-PVA and iodine complex may due to the higher thermal stability of the aggregation of the HI-PVA in solution because of a didiol crosslink between each molecule.

(4) Two resonance Raman shifts appear at 162 and 110 cm^{-1}, which is attributed to I$_5^-$ and I$_3^-$, respectively, for HI-PVA solution. In addition, with lower boric acid concentration, a new band appears at approximately 178 cm^{-1}, which may be attributed to the pentaiodide ions having distorted combinations of I$_2$ and I$_3^-$. There are two types of polyiodines, i.e., linear I$_5^-$ and bent complex of I$_2$ and I$_3^-$, in HI-PVA solution, and this may be the

reason that the λ_{max} values for the HI-PVA are smaller than those for S-PVA or A-PVA.

(5) We proposed a model of the HI-PVA and iodine complexes in which the complex basically forms the same structure as in that for A-PVA or S-PVA, i.e., polyiodine is surrounded by extended PVA molecules. One of the experimental results supporting this extended conformation for HI-PVA and iodine complex is the acceleration of the complex formation by the chain extension demonstrated by X-ray diffraction studies. In this model, the HI-PVA chains with an extended but slightly helical conformation due to successive intramolecular hydrogen bonding, surround polyiodine, and each PVA chain aggregate through didiol crosslinks between the PVA chains.

(6) For the iodinated drawn HI-PVA film, only weak and broad peaks can be observed at approximately $2\theta=29$ ^{o}, which corresponds to polyiodine with an interatom period of 0.31 nm, and at approximately $2\theta=61$ ^{o} corresponds to the second order reflection of the polyiodine complex. Both peaks are weaker and broader than those for the A-PVA film, while the peaks at approximately $2\theta=13.5$ ^{o} on the equatorial profile corresponds to the average distance between polyiodine; further, the extended PVA chains cannot be observed in the HI-PVA film. These results suggest that the capability of polyiodine complex formation in the HI-PVA films is very low even in an extended mode. In addition, the extraordinary broadening of the X-ray diffraction peak at $2\theta=75$ ^{o}, which corresponds to the crystal spacing, indicate that the iodine sorption takes place not only in the

noncrystalline region but also in the crystalline region in HI-PVA films.

References

(1) Miyazaki, T.; Katayama, S.; Funai, E.; Tsuji, Y.; Sakurai, S. *Polymer* **2005**, 46, 7436 and references therein.

(2) Takamiya, H.; Tanahashi, Y.; Matsuyama, T.; Tanigami, T.; Yamaura, K.; Matsuzawa, S. *J Applied Polym Sci* **1993**, 50, 1807.

(3) Yamamoto, T.; Yoda, S.; Takase, H.; Sangen, O.; Fukae, R.; Kamachi, M.; Sato, T. *Polymer J* **1991**, 23, 185.

(4) Finch, C. A. *Polyvinyl Alcohol-Developments*; John Wley & Sons: New York, **1992**, 757.

(5) Nakajima, A. *Kobunshi Kagaku* **1949**, 6, 451.

(6) Moritani, T.; Kuruma, I.; Shibatani, K.; Fujiwara, Y. *Macromolecules* **1972**, 5, 577.

(7) DeMember, JR.; Haas, HC.; MacDonald, RL. *J Polym Sci, Polym Lett Ed* **1972**, 10, 385.

(8) Matsuzawa, S.; Yamaura, K.; Noguchi, H. *Makromol Chem* **1974**, 175, 31.

(9) Noguchi, H.; Jyodai, H.; Matsuzawa, S. *J Polym Sci* **1997**, 1701.

(10) Maeda, H.; Morishima, Y.; Kamachi, K. *Polym Preprints Jpn* **1994**, 43, 3437, *Rep of the PVAL Committee* **1994**, 105, 75.

(11) Deuel, H.; Neukom, H. *Makromol Chem* **1949**, 3, 13.

(12) Shibayama, M.; Sato, M.; Kimura, Y.; Fujiwara, H.; Nomura, S. *Polymer* **1988**, 29, 336.

(13) Hayashi, S.; Hirai, Y.; Hojo, N.; Sugita, H.; Kyogoku, Y. *J Polym Sci Polym Lett Ed* **1982**, 20, 69.

(14) Yokota, T.; Kimura, Y. *Makromol Chem* **1989**, 190, 939.

(15) Yokoyama, T.; Kaneyuki, K.; Sato, H.; Hamamatsu, H.; Ohta, T. *Bull Chem Soc Jpn* **1995,** 68, 469.

(16) Choi, Y.S.; Miyasaka, K. *Polym J* **1991,** 23, 977.

(17) Matsuzawa, S.; Yamaura, K.; Tanigami, T.; Somura, T.; Nakada, M. *Polym Commun* **1987**, 28, 105.

(18) Lin, H.L.; Liu, Y.F.; Yu, T.L.; Liu, W.H.; Rwei, S.P. *Polymer* **2005**, 46, 5541 and references there in.

(19) Heyde, M.E.; Rimai, L.; Kilponen, R.G.; Gill, D. *J Am Chem Soc* **1972**, 94, 5222.

(20) Inagaki, F.; Harada, I.; Shimanouchi, T.; Tasumi, M. *Bull Chem Soc Jpn* **1972**, 45, 3384.

(21) Teitelbaum, R.C.; Ruby, S.L.; Marks, T.J. *J Am Chem Soc* **1980**, 102, 3322.

(22) Miyasaka, K. *Adv in Polym Sci* **1993**, 108, 91 and references their in.

(23) Oishi, Y.; Yamamoto, H.; Miyasaka, K. *Polymer J* **1987**, 19, 1261.

(24) Kojima, Y.; Furuhata, K.; Miyasaka, K. *J Appl Polym Sci* **1985**, 30, 1617.

Summary

In this thesis, details of the preparation and the characterization of the highly isotactic poly(vinyl alcohol)s (HI-PVAs) derived from poly(*tert*-butyl vinyl ether) (poly*t*BVE) have been dealt with. In addition, some basic physical properties of PVA samples with different tacticities including HI-PVA have been systematically examined by different analytical methods as functions of the *mm* fraction (f_{mm}) at the wide range. Intramolecular and intermolecular hydrogen bondings are also characterized for dried and hydrated HI-PVA films in detail by using high-resolution solid-state ^{13}C NMR spectroscopy.

In Chapter 2, the preparation and characterization of HI-PVAs derived from poly*t*BVE polymerized with $BF_3{\cdot}OEt_2$ were investigated. The *mm* fraction (f_{mm}) increased with decreasing $BF_3{\cdot}OEt_2$ concentration, and it reached as high as 0.78–0.79, which seems to be the highest value of all the so-called isotactic PVAs reported so far; the catalyst concentration was reduced to below 0.5×10^{-3} mole/l. An increase in f_{mm} may be caused by highly isospecific propagation of a new kind of species, which is thought to be generated from the ligand exchange of BF_3 complex from ether to water. We also studied the polymerization of *t*BVE with various BF_3 complexes such as $BF_3{\cdot}2CH_3COOH$, $BF_3{\cdot}2CH_3OH$, and $BF_3{\cdot}2H_2O$. f_{mm} increased in the following order: $BF_3{\cdot}2CH_3COOH$ < $BF_3{\cdot}OEt_2$ < $BF_3{\cdot}2CH_3OH$ < $BF_3{\cdot}2H_2O$, and it increased with reducing the catalyst concentration for

each type of catalyst.

In Chapter 3, we studied the polymerization of tBVE and benzyl vinyl ether (BzVE) with heterogeneous catalysts, that is, modified Ziegler type (Vandenberg type) catalysts and metal sulfate-sulfuric acid complexes. Vandenberg type catalysts yielded highly isotactic poly$t$BVEs with relatively narrow molecular weight distributions and high molecular weights at high temperatures; the resultant poly$t$BVEs were then converted into stereoregular PVAs.   With a titanium based Vandenberg type catalyst, a relatively high isotactic PVA, which has a f_{mm} fraction of 0.52, was obtained from the poly$t$BVE polymerized at 30 ^{o}C.   From NMR studies, it was found that the content of the triad tacticity of PVAs derived from poly$t$BVE catalyzed by titanium based catalysts agreed with the value calculated from the chain-end control model (Bovey's model).   This fact suggests that the steric structure of the adding monomer in this system is determined by using the same mechanism as that used in the homogeneous BF_3 complexes catalysts system.   In contrast, the metal sulfate-sulfuric acid complexes showed significantly low activity with tBVE polymerization.

In Chapter 4, some basic physical properties, structure and hydrogen bonding have been characterized for different stereoregular PVA films including HI-PVAs as functions of the f_{mm} by using different analytical methods.   The melting temperature, degree of crystallinity, and ^{13}C spin-lattice relaxation time of the crystalline component were found to have their own clear minima at the f_{mm} of about 0.4 - 0.5.   This fact suggests

that structural disordering associated with the decrease in crystallinity may be most strongly induced at this f_{mm}.   The formation of the new crystal form of PVA has been reconfirmed for HI-PVAs with the f_{mm} higher than about 0.55 by FT IR spectroscopy and the structure and hydrogen bonding have been investigated in detail by solid-state ^{13}C NMR spectroscopy.   It was found that all OH groups were allowed to form successive intramolecular hydrogen bonding along the respective chains in the crystalline region for HI-PVAs with the f_{mm} higher than about 0.7.   Since these chains should contain some amount of r units even in the crystalline region, a slightly helical structure with a considerably long period may be adopted by them as an energetically stable state.   On the basis of the line shape analysis of the CP/MAS ^{13}C NMR spectra of the crystalline components, structural causes of the appearance of the minima of the physical values described above were also discussed in relation to the introduction of disordered units mainly associated with hydrogen bonding to the syndiotactic or isotactic sequences forming successive intermolecular or intramolecular hydrogen bonding, respectively.

In Chapter 5, the structure and hydrogen bonding of the hydrated stereoregular PVA films have been investigated by high-resolution solid-state ^{13}C NMR spectroscopy.   It was found by the ^{13}C spin-lattice relaxation analysis that there existed three components with different T_{1C} values assigned to the crystalline, less mobile, and mobile components for the hydrated syndiotactic PVA (S-PVA) and HI-PVA films.   The line shape analysis indicated that the probability of intramolecular hydrogen bonding

was appreciably increased in the crystalline region for the S-PVA films by the hydration but a slightly helical structure, which was probably allowed by the formation of the successive intramolecular hydrogen bondings along the chains in the crystalline region, seemed not to undergo any significant change by the hydration for HI-PVA. This fact indicated that intramolecular hydrogen bonding was more stable in the hydrated state in the crystalline region. As for the less mobile component, the line shape of the CH resonance line for the hydrated S-PVA or HI-PVA films was found to be very similar to that of the corresponding crystalline component, probably being due to the successive formation of intermolecular or intramolecular hydrogen bonding in the interfacial region, which mainly contributed to the less mobile component, for the S-PVA or HI-PVA films even in the hydrated state. The mole fractions of the *mm*, *mr* and *rr* sequences were also estimated for the mobile component that was produced in each stereoregular PVA sample by swelling with water and it has been concluded that no prominent preferential partitioning of the *mm, mr* and *rr* sequences occur in the crystalline and noncrystalline regions for the PVA films with different tacticities.

In Chapter 6, dynamic viscoelasticity of HI-PVA (f_{mm}=0.78) was investigated to compare with that of S-PVA (f_{mm}=0.14) and commercial A-PVA (f_{mm}=0.22). In the noncrystalline region, the β_a (local twisting motion) and α_a (micro-Brownian motion) dispersions occurring at around -10 ˚C and 70 ˚C were nearly the same, in both magnitude and location, for the HI-PVA and S-PVA having an almost identical degree of crystallinity.

On the other hand, in the crystalline region, the β_c and α_c dispersions of HI-PVA were somewhat different from those of ordinary PVAs. The β_c dispersion (local motion in crystals due to defects) was clearly observed for HI-PVA but not for S-PVA and A-PVA. The α_c dispersion (axial motion of the chain in the crystal lattices) was observed for all PVA films but its temperature increased in the order of HI-PVA > S-PVA > A-PVA, which well corresponded to the order of the melting temperature and ^{13}C spin-lattice relaxation time (T_{1C}) of each stereoregular PVA. These differences may be attributed to a difference of the magnitude of intermolecular and/or intramolecular hydrogen bonding in the crystals of respective PVAs. Specifically, the successive intramolecular bonding in the HI-PVA crystal appeared to reduce the magnitude of the intermolecular bonding thereby allowing the chain to exhibit the β_c motion. This successive bonding would also stiffen the chain backbone thereby increasing the α_c dispersion temperature.

In Chapter 7, we studied the complex formation of the HI-PVA with iodine comparing it with that for A-PVA and S-PVA in aqueous solutions and in the film state. Without boric acid, a color change, which occurs due to the formation of PVA-iodine complex, was not observed for the HI-PVA solution in contrast to the case of the S-PVA or A-PVA. On the other hand, the boric acid enhanced the formation of the complex over a wide range of f_{mm} of PVAs. The absorbance at λ_{max} of PVA-iodine complexes highly depended on the f_{mm}, and PVA with f_{mm}=~0.5 showed no color development. This result agrees with the case for the physical

187

properties of stereoregular PVAs, i.e., the plots of $T\alpha_c$, T_m, χ_c, and T_{1C} against f_{mm} show the respective minima at f_{mm}=0.4–0.5. Two resonance Raman shifts appeared at 162 and 110 cm^{-1}, which can be attributed to I_5^- and I_3^-, respectively, for the HI-PVA solution. In addition, with a lower boric acid concentration, a new band appeared at approximately 178 cm^{-1}; this can be attributed to the pentaiodide ions having distorted combinations of I_2 and I_3^-. On the basis of the investigations by Raman scattering, X-ray diffraction, and solid-state ^{13}C NMR spectroscopy, we proposed a model of the HI-PVA and iodine complexes in which the complex basically forms the same structure as in the case of A-PVA or S-PVA, i.e., polyiodine may be surrounded by extended PVA molecules. In this model, the HI-PVA chains with an extended and slightly helical conformation due to successive intramolecular hydrogen bonding surrounded a polyiodine, and each PVA chain aggregates through didiol crosslinks between the PVA molecules.

List of Publications

Chapter 2   "Preparation of Highly Isotactic Poly(vinyl alcohol)s Derived from Poly(*tert*-butyl vinyl ether)s" Hiroyuki Ohgi and Toshiaki Sato, *Macromolecules* **1999**, 32, 2403.

Chapter 3   "Heterogeneous Cationic Polymerization of *tert*-Butyl Vinyl Ether" Hiroyuki Ohgi and Toshiaki Sato, *Polymer* **2002**, 43, 3829.

Chapter 4   "Some Physical Properties, Structure and Hydrogen Bonding of Highly Isotactic Poly(vinyl alcohol) Films" Hiroyuki Ohgi, Toshiaki Sato, Shaohua Hu, and Fumitaka Horii, *Polymer* **2006**, 47,1324.

Chapter 5   "Solid-State ^{13}C NMR Investigation of the Structure and Hydrogen Bonding for Stereoregular Poly(vinyl alcohol) Films in the Hydrated State" Hiroyuki Ohgi, Hu Yang, Toshiaki Sato, and Fumitaka Horii,

Polymer **2007**, 48, 3850.

Chapter 6   "Viscoelastic Behavior of Highly Isotactic Poly(vinyl alcohol) Films"

Hiroyuki Ohgi, Toshiaki Sato, Hiroshi Watanabe, and Fumitaka Horii,

Polym. J. **2006**, 38, 1055.

Chapter 7   "Investigation of the Complex Formation between Highly Isotactic Poly(vinyl alcohol) and Iodine"

Hiroyuki Ohgi, Toshiaki Sato, Nobuhiro Moriguchi, Kumiko Oishi, Mikiko Ohgi, and Fumitaka Horii,

in preparation.

Acknowledgements

Kyoto, 2007   *Hiroyuki Ohgi*